A pure eulerian method with interface capturing for multi-material fluid flows in dimension 1, 2 and 3

Jean-Philippe Braeunig

ENSC N° 2007/85

THESE DE DOCTORAT
DE L'ECOLE NORMALE SUPERIEURE DE CACHAN

Présentée par

Jean-Philippe BRAEUNIG

pour obtenir le grade de

DOCTEUR DE L'ECOLE NORMALE SUPERIEURE DE CACHAN

Domaine :
MATHEMATIQUES APPLIQUEES

Sujet de la thèse :

Sur la simulation d'écoulements multi-matériaux par une méthode eulérienne directe avec capture d'interfaces en dimensions 1, 2 et 3.

Thèse présentée et soutenue à Cachan le 17 décembre 2007 devant le jury composé de :

François ALOUGES	Professeur, Paris XI	Rapporteur
Benoît DESJARDINS	Professeur, ENS Ulm	Directeur de thèse
Bruno DESPRES	Professeur, Paris VI	Examinateur
Jean-Michel GHIDAGLIA	Professeur, ENS Cachan	Examinateur
Patrick LE TALLEC	Professeur, Polytechnique	Rapporteur
Jean OVADIA	Ingénieur, CEA	Examinateur
David YOUNGS	Ingénieur, AWE	Examinateur

Laboratoire Centre de Mathématiques et de Leurs Applications
(ENS CACHAN/CNRS/UMR 8536)
61, avenue du Président Wilson, 94235 CACHAN CEDEX (France)

Sur la simulation d'écoulements multi-matériaux par une méthode eulérienne directe avec capture d'interfaces en dimensions 1, 2 et 3.

Résumé :
La méthode présentée dans ce mémoire vise à résoudre numériquement les équations d'Euler en 2D/3D modélisant l'écoulement de plusieurs matériaux compressibles, non-miscibles et de nature différentes. Il s'agit en particulier de reconstruire une interface d'épaisseur nulle entre ces matériaux, sans introduire de mélange entre eux. L'originalité de cette méthode purement eulérienne réside dans l'utilisation d'un schéma volumes finis direct. Le concept de "condensat" est introduit et étudié dans ce mémoire, qui permet de calculer l'évolution de l'interface dans la grille eulérienne fixe. De plus, cette méthode permet un glissement parfait des matériaux les uns par rapport aux autres et une conservation locale des grandeurs eulériennes. La qualité de la méthode est évaluée par des cas-tests académiques ainsi que par des cas-tests éprouvant la robustesse de la méthode.
Mots Clefs :
hydrodynamique compressible, schéma numérique, méthode directe, reconstruction d'interfaces, glissement, interfaces.

Abstract :
The method described in this report is designed to simulate multi-material fluid flows, by solving compressible Euler equations with sharp interface capturing, in dimension 2 and 3. Materials are supposed to be non-miscible and to follow different equations of state. The main purpose of this work is to design an interface reconstruction method with no diffusion at all between materials of any eulerian quantity. One novelty of our approach is the use of a pure eulerian finite volume scheme in an interface reconstruction method. A new concept is introduced, the "condensate", which allows to handle mixed cells containing two or more materials and to calculate the evolution of the interface on the fixed eulerian grid. Moreover, this method allows a free sliding of materials on each others. The accuracy of the method is evaluated on academic $1D$ benchmarks and its robustness is tested with severe $2D$ benchmarks.
Key words :
compressible hydrodynamic, numerical scheme, pure eulerian method, interface capturing, sliding, interfaces.

Accuracy is robustness's enemy.
Robustness is accuracy's enemy.
Good luck!

Remerciements

Cette thèse a débuté en décembre 2004, un mois après avoir émis le souhait de me lancer dans ce projet. Cette réactivité exceptionnelle, compte tenu des aspects administratifs liés a mon statut de salarié, témoigne du soutien que Benoît Desjardins m'a apporté et de l'ouverture d'esprit de ma hiérarchie au CEA, que je tiens à remercier pour cette liberté qu'elle m'a offerte. Ce soutien et cette confiance de la part de Benoît ont été constants, agrémentés de ses remarques pertinentes instantannées, de sa bonne humeur légendaire et même d'un saucisson ramené de Corse, ce qui en fait haut la main le meilleur chef que j'ai connu !
C'est le laboratoire CMLA de l'ENS de Cachan qui m'a accueilli pour réaliser cette thèse. J'y ai rencontré des chercheurs passionnés et des personnalités d'une très grande richesse. En particulier, Jean-Michel Ghidaglia, qui a suivi ce travail constamment, m'a prodigué ses conseils conjuguant rigueur et décontraction.
A tous les deux, je veux exprimer ma reconnaissance, mon respect et mon amitié.
Je tiens également à remercier Patrick Le Tallec et François Alouges qui ont accepté de rapporter cette thèse, Bruno Després, Jean Ovadia et David Youngs qui ont accepté de faire parti du jury, ainsi que tous pour leurs conseils et remarques à propos de ce travail.
Merci à mes collègues au CEA, pour leur soutien et leur patience à mon égard, tout particulièrement à Renaud Motte et Eric Van Renthergem pour leur bienveillance et leur relecture attentive de ce rapport.

A titre personnel, un immense merci á ma famille pour son affection et son soutien inconditionnel.
Merci à Marie d'aimer aussi les ours !
Merci enfin, pour tout ce qu'ils m'ont apporté et pour leur fidélité depuis toutes ces années, à mes amis d'Alsace et mes amis de Bordeaux.
Cette thèse leur est dédiée.

Table des matières

Chapitre 1

Introduction

Ce mémoire traite de la simulation numérique des écoulements compressibles multi-matériaux. Par écoulements, l'on entend que la physique concernée est l'évolution des gaz, des liquides, voire des matériaux solides lorsque les contraintes y sont telles que l'on peut les considérer comme des fluides [89]. De façon générique, chacun de ces milieux sera appelé matériau. Du point de vue de la simulation numérique, un matériau est principalement défini par son équation d'état, c'est-à-dire la loi qui relie ses quantités thermodynamiques (densité, énergie interne, pression). Selon ce critère, les phases d'un même fluide pourront selon le cas être considérées comme des matériaux différents : l'eau en phase gazeuse ou en phase liquide sont considérées comme des matériaux différents, car d'équations d'état ou de caractéristiques physiques différentes. Par multi-matériaux, l'on entend que le système physique étudié contient deux ou plusieurs matériaux distincts. Dans le cas ou les matériaux sont différentes phases du même fluide, on parle aussi d'écoulements multi-phasiques. Chacun des matériaux est décrit par les équations d'Euler, mais en prenant en compte l'interaction entre eux aux interfaces. Cependant, ces interactions peuvent être de nature extrêmement différentes. Considérons par exemple de l'eau dans un verre. En soufflant dans le verre, l'air se met en mouvement et la surface de l'eau se ride sous l'effet du mouvement de l'air pendant quelques secondes. A l'oeil nu, on ne distingue pas de mélange entre l'air et l'eau, mais une interface nette entre l'air et l'eau qui évolue au cours du temps. Si le verre d'eau est laissé à l'air libre, l'eau aura vraisemblablement disparue au bout de quelques jours par évaporation. L'interface entre l'eau et l'air n'est donc pas une frontière absolue. Si du lait est versé dans de l'eau, l'interface entre les fluides ne pourra pas

être distinguée, car ils se mélangeront jusqu'à former un mélange homogène dans tout le verre. En revanche, de l'huile versée dans de l'eau donnera lieu à une interface nette entre les deux fluides et l'écoulement se stabilisera sous l'effet de la tension de surface et de la différence de densité entre l'eau et l'huile, jusqu'à ce que toute l'huile flotte au dessus de l'eau, créant ainsi une interface horizontale. L'interaction entre les matériaux dépend donc des caractéristiques intrinsèques de chacun des matériaux (loi de comportement, compressibilité), du type d'écoulement (laminaire, turbulent, élasto plastique, phase dispersée, etc.), des caractéristiques physiques de l'interaction entre les matériaux (miscibilité, pression de vapeur saturante, tension de surface, interaction électrostatique, friction, etc.). Ce sont les échelles de temps et d'espace dans la simulation qui permettront de juger de la fidélité de la restitution de la physique traitée. Les modèles physiques et les méthodes numériques disponibles pour traiter ces différentes natures d'écoulement sont de ce fait très nombreux.

1.1 Modèles physiques

1.1.1 Diffusion des matériaux

Dans le cas de fluides miscibles, la diffusion d'une interface peut être due à l'agitation moléculaire, qui peut être traitée par un opérateur de diffusion. Dans d'autres situations, l'interface peut être soumise à des instabilités hydrodynamiques. Citons les plus connues [49] :

- l'instabilité de Kelvin-Helmholtz qui intervient dans les écoulements de cisaillement, lorsque les vitesses tangentielles à l'interface sont différentes dans chacun des matériaux. Par exemple, des vagues créées par le vent à la surface d'un étang.
- l'instabilité de Rayleigh-Taylor qui intervient lorsqu'une accélération, la gravité par exemple, existe dans un écoulement de matériaux dont les densités sont différentes. Cette instabilité se développe si le gradient de densité à l'interface est dans le sens inverse de l'accélération. Dans le cas contraire, la force de flottabilité, i.e. la poussé d'Archimède, stabilise l'écoulement. Ainsi, par exemple de l'air au dessus de l'eau dans le champ de gravité terrestre, dirigé vers le bas, est un système stable, alors que de l'eau au dessus de l'air est un système instable.
- l'instabilité de Richtmyer-Meshkov, qui est un cas limite d'instabi-

lité de Rayleigh-Taylor avec une accélération impulsionnelle, intervient lorsqu'une onde de choc traverse une interface entre deux matériaux d'impédances acoustiques [1] différentes. L'instabilité se développe quel que soit le sens de propagation du choc par rapport aux matériaux. Les gouttes projetées vers le haut à la surface de l'eau dans un seau tombant au sol relèvent d'un type d'instabilité de Richtmyer-Meshkov.

Chacune de ces instabilités est un processus qui tend à mélanger les matériaux et qui peut mener à un écoulement turbulent. Différentes stratégies existent pour les simuler. Une première, très coûteuse en puissance de calcul et en général inabordable, est la simulation numérique directe (DNS : Direct Numerical Simulation) qui vise à calculer les instabilités jusqu'à la plus petite échelle de l'écoulement. Cette stratégie est cependant employée à des fins de validation de modèles moyennés [30]. En effet, la stratégie la plus courante, appelée RANS (Reynolds Averaged Navier Stokes) pour traiter ces écoulements instables consiste à réécrire les équations de Navier-Stokes en considérant les variables physiques comme la somme de quantités moyennes et de perturbations de ces quantités qui rend compte des petites échelles. La difficulté est de trouver des relations de fermeture au nouveau système portant sur les grandeurs moyennes et les corrélations des parties fluctuantes, pour simuler l'écoulement de façon suffisamment réaliste. Dans les modèles de type LES (Large Eddy Simulation), une échelle de coupure est introduite dans la simulation de l'écoulement, en dessous de laquelle le mélange des matériaux par les petits tourbillons est modélisé par de la diffusion turbulente. Cette échelle de coupure est comprise entre l'échelle de Kolmogorov et l'échelle intégrale de turbulence, respectivement la taille des plus petits tourbillons qui contiennent de l'énergie et la taille des plus grands tourbillons. Le coefficient de diffusion est calculé en fonction de l'écoulement moyen, par exemple le modèle de *Smagorinsky* [74], ou par des équations supplémentaires. Citons les modèles $k-l$ [29] ou $k-\varepsilon$ [49],[40],[84]. Il existe aussi des stratégies de type ILES (Implicit LES) [42] ou MILES (Monotonic Implicit LES) [30], [88], dans lesquelles la diffusion numérique du schéma est utilisée ou éventuellement modifiée par des termes supplémentaires dans les équations résolues, de sorte que celle-ci est calibrée pour simuler la diffusion turbulente. Il existe évidemment des modèles de mélange turbulent bien plus sophistiqués, par exemple le modèle développé par *D. L. Youngs* [87] ou celui de *Llor et al* [54]. Ces derniers modèles visent à capturer l'évolution

[1] l'impédance acoustique est ρc^2, ρ la densité, c la vitesse du son.

du mélange turbulent des fluides sous l'effet des intabilités hydrodynamiques citées précédemment, en cherchant à capturer l'évolution de la longueur caractéristique de mélange, un taux de mélange moléculaire dans le mélange et une taille caractéristique des tourbillons par rapport à celle de la zone de mélange [2]. Le système est décrit par des structures hydrodynamiques auxquelles on associe un champ de vitesse et un modèle de turbulence $k - \varepsilon$ propre pour le modèle *2SFK*. Une caractéristique importante de ces modèles est qu'ils autorisent le démélange des fluides, lorsque la force de flottabilitté est présente.

1.1.2 Phases dispersées

Lorsqu'un des matériaux ne peut pas être considéré comme un milieu continu, dans le cas de phases dispersées (particules ou gouttelettes) au sein d'un fluide continu, l'interface entre les matériaux ne peut pas être calculée pour décrire l'évolution du système [68].

Une stratégie est de traiter la phase dispersée par des modèles de type Boltzmann, sous forme d'équations cinétiques, qui prennent en compte les interactions entre les particules (choc, fragmentation, coalescence, etc.). La phase continue est traitée par un modèle de type eulérien [9], [57]. Le couplage entre les phases est modélisé suivant la complexité de la physique traitée par des échanges de quantité de mouvement, d'énergie, prise en compte de la turbulence induite par les particules, etc. Cependant, à des fins de validation de ces modèles, l'approche simulation numérique directe DNS peut là aussi être utilisée sur de petits échantillons de particules ou des interactions unitaires.

1.1.3 Interfaces

Les écoulements multi-matériaux dont l'interface doit être suivie précisément ou reconstruite sont nombreux. Le critère en est en général le temps de diffusion très grand, ou infini dans le cas de fluides non-miscibles, par rapport à la durée du phénomène à simuler. Cette situation est très courante, notamment lorsque les matériaux présents dans le système ne sont pas dans la même phase, par exemple liquide et gaz [48]. Par ailleurs, dans le cas de phénomènes instationnaires rapides, la diffusion des matériaux peut simplement être négligeable à l'échelle spatiale envisagée. Outre l'aspect to-

[2] nombre de Von Karmann

pologique de la reconstruction d'interface, ce traitement numérique permet également l'introduction de modèles de couplage plus complexes entre les matériaux. Par exemple, le suivi de fronts réactifs ou encore le changement de phase, où l'interface est localement le siège d'une transition d'une phase à une autre. Dans les écoulements impliquant des matériaux élasto-plastiques ou soumis à une tension de surface, la reconstruction d'interface permet le calcul des contraintes entre les matériaux, [53] et de gérer des phénomènes d'endommagement et de recompaction. Enfin, les caractéristiques du contact entre les matériaux peuvent être de natures différentes : adhérence, mais aussi glissement parfait ou friction. Dans ce dernier cas, seul un traitement explicite local à l'interface peut restituer ces conditions.

1.2 Méthodes numériques

Nous allons maintenant aborder la question de la résolution numérique de ces modèles physiques. Les principales méthodes se divisent en deux catégories : soit de type Lagrange où les équations d'évolution sont écrites dans le référentiel du fluide, soit de type Euler où les équations sont écrites dans un référentiel extérieur au fluide. Les variables peuvent être discrétisées aux mailles, aux noeuds ou aux faces des mailles, selon la méthode. On peut également citer les méthodes de type spectral [19], particulaire [16], [23] ou SPH [80] (Smoothed Particle Hydrodynamics), que nous n'aborderons pas ici, car trop peu liées à la méthode développée dans ce mémoire.

1.2.1 Méthodes lagrangiennes

Les méthodes lagrangiennes sont très naturelles pour capturer l'interface et traiter le contact entre les matériaux. Le volume Ω_m occupé par un matériaux m est discrétisé en un maillage dont les noeuds sur sa frontière $\partial\Omega_m$ constituent l'interface. Un noeud du maillage est déplacé à la vitesse matérielle calculée par le schéma lagrangien. Le mouvement des noeuds aux frontières des matériaux définit naturellement le mouvement des interfaces. Chaque matériau peut être considéré comme un bloc indépendant interagissant avec les autres via sa frontière. Ce point de vue est très pratique pour la prise en compte de modèles de contact entre les matériaux. Les schémas lagrangiens sont conservatifs par bloc, et par conséquent pour chaque matériau. Les quantités de mouvement et énergies totales ne sont pas toujours stricte-

ment conservées du fait, dans la plupart des méthodes actuelles, du décalage de la discrétisation des vitesses (aux noeuds ou aux faces) par rapport aux densités, énergies interne et pression (au centre des mailles). Un schéma de référence est aujourd'hui encore celui de *Wilkins* [83], malgré des défauts bien identifiés, tels que la dépendance des résultats aux coefficients de pseudo viscosité et au filtrage des modes parasites (antidérive). Cependant, des travaux ont été menés pour accroître la consistance de ces schémas par rapport aux variables lagrangiennes [56], [2], [3], ainsi que le traitement de l'aspect faiblement hyperbolique des équations d'Euler en variables lagrangiennes, voir *Després-Mazeran* [26].
Les coordonnées lagrangiennes (X, Y) d'un point P évoluant dans l'écoulement sont fonctions de sa position (x, y) à $t = 0$. Les fonctions $X(x, y, t)$ et $Y(x, y, t)$ sont alors solutions des équations des trajectoires :

$$\begin{cases} X(x,y,0) = x, \\ Y(x,y,0) = y, \\ \\ \dfrac{\partial X}{\partial t} = u(X,Y,t), \\ \\ \dfrac{\partial Y}{\partial t} = v(X,Y,t), \end{cases} \tag{1.1}$$

avec (u, v) les coordonnées du vecteur vitesse V dans le référentiel de l'écoulement.
Les équations d'Euler sous forme lagrangienne s'écrivent alors :

$$\begin{cases} \rho \dfrac{\partial}{\partial t}\left(\dfrac{1}{\rho}\right) - \nabla_X \cdot (V) = 0, \\ \rho \dfrac{\partial V}{\partial t} + \nabla_X (P) = 0, \\ \rho \dfrac{\partial E}{\partial t} + \nabla_X \cdot (PV) = 0, \end{cases} \tag{1.2}$$

avec ρ la densité, V le vecteur vitesse, P la pression, E l'énergie totale spécifique.
Les méthodes lagrangiennes utilisant une discrétisation de type Galerkine-Discontinu [2] sont très précises pour capturer les discontinuités de contact et donc les interfaces entre les matériaux. Cependant, les méthodes lagrangiennes sont malheureusement limitées aux écoulements faiblement rotationnels, puisque les noeuds suivent l'écoulement et que les volumes des mailles

doivent rester positifs, i.e. que les mailles ne se croisent pas. La méthode ALE (Arbitrary Lagrangian Eulerian) [12], [55] permet d'étendre les méthodes lagrangiennes à des écoulements plus complexes, mais au prix de remaillages lorsque le maillage contient des mailles trop déformées (projection des grandeurs de l'écoulement sur un maillage régularisé) selon des critères de qualité du maillage [45] [4],[11]. La question de la reconstruction des interfaces entre les matériaux se pose alors comme pour les méthodes eulériennes si l'on ne se restreint pas à un remaillage par matériau. Une reconstruction des interfaces par des segments de droites dans des mailles mixtes peut se révéler très complexe sur les maillages non structurés qui sont souvent utilisés dans les méthodes lagrangiennes. Pour les écoulements très complexes, cette méthode dégénère globalement en un schéma eulérien, de type Lagrange-Projection, que nous aborderons dans la section concernant les méthodes eulériennes. Par ailleurs, il existe également des méthodes extrêmement complexes combinant des méthodes ALE à des méthodes de raffinement de maillage AMR par bloc (Adaptive Mesh Refinement), développées par exemple par *Koniges et al* [47] [76].

1.2.2 Méthodes eulériennes

Les méthodes eulériennes sont bien adaptées aux écoulements très complexes et notamment ceux sujets à des instabilités hydrodynamiques créant des tourbillons. En effet, le maillage étant fixé, il n'existe pas de contrainte géométrique pour capturer la complexité de l'écoulement. Différentes méthodes de discrétisation des équations d'Euler en variables eulériennes existent. Les trois grandes catégories sont :

- les différences finies (DF) : la discrétisation des équations consiste à approcher les différentes dérivées par un développement limité [5]. Ces schémas peuvent être très efficaces en terme de temps de calcul et d'ordre de précision [73]. Cependant, il peut s'avérer délicat de traiter des modèles physiques et des géométries complexes.

- les éléments finis (EF) : il s'agit de projeter la solution du problème continu sur un espace de fonctions de base dont le support est contenu dans les mailles voisines de chaque noeud du maillage. Les coefficients associés à chaque fonction de base doivent être calculés, ce qui détermine la solution. Pour ce faire, on écrit les équations sous une forme variation-

nelle, ce qui conduit à un système linéaire à résoudre pour déterminer ces coefficients. L'ordre de la méthode dépend de la complexité des fonctions de base que l'on choisit, qui peuvent être théoriquement des polynômes d'ordre aussi élevés que l'on souhaite. Ces méthodes sont bien maitrisées mathématiquement [38], [61], [90], [17], [7], [65] et capturent bien les discontinuités dans les écoulements. De plus, des extensions de cette approche aux écoulements multi-matériaux existent, voir *Glowinski et al* [37].

- les volumes finis (VF) : Chaque maille est un volume de contrôle Ω au sens physique, dont la surface fermée $\partial\Omega$ constituant sa frontière est parcourue par des flux d'échange avec les autres mailles. L'approche VF consiste à considérer que l'ensemble du fluide contenu dans la maille Ω est dans le même état (de pression, de densité, etc.) et d'intégrer le système d'équations sur cette maille. Cette intégration fera apparaître des flux sur la surface $\partial\Omega$ qui seront discrétisés pour obtenir un schéma numérique. Ces flux sont souvent calculés à l'aide d'un problème de Riemann sur la face de la maille [78]. Les plus célèbres sont, chronologiquement, ceux de *Godunov* [39], de *Van Leer* [79], de *Roe* [67] ou *Osher-Solomon* [59]. Nous reviendrons sur cette approche dans le corps du mémoire, car c'est le type de schéma que nous avons choisi : c'est le schéma VFFC de *Ghidaglia et al* [34] qui va être utilisé dans le cadre de ce mémoire.
  Dans les méthodes de type Volumes Finis, le traitement numérique des équations est très proche de la physique traitée et extensible à des modèles complexes. En effet, comme nous le verrons dans les prochains chapitres, la méthode numérique développée dans ce mémoire met en jeu un calcul explicite des flux des variables entre les mailles ainsi qu'au travers des interfaces entre les matériaux. Ce point de vue est très appréciable pour la résolution de systèmes de loi de conservation. Une introduction á ces schémas se trouve dans [32] et [10].

1.2.3 Le schéma Lagrange-Projection

Le schéma Lagrange-Projection multi-matériaux, introduit par *Noh-Woodward* [58], *Woodward-Collela* [21] [22], *Youngs* [85], appartient à la famille des méthodes eulériennes. Cette approche peut cependant être assimilée à une méthode de type ALE. En effet, ce schéma utilise deux étapes : une étape

lagrangienne pendant laquelle les noeuds du maillage sont déplacés, puis une étape de projection où les grandeurs calculées sur le maillage déformé sont projetées sur le maillage eulérien. Les vitesses sont discrétisées sur un maillage décalé (aux noeuds ou aux faces) par rapport aux autres variables (densité, énergie, pression) qui sont discrétisées au centre des mailles. Ce schéma permet de simuler des écoulements multi-matériaux avec reconstruction des interfaces par des segments de droites dans les mailles mixtes. La position de l'interface est déterminée dans une maille mixte en fonction des fractions volumiques dans les mailles voisines. Cette reconstruction des interfaces permet alors de calculer la proportion de chacun des matériaux présents dans le volume de fluide qui change de maille lors de la phase de projection. Ce schéma a pour avantage d'être précis pour le suivi des interfaces et permet de traiter des modèles plus complexes [25]. Cependant, cette méthode est relativement diffusive et la reconstruction d'interfaces n'autorise pas le glissement entre les matériaux, car les vitesses sont communes à tous les matériaux présents dans une maille mixte, du fait de leur discrétisation sur un maillage décalé.

1.3 Méthodes multi-matériaux

Comme pour les schémas numériques, la stratégie à adopter pour traiter les écoulements multi-matériaux dépend principalement du modèle physique que l'on considère. Dans certaines applications, seule la géométrie des matériaux a de l'intérêt, alors que dans d'autres, le traitement de la physique à l'interface est fondamental pour la précision globale de la simulation.

1.3.1 Interfaces diffuses

Il s'agit de capturer l'évolution des matériaux via une variable, par exemple la fraction volumique α_m pour le matériau m, dont l'équation s'ajoute au système à résoudre. Cet approche a été étudiée par exemple par *Anderson et al* [6] pour le traitement de différentes physiques et par *Serrin et al* [71] où la cohérence mécanique et thermodynamique du modèle est étudiée. Dans le cas des équations d'Euler, il s'agit d'une équation d'advection de cette variable du type $\partial_t(\alpha_m\rho) + \nabla \cdot (\alpha_m\rho u) = 0$. Cette méthode ne permet pas de capturer précisément la position de l'interface, car cette variable est soumise à la diffusion numérique du schéma employé. Une approxima-

tion peut cependant en être faite en considérant par exemple que l'interface est confondue avec l'isovaleur $\alpha_m = 0.5$. De plus, la conservativité locale des variables n'est pas assurée et cette technique nécessite de construire une équation d'état de mélange des matériaux pour écrire le schéma dans les mailles où $0 < \alpha_m < 1$, ce qui peut se révéler délicat pour des matériaux de natures très différentes. Cependant, cette stratégie est bien adaptée pour capturer l'évolution du mélange entre deux gaz par exemple, car la diffusion numérique entre eux peut être assimilée à de la diffusion moléculaire ou turbulente. C'est la stratégie développée dans les méthodes de type ILES (Implicit LES) que nous évoquions dans la section Modèles Physiques 1.1. La précision du calcul de la position de l'interface peut être améliorée en utilisant des schémas de très grande précision spatiale, cf. *Després et Lagoutière* [27] ou des maillages très raffinés à l'aide de méthode d'adaptation de maillage AMR (Adaptative Mesh Refinement) par exemple. Cependant, ces améliorations ne permettent pas de s'affranchir d'un modèle de mélange des fluides dans les mailles où $0 < \alpha_m < 1$.

1.3.2 Méthodes Level Set

Ces méthodes, introduites par *Osher et Sethian* [77], [72] sont élaborées avec une stratégie de départ assez proche de la méthode VOF (Volume Of Fluid). Il s'agit ici d'advecter à la vitesse des matériaux v_m une fonction distance ϕ, dont l'isovaleur 0 représente l'interface, par une équation du type $\partial_t \phi + v_m \cdot \nabla \phi = 0$. Un matériau sera repéré par la région de l'espace où la fonction est positive, l'autre matériau par la région où la fonction est négative. Les mailles où la fonction s'annule sont considérées mixtes, c'est-à-dire contenant plusieurs matériaux. Ce procédé permet de reconstruire une interface d'épaisseur nulle, mais basée sur la fonction distance ϕ qui est soumise, ainsi que les variables du système, à la diffusion numérique entre les matériaux. La précision de la méthode peut être améliorée en utilisant des algorithmes basés sur les équations d'Hamilton-Jacobi [60] qui permettent de raidir les fronts de la fonction distance ϕ et donc de positionner l'interface plus précisément. Cette méthode n'est pas conservative, mais il existe des corrections adaptées [75], [50]. De plus, l'écriture du schéma numérique à partir de valeurs moyennes entre les matériaux dans les mailles mixtes peut provoquer des oscillations ou des instabilités numériques qui nécessitent des traitements spécifiques [1], [46].

1.3.3 Méthodes Front Tracking

Il s'agit ici de suivre explicitement l'interface entre les fluides. Cette méthode consiste à suivre le mouvement de particules lagrangiennes situées sur l'interface [24],[36]. La vitesse de l'interface est calculée en déterminant la vitesse de la discontinuité de contact via la résolution d'un problème de Riemann. Elles sont très efficaces pour la simulation d'instabilités hydrodynamiques, par exemple dans le cas des équations d'Euler incompressible avec tension de surface [43]. Ces méthodes ne sont pas intrinsèquement conservatives, mais des extensions conservatives en masse existent, [20].

1.3.4 Méthodes de reconstruction d'interfaces

Ces méthodes font partie de la famille des méthodes VOF (Volume Of Fluid). Les bases de ces méthodes peuvent être trouvées dans les publications de *Noh-Woodward* [58], de *Youngs* [85], de *Zaleski et al* [62], [48], ou encore de *Puckett, Rider et al* [63]. Les matériaux sont repérés par le volume qu'ils occupent dans chaque maille. Une maille est dite mixte, i.e. contenant plus d'un matériau, ou pure si elle ne contient qu'un seul matériau. Il s'agit de reconstruire et de faire évoluer les interfaces dans les écoulements multi-matériaux en les discrétisant par des segments de droite en $2D$, des plans en $3D$, qui séparent les matériaux. Dans une maille mixte, les matériaux sont purs de part et d'autre de l'interface et possèdent chacun leurs propres densité, énergie interne et pression. Ces méthodes sont toutes conservatives en masse, car elles sont construites de sorte qu'il n'y ait aucun échange de masse au travers des interfaces. Certains auteurs envisagent de reconstruire les interfaces à l'aide de courbes plus complexes ou de faire évoluer des objets mathématiques permettant de reconstruire les interfaces de manière plus efficace, par exemple la méthode MOF de *Shashkov et al* [31], mais l'intégration dans un code d'hydrodynamique de ces traitements peut s'avérer délicate. Les méthodes de reconstruction d'interfaces sont efficaces pour les écoulements dans lesquels les matériaux ont des densités ou des caractéristiques physiques très différentes. En effet, ces méthodes ne nécessitent pas de calculer une équation d'état de mélange, ce qui représente un avantage important pour traiter des écoulements de matériaux aussi différents en terme de masse et de compressibilité que l'eau et l'air par exemple.

1.4 Hypothèses physiques dans ce mémoire

Le cadre physique adopté dans tout le mémoire est le suivant : les écoulements multi-matériaux sont supposés compressibles, laminaires, instationnaires et soumis à de grandes déformations. Le modèle de fluide que nous considérons est celui des équations d'Euler en régime compressible, car le nombre de Reynolds est ici supposé assez grand pour que la viscosité moléculaire puisse être négligée. Les matériaux sont supposés être non miscibles et séparés par une interface d'épaisseur nulle, avec un glissement parfait des matériaux les uns par rapport aux autres. Chaque matériau est pur et caractérisé par sa propre équation d'état. Par exemple, ce contexte est bien adapté à la simulation de l'interaction d'une onde de choc se propageant dans l'air avec une goutte d'eau, comme le système décrit par *Takayama et al* dans [46].
Les équations d'Euler compressible en dimension d'espace d peuvent être écrites sous forme conservative comme suit :

$$\begin{cases} \partial_t \rho + \operatorname{div}(\rho u) = 0, \\ \partial_t(\rho u) + \operatorname{div}(\rho u \otimes u) + \nabla p = 0, \\ \partial_t(\rho E) + \operatorname{div}((\rho E + p)u) = 0, \end{cases} \tag{1.3}$$

avec ρ la densité, $u \in \mathbb{R}^d$ le champ de vitesse, e l'énergie interne spécifique, p la pression, et $E = e + |u|^2/2$ l'énergie totale spécifique. Une équation d'état de la forme $EOS(\rho, e, p) = 0$ est donnée par hypothèse pour clore ce système.
De plus, ce système d'équations peut s'écrire sous une forme conservative générique et posant $V = (\rho, \rho u, \rho E)^t$ le vecteur des variables conservatives et F la matrice des flux de ces variables définie comme suit :

$$\begin{array}{rccc} F: & \mathbb{R}^{d+2} & \longrightarrow & \mathbb{R}^{d+2} \times \mathbb{R}^d \\ & V & \longmapsto & F(V). \end{array}$$

Pour tout vecteur unitaire $n \in \mathbb{R}^d$, $F(V) \cdot n$ est défini en fonction de V par :

$$F(V) \cdot n = (\rho(u \cdot n), \rho u(u \cdot n) + pn, (\rho E + p)(u \cdot n))^t. \tag{1.4}$$

Les équations d'Euler sous forme conservative (1.3) peuvent donc être réécrites sous une forme conservative générique :

$$\partial_t V + \operatorname{div} F(V) = 0. \tag{1.5}$$

Les équations d'Euler ne prennent pas en compte la dissipation d'énergie qui intervient dans quasiment tous les systèmes physiques. Elle intervient par frottement dans les écoulements de fluides dû à la viscosité, par conduction thermique, ou par de quelconques processus irréversibles. Les équations d'Euler décrivent un système adiabatique en l'absence de chocs dans l'écoulement, donc sans dissipation. Cependant, les erreurs de discrétisation du schéma qui les résout doivent tendre à faire augmenter l'entropie physique, comme le feraient des processus de dissipation dans les systèmes réels, voir la conférence de *Balian* [8]. Dans le cas où des ondes de choc sont présentes dans l'écoulement, le schéma doit être suffisamment dissipatif pour rendre compte de la dissipation physique d'entropie intervenant dans ce phénomène.
Par conséquent, en accord avec le Second Principe de la Thermodynamique, le comportement des solutions des équations d'Euler est soumis à l'inégalité suivante [44] :

$$\partial_t(\rho s) + \mathrm{div}\,(\rho u s) \geq 0, \tag{1.6}$$

avec s l'entropie physique spécifique.

1.5 Introduction à la méthode VFFC-NIP

La méthode de reconstruction d'interfaces originale, nommée *NIP* (Natural Interface Positioning), a été développée par *J.-P. Braeunig, B. Desjardins et J.-M. Ghidaglia* lors de ce projet de thèse et est une extension aux écoulements multi-matériaux du schéma volume fini VFFC (Volume Fini à Flux Caractéristiques) introduit par *Ghidaglia et al* [34]. C'est un schéma eulérien direct, c'est-à-dire que toutes les directions de l'espace et tous les termes des équations d'Euler sont traités en une seule étape. Toutes les variables eulériennes $(\rho, \rho u, \rho E)$ sont centrées aux mailles. L'interface entre les matériaux dans une maille mixte est représentée par une ligne en $2D$ et un plan en $3D$, sachant que s'il existe plusieurs fragments d'un même matériau dans une maille, ils seront agglomérés et représentés par un seul volume dans la maille. Nous définissons :

- une maille pure mp, comme une maille ne contenant qu'un seul matériau m auquel on associe un vecteur des variables $(\rho_m, \rho_m u_m, \rho_m E_m)$ centré dans le volume de la maille Vol_{mp},

- une maille mixte mm, comme une maille contenant nm matériaux distincts. A chaque matériau k on associe un vecteur des variables $V_k = (\rho_k, \rho_k u_k, \rho_k E_k)^t$ centré dans le volume partiel Vol_k qu'il occupe dans la maille. L'ensemble des matériaux k occupe l'ensemble du volume Vol_C de la maille de sorte que :

$$\sum_{k=1}^{nm} Vol_k = Vol_C.$$

  De plus, à chaque matériau k est associé une pression p_k via une équation d'état $EOS_k(\rho_k, e_k, p_k) = 0$.

L'idée principale est de faire évoluer les interfaces en utilisant une décomposition directionnelle robuste dans les mailles mixtes, sans perdre la précision du schéma dans les mailles à l'intérieur des matériaux. Cette stratégie nous contraint à ne considérer que des maillages structurés orthogonaux. Les informations *2D/3D* dans les volumes partiels sont utilisées dans chaque étape de la décomposition directionnelle, dans le but d'assurer le glissement parfait des matériaux les uns par rapport aux autres. Ceci est réalisé en imposant une vitesse normale à l'interface égale de part et d'autre de l'interface pour qu'il n'y ait pas d'interpénétration des matériaux, mais en n'imposant aucune contrainte sur la vitesse tangentielle. De plus, le gradient de pression est imposé normal à l'interface.
La méthode est localement conservative pour chacune des variables eulériennes $(\rho, \rho u, \rho E)$, car l'évolution des volumes partiels dans les mailles mixtes est calculée par un schéma conservatif au même titre que pour les mailles pures. Considérons l'équation de conservation suivante :

$$\partial_t v + \partial_x f = 0.$$

Un schéma est dit localement conservatif si il peut s'écrire sous une *forme conservative*, c'est-à-dire en $1D$:

$$\frac{v_i^{n+1} - v_i^n}{dt} + \frac{f_{i,i+1}^{n,n+1} - f_{i-1,i}^{n,n+1}}{dx} = 0.$$

avec $dt = t^{n+1} - t^n$ le pas de temps, dx le pas d'espace, v_i^n la valeur de la variable v dans la maille i au temps t^n, $f_{i,i+1}^{n,n+1}$ le flux de la variable v de la maille i vers la maille $i+1$ entre t^n et t^{n+1}.
La forme conservative des équations que nous allons effectivement résoudre

dans la méthode est fondamentale, non seulement pour le respect de la conservation des variables au niveau discret, mais aussi pour bien capturer les solutions faibles du système d'équations aux dérivées partielles lorsque des discontinuités se propagent dans l'écoulement. Il s'agit en particulier d'assurer que ces ondes se propagent à la bonne vitesse, ce qui ne peut pas être assuré par un schéma non conservatif, cf *LeVeque* [51] et une mise en évidence concrète du problème dans [18]. Pour écrire l'équation d'évolution des grandeurs dans les volumes partiels, nous avons introduit un objet que nous avons nommé "Condensat" qui est constitué d'une agglomération de mailles mixtes consécutives et que l'on peut considérer comme un masque lagrangien sur le maillage eulérien au voisinage des interfaces. Des définitions plus précises seront données dans le corps du mémoire.

1.6 Plan du mémoire

Tout d'abord, dans le chapitre 2 nous allons présenter succintement le schéma VFFC monofluide qui sous-tend la méthode. Puis nous décrirons la méthode de reconstruction d'interface en une dimension d'espace ainsi qu'un résultat concernant la croissance de l'entropie dans ce que nous appellerons un condensat. Puis l'extension au cas multi-dimensionnel sera présentée algorithmiquement. Des limitations sur les variations des inconnues du système sont établies, dûes au non respect de la condition CFL dans les mailles mixtes. Le caractère entropique de la méthode en dimension supérieure à un est discuté. Puis, quelques cas-tests sont exposés, montrant la capacité de la méthode à traiter les écoulements violents, c'est-à-dire des écoulements où sont présents de forts gradients, des nombres de Mach élevés ou encore des différences de densité ou de compressibilité importantes entre les matériaux. Dans le chapitre 3, un système constitué d'une masse d'eau s'écrasant sur le sol est simulé en faisant varier la vitesse de chute initiale.

Chapitre 2

Présentation de la méthode VFFC-NIP

A pure Eulerian scheme for multi-material fluid flows

J.-P. Braeunig [1], B. Desjardins [2], J.-M. Ghidaglia [3]

Abstract

The purpose of this note is to present a new numerical scheme for multi-material fluid flow in dimension $d \geq 1$. It is a pure Eulerian conservative scheme that allows to compute sharp interfaces between non miscible fluids. The underlying flux scheme in single material cells is the so called FVCF scheme, whereas interface reconstruction and directional splitting is used in multi-material cells. One of the novelty of our approach is the introduction of the concept of "condensate" which allows to handle mixed cells containing two or more materials.

[1]CEA/DIF Bruyères-le-Châtel, 91297 Arpajon Cedex, France
[2]MOMA, 10 rue Lincoln, 75008 Paris, France
[3]CMLA ENS Cachan, 61 av. du président Wilson, 94235 Cachan cedex, France

2.1 Introduction

The numerical simulation of fluid material interfaces encompasses a wide range of numerical methods, depending on the various physical situations, in particular the relevant space and time scales involved. A diffuse interface, with mixing of materials at the molecular scale, can be treated for instance with diffusion. If the mixing is driven by hydrodynamic instabilities in the fully turbulent regime, then it may be treated with turbulence models in a statistical approach. In the case where the diffusion scale between materials can be neglected with respect to macroscopic hydrodynamic structures, then the interface motion may be represented with sharp interfaces. In this case, contact properties between materials may be modelled by exact sliding, no slip condition, or friction.

The physical assumptions of this work are the following : the multi-material fluid flow is assumed to be compressible, laminar, subject to large and transient deformations. The fluid model addressed here is the compressible Euler equations, because the Reynolds number is assumed to be so high that molecular viscosity inside materials is neglected : materials are considered as immiscible and separated by a sharp interface, with perfect sliding of one material on each others. Each material is pure and characterized by its own equation of state. For instance, this set of assumptions is well adapted to simulate the interaction between a shock wave propagating in the air and a water droplet, as described in *Takayama* [46].

The compressible Euler equations in dimension of space d can be written in a conservative form as follows :

$$\begin{cases} \partial_t \rho + \operatorname{div}(\rho u) = 0, \\ \partial_t(\rho u) + \operatorname{div}(\rho u \otimes u) + \nabla p = 0, \\ \partial_t(\rho E) + \operatorname{div}((\rho E + p)u) = 0, \end{cases} \tag{2.1}$$

where ρ denotes the density, $u \in \mathbb{R}^d$ the velocity field, e the specific internal energy, p the pressure, and $E = e + |u|^2/2$ the specific total energy. An equation of state of the form $EOS(\rho, e, p) = 0$ is provided in order to close the system.

This system does not take into account energy dissipation that occurs in nearly all physical systems. This is happening in viscous flows or any dissipation processes with irreversible behavior. Eulerian equations describe an adiabatic system when no shock waves are present in the fluid, but errors of

discretization of the scheme must lead to an increase of entropy, as dissipation processes do in real systems. When a shock wave is present, dissipation of the scheme have to represent the physical dissipation of entropy occurring in this discontinuity. Therefore, according to the second principle of thermodynamics, Euler equations are supplemented with an entropy inequality :

$$\partial_t(\rho s) + \operatorname{div}(\rho u s) \geq 0, \tag{2.2}$$

with s the specific entropy.

This system of conservation laws can be written in a generic conservative form : let $V = (\rho, \rho u, \rho E)^t$ be the unknown vector of conservative variables and the flux F be a matrix valued function defined as :

$$\begin{array}{rccc} F: & \mathbb{R}^{d+2} & \longrightarrow & \mathbb{R}^{d+2} \times \mathbb{R}^d \\ & V & \longmapsto & F(V). \end{array}$$

For all direction $n \in \mathbb{R}^d$, $F(V) \cdot n$ is given in terms of V by :

$$F(V) \cdot n = (\rho(u \cdot n), \rho u(u \cdot n) + pn, (\rho E + p)(u \cdot n)). \tag{2.3}$$

The compressible Euler equations (1.3) then can be rewritten as follows :

$$\partial_t V + \operatorname{div} F(V) = 0. \tag{2.4}$$

Multi-material fluid flows computation may be treated with many different numerical strategies. Lagrangian methods are very natural to capture interface motion and contact between different materials. Material volumes are meshed and nodes at the boundary of each material represent the interfaces. The Lagrangian evolution of these nodes naturally defines the interface motion. One can consider each meshed material as one independent block, interacting with the others through their boundaries. Most of Lagrangian schemes preserve mass conservation by block, therefore on each material. Conservation of momentum and total energy are rarely ensured in a strict sense when one use staggered grids for velocity and pressure. Unfortunately, accuracy and robustness of Lagrangian schemes are limited by large mesh distortion.

Eulerian methods can be very accurate on shock or rarefaction waves with high space discretization order. A great variety of schemes for single phase flow computation exists among three main families : finite element methods,

finite differences, and finite volume methods. The finite element method can be very accurate by using high order base functions, but it might be difficult to extend it to complex physics or interface capturing. The formalism of finite volumes methods is close to the mechanical viewpoint, very generic for different types of physical applications. Thus it might be easier to add physical models as surface tension or turbulent diffusion for instance. The discretization order is limited, but this method is very accurate for hydrodynamic shock waves, because of the similarity between numerical treatment and mechanics.

The extension of Eulerian schemes to multi-material fluid flows can be obtained by various techniques. One is to introduce the mass fraction c_α of material α and to let it evolve according to the material velocity. The cell is called a pure cell if a material α satisfies $c_\alpha = 1$ and is called a mixed cell if $c_\alpha \in]0, 1[$. Pure cells filled by material α are calculated in the same manner as for the single phase method. Mixed cells evolution is computed using a mixing equation of state that takes into account material mass fractions. The drawback here is the interface numerical diffusion, which prevents sharp interface capturing. However, it exists very accurate methods that limit this diffusion, see *Després and Lagoutière* [27]. In another type of method, called *Level Set Methods* [77], a signed distance function ϕ is defined instead of mass fractions, advected by the material velocity. The materials position is determined according to the sign of this function. For instance, negative values are associated with material 1, positive values to material 2 and isovalue 0 corresponds to the interface position in the domain. Mixed cells are defined by the set where the function ϕ vanishes. This method gives smooth curves of a sharp interface between materials, dealing with complex or singular geometry. Nevertheless, the interface is sharp, but not the quantities that are averaged in the mixed cells to write scheme fluxes, for instance. Thus variables conservation is not guaranteed without specific corrections and spurious oscillations may appear, [1].

Quantities sharpness and conservation at interfaces may be obtained using a subgrid interface reconstruction. In mixed cells, the interface is approximated by straight lines by most authors, but sometimes by more complex curves separating materials, or more complex theory by *Shashkov et al* [31] for instance. A famous method using sharp interface reconstruction is the Lagrange-Remap Finite Volume scheme, developed by *Noh-Woodward* [58] and improved by *D.L. Youngs* [85], belonging to the family of Volume of Fluid (VOF) methods. The first step is Lagrangian, while mesh nodes are

moving. The second one is a remapping of Lagrangian cells on the original Eulerian mesh, by exchanging volume fluxes between cells corresponding to the Lagrangian motion of cell edges. Interface position in a mixed cell is determined according to partial volumes of the materials and according to the interface normal vector calculated using the volume fractions in neighboring cells. Thus the ratio of each material in volume fluxes is known by geometrical considerations. Some methods with the same kind of operator splitting are used for incompressible multi-material fluid flows as for instance *Zaleski et al* [48]. These methods give sharp interfaces for materials and discontinuous quantities in mixed cells, dealing with large deformations and transient flows. The drawback of these methods is the limited accuracy of the single phase scheme. Moreover, special treatments at material interfaces, such as sliding, are not possible.
The method described in this work, named *NIP* (Natural Interface Positioning), has been developed by *J.-P. Braeunig, B. Desjardins and J.-M. Ghidaglia* and is an extension to multi-material fluid flow of the so called Finite Volume with Characteristic Flux (FVCF) scheme, introduced by *Ghidaglia et al* [34]. This is a cell centered pure Eulerian scheme, in which material interfaces are represented by a discontinuous piecewise linear curve. Let us define pure and mixed cells as follows : a cell C of volume Vol_C may contain nm materials, each of them filling a partial volume Vol_k with

$$\sum_{k=1}^{nm} Vol_k = Vol_C.$$

A centered variable vector $V_k = (\rho_k, \rho_k u_k, \rho_k E_k)^t$ and an equation of state $EOS_k(\rho_k, e_k, p_k) = 0$ are also associated with each material $k \leq nm$. We shall say that the cell C is a *pure cell* if $nm = 1$, and a *mixed cell* otherwise.

The main idea is to let interfaces evolve through a directional splitting scheme, without loosing the accuracy of the pure Eulerian scheme in bulk materials. Of course, this scheme is restricted to structured cartesian meshes. The interface capturing method NIP uses *2D/3D* informations of partial volumes for each direction, imposing materials sliding on each others. The method preserves local conservation of each component of the variable vector $V = (\rho, \rho u, \rho E)^t$ by writing a conservative scheme of these variables even on partial volumes. Considering a conservation equation of the form :

$$\partial_t v + \partial_x f = 0,$$

the conservative form for a scheme is defined here in $1D$ as follows :

$$\frac{v_i^{n+1} - v_i^n}{dt} + \frac{f_{i,i+1}^{n,n+1} - f_{i-1,i}^{n,n+1}}{dx} = 0,$$

with $dt = t^{n+1} - t^n$ the time step, dx the space step, v_i^n variable v value in cell i a time t^n, $f_{i,i+1}^{n,n+1}$ the flux of variable v from cell i to cell $i+1$ between time t^n and t^{n+1}.
Conservative form of the scheme is not only necessary to ensure conservation of variables at discrete level, but it is also necessary to compute the right weak solution of the partial derivative equations system when discontinuities are propagating in the flow. In particular, velocities of these waves cannot properly be computed when using non conservative schemes, see *LeVeque* [51].

2.2 Single material system

2.2.1 Finite volume schemes

The chosen numerical scheme is of finite volume type with cell centered variables V. Variables V in a single material cell are then constant in space and represent the average value of the solution. Some other families of schemes also belong to the finite volume family with cell centered variables, except the velocities that may be given on nodes [85] or on edges [21].

The system is integrated over a volume Ω, set with an outgoing normal n on its boundary surface Γ. We consider the system of partial differential equations :

$$\partial_t V + \operatorname{div} F(V) = 0.$$

This system is then integrated over a fixed volume Ω :

$$\int_\Omega \left(\partial_t V + \operatorname{div} F(V)\right) d\tau = \frac{d}{dt}\int_\Omega V d\tau + \int_\Gamma F \cdot n ds.$$

The volume Ω is set, then the finite volume scheme can be written on a cell Ω_i bounded by F_i planar edges in this way :

$$|\Omega_i|\frac{V_i^{n+1} - V_i^n}{dt} + \sum_{f=1}^{F_i} |A_f|\phi_f = 0, \quad \text{with} \quad V_i^n = \frac{1}{|\Omega_i|}\int_{\Omega_i} V^n d\tau$$

denoting the averaged value of the solution at time t^n in Ω_i, dt the time step, A_f the edge f area and

$$\phi_f = \frac{1}{|A_f|} \int_{\Gamma_f} F \cdot n_f \, ds$$

the flux through edge f in the direction of its outward normal vector n_f.

The robustness and accuracy of a finite volume scheme depends on the flux approximation $\phi_f(V_\ell, V_r)$ through the common edge Γ_f, between left and right neighboring cells C_ℓ and C_r of variable vectors V_ℓ and V_r. This scheme has a conservative form and the variables V evolution is conservative if and only if we have : $\phi_f(V_\ell, V_r) = -\phi_f(V_r, V_\ell)$.

Remark 1. *The Finite Volume method described in this section is well defined in the case of pure cells. In mixed cells, conservative variables and pressures are not defined. The purpose of this work is to find a way to extend a Finite Volume scheme to multi-material fluid flows.*

Remark 2. *Note that in this work, we only consider cartesian structured meshes. This hypothesis is strongly used for the multi-material extension.*

2.2.2 Finite Volume with Characteristic Flux scheme

The so called "FVCF" scheme, that stands for "Finite Volume scheme with Characteristic Fluxes", due to *Ghidaglia et al* [34] in 2001, is a finite volume scheme with cell centered variables, including the velocity vector. In this scheme, conservation laws are discretized by calculating numerical fluxes ϕ_f through mesh edges. These fluxes ϕ_f are expressed in terms of cell defined physical fluxes F, and not cells variables V. Introducing $(e_i)_{i=1,\dots,d}$ the canonical orthonormal basis of $\mathbb{R}^d$, we consider the generic system of partial derivative equations in d dimensions of space :

$$\partial_t V + \sum_{i=1}^{d} \partial_i F^i(V) = 0, \qquad \text{where} \quad F^i(V) = F(V) \cdot e_i.$$

The one and only hypothesis to use this scheme is that the system is hyperbolic, i.e. the jacobian matrix $J(V, n)$ can be diagonalized with real eigenvalues, where $J(V, n)$ is defined as a function of the direction $n \in \mathbb{S}^{d-1}$:

$$J(V, n) = \frac{\partial (F(V) \cdot n)}{\partial V}. \tag{2.5}$$

The system of conservation laws can be written in a non conservative form using the jacobian matrix :

$$\partial_t V + \sum_{i=1}^{d} J(V, e_i)\partial_i V = 0. \tag{2.6}$$

Let us multiply the above equation by the jacobian matrix $J(V, n)$. Then the normal flux in direction $n \in \mathbb{R}^d$ is given by the following equation :

$$\partial_t(F(V)\cdot n) + \sum_{i=1}^{d} J(V, n)J(V, e_i)J(V, n)^{-1}\partial_i(F(V)\cdot n) = 0. \tag{2.7}$$

The *FVCF* flux through Γ is calculated using the flux equation, linearized around an approximation of variables V_Γ on Γ :

$$\partial_t(F(V)\cdot n) + \sum_{i=1}^{d} J(V_\Gamma, n)J(V_\Gamma, e_i)J(V_\Gamma, n)^{-1}\partial_i(F(V)\cdot n) = 0, \tag{2.8}$$

where V_Γ denotes an average of variables in neighboring cells C_ℓ and C_r that have the common edge Γ. As an example, one may take a 1D linear interpolation which leads to :

$$V_\Gamma = \frac{Vol_r V_\ell + Vol_\ell V_r}{Vol_r + Vol_\ell}.$$

Since V_Γ is assumed to be locally constant on the face Γ, there is no tangential gradient of the flux. Restricting then to evolutions in the normal direction n to the face Γ and neglecting fluxes on cell corners, equation (2.8) reduces to :

$$\partial_t(F(V)\cdot n) + J(V_\Gamma, n)\partial_n(F(V)\cdot n) = 0, \quad \text{where} \quad \partial_n = n\cdot\nabla. \tag{2.9}$$

This system can be diagonalized in $\mathbb{R}^d$ according to the hyperbolicity hypothesis, thus eigenvalues $\lambda_k(V_\Gamma, n)$, left and right eigenvectors $\ell_k(V_\Gamma, n)$ and $r_k(V_\Gamma, n)$ can be calculated :

$$\begin{array}{ll} {}^tJ(V_\Gamma, n)\cdot\ell_k(V_\Gamma, n) & = \lambda_k(V_\Gamma, n)\ \ell_k(V_\Gamma, n), \\ J(V_\Gamma, n)\cdot r_k(V_\Gamma, n) & = \lambda_k(V_\Gamma, n)\ r_k(V_\Gamma, n), \\ diag(\lambda(V_\Gamma, n)) & = L(V_\Gamma, n)\ J(V_\Gamma, n)\ R(V_\Gamma, n). \end{array} \tag{2.10}$$

It turns out that local Riemann invariants $\ell_k(V_\Gamma, n)(F(V)\cdot n)$ are advected along n with velocity $\lambda_k(V_\Gamma, n)$:

$$(\partial_t + \lambda_k(V_\Gamma, n)\partial_n)\left(\ell_k(V_\Gamma, n)(F(V)\cdot n)\right) = 0. \tag{2.11}$$

with in two dimension of space *(2D)*, $u = (u_x, u_y)$, $n = (n_x, n_y)$, $t \cdot n = 0$,

$$\begin{array}{l} \lambda_1(V, n) = (u \cdot n) - c, \\ \lambda_2(V, n) = (u \cdot n), \\ \lambda_3(V, n) = (u \cdot n), \\ \lambda_4(V, n) = (u \cdot n) + c, \end{array} \tag{2.12}$$

$$R(V, n) = \begin{pmatrix} 1 & 1 & 0 & 1 \\ u_x - c\ n_x & u_x & t_x & u_x + c\ n_x \\ u_y - c\ n_y & u_y & t_y & u_y + c\ n_y \\ H - (n \cdot u)\ c & H - c^2/k & (t \cdot u) & H + (n \cdot u)\ c \end{pmatrix}, \tag{2.13}$$

$$L(V, n) = \begin{pmatrix} \dfrac{K + (n \cdot u)\ c}{2\ c^2} & \dfrac{(H - |u|^2)\ k}{c^2} & -(t \cdot u) & \dfrac{K - (n \cdot u)\ c}{2\ c^2} \\ \dfrac{-k\ u_x - n_x\ c}{2\ c^2} & \dfrac{u_x\ k}{c^2} & t_x & \dfrac{-k\ u_x + n_x\ c}{2\ c^2} \\ \dfrac{-k\ u_y - n_y\ c}{2\ c^2} & \dfrac{u_y\ k}{c^2} & t_y & \dfrac{-k\ u_y + n_y\ c}{2\ c^2} \\ \dfrac{k}{2\ c^2} & \dfrac{-k}{c^2} & 0 & \dfrac{k}{2\ c^2} \end{pmatrix} \tag{2.14}$$

$$\begin{array}{l} c^2 = \left(\dfrac{\partial p}{\partial \rho}\right)_s, \\ H = e + p/\rho + |u|^2/2, \\ k = \dfrac{1}{\rho}\left(\dfrac{\partial p}{\partial e}\right)_\rho, \\ K = c^2 + k(|u|^2 - H), \end{array} \tag{2.15}$$

Let be the normal unit vector $n = n_{\ell r}$ of edge Γ, directed from cell C_ℓ to cell C_r. The solution of equation (2.11) can be computed analytically by using the method of characteristics, and discretized by simple upwinding :

- if $\lambda_k(V_\Gamma, n) > 0$, then $\ell_k(V_\Gamma, n)\phi(\Gamma, n) = \ell_k(V_\Gamma, n)(F(V_\ell) \cdot n)$,
- if $\lambda_k(V_\Gamma, n) < 0$, then $\ell_k(V_\Gamma, n)\phi(\Gamma, n) = \ell_k(V_\Gamma, n)(F(V_r) \cdot n)$,
- if $\lambda_k(V_\Gamma, n) = 0$, then $\ell_k(V_\Gamma, n)\phi(\Gamma, n) = \ell_k(V_\Gamma, n)\left(\frac{F(V_\ell) + F(V_r)}{2} \cdot n\right)$.

The flux in the physical space is obtain by projection on the physical base $r_k(V_\Gamma, n)$. Then the *FVCF* flux is written in the following form :

$$\phi(\Gamma, n_{\ell r}) = \left(\frac{F(V_\ell) + F(V_r)}{2} - sign(J(V_\Gamma, n_{\ell r}))\frac{F(V_r) - F(V_\ell)}{2}\right) \cdot n_{\ell r}, \tag{2.16}$$

where the sign matrix is given by

$$sign(J(V_\Gamma, n_{\ell r})) = R(V_\Gamma, n)\ diag(sign(\lambda(V_\Gamma, n)))\ L(V_\Gamma, n).$$

Remark 3. *The FVCF flux on face* Γ *is constituted of an average of fluxes in neighboring cells added to an upwinding flux. The difference with Roe or Van Leer schemes is that the upwinding term here only involves fluxes* F *and not the primal variables* V*. Since eigenvalues and eigenvectors of the Jacobian matrix are known analytically, the calculation of the FVCF flux is straightforward. This scheme is then very generic for different systems of conservation laws and for different equations of state. See FVCF flux calculation for different systems of conservation laws in [33].*

Remark 4. *Some improvements of the scheme consistency using a modified sign function and correction for positive rate of entropy dissipation can be found in the report of de Vuyst [82].*

The time step dt is given by the scheme stability *CFL* condition (*Courant-Friedrichs-Levy*) :

$$dt < \min_i \left(\frac{Vol_i}{A \quad \max_k |(\lambda_i)_k|}\right) \tag{2.17}$$

with A the area of face Γ.

Remark 5. *Note that no assumption has been made on the nature of the system of conservation laws solved using this scheme. Even for non-hyperbolic systems, this scheme can be used as it is described in the PhD Thesis of Rovarch [69]. Moreover, a generic code has been built to solve almost any system of conservation laws, just describing the variables vector and the associated flux.*

2.2.3 Second order in space : *MUSCL* method

The second order in space is obtained by a reconstruction of each variable $V = (\rho, \rho u, \rho E)^t$ on cells edges, following MUSCL method of Van Leer [79]. A monotonic slope limiter is used to reconstruct left and right values $V_\Gamma(C_\ell)$ and $V_\Gamma(C_r)$ on the edge Γ between cells C_ℓ and C_r :

$$\begin{cases} V_\Gamma(C_\ell) &= V(C_\ell) + \dfrac{\varphi(\theta_\ell)}{2}(V(C_r) - V(C_\ell)), \\ V_\Gamma(C_r) &= V(C_r) - \dfrac{\varphi(\theta_r)}{2}(V(C_r) - V(C_\ell)), \end{cases} \tag{2.18}$$

θ_ℓ and θ_r denoting the slope ratios centered respectively on C_ℓ and C_r. Let $C_{\ell\ell}$ be the left neighbor of C_ℓ and C_{rr} the right neighbor of C_r. For each coordinate k of the variables vector V in cell C :

$$\begin{aligned} (\theta_\ell)_k &= \frac{V(C_r)_k - V(C_\ell)_k}{V(C_\ell)_k - V(C_{\ell\ell})_k} \\ (\theta_r)_k &= \frac{V(C_{rr})_k - V(C_r)_k}{V(C_r)_k - V(C_\ell)_k} \end{aligned}$$

The *minmod* slope limiter function is $\varphi(\theta) = \max(0, \min(\theta, 1))$ and is the only one that preserves a strict monotonic reconstruction, needed for the scheme stability.

Remark 6. *Instead of reconstructing the variable vector $V = (\rho, \rho u, \rho E)^t$, one can choose to perform this operation on primitive variables $W = (\rho, u, e)^t$, with e the specific internal energy and $e = E - 1/2 \|u\|^2$. This choice can be relevant for real equations of state of the form $p = P(\rho, e)$, because a monotonic reconstruction of ρ and e provides a monotonic value for p. That might not be the case by reconstruction of the variable vector $V = (\rho, \rho u, \rho E)^t$. Therefore our choice is to perform the reconstruction on primitive variables W.*

The physical flux $F(V) \cdot n = (\rho(u \cdot n), \rho u(u \cdot n) + pn, (\rho E + p)(u \cdot n))$ is a function of variables $V = (\rho, \rho u, \rho E)^t$ and of the equation of state which gives the associated pressure p. Thus second order fluxes in cells C_ℓ and C_r read as $F_\Gamma(C_\ell) = F(V_\Gamma(C_\ell))$ and $F_\Gamma(C_r) = F(V_\Gamma(C_r))$.

Computation of the eigenvalues on the edge Γ

The variable vector V_Γ on edge Γ is approximated by an average of left and right values. One can use for this average the neighboring cells volumes Vol_ℓ and Vol_r :

$$V_\Gamma = \frac{Vol_r V_\Gamma(C_\ell) + Vol_\ell V_\Gamma(C_r)}{Vol_\ell + Vol_r} \tag{2.19}$$

The eigenvalues $\lambda_\Gamma = \lambda(V_\Gamma, n)$, the left eigenvector matrix $L_\Gamma = L(V_\Gamma, n)$ and the right eigenvector matrix $R_\Gamma = R(V_\Gamma, n)$ can then be calculated and are functions of V_Γ and of the equation of state with same definitions as in Section 2.2.2.

Calculation of the numerical fluxes

With this *MUSCL* method, we obtain a second order *FVCF* flux, using the system sign matrix and right and left reconstructed flux values on Γ :

$$\phi_\Gamma = \frac{F_\Gamma(C_r) + F_\Gamma(C_\ell)}{2} - sign(A_\Gamma)\frac{F_\Gamma(C_r) - F_\Gamma(C_\ell)}{2} \tag{2.20}$$

with $sign(A_\Gamma) = R_\Gamma \, diag(sign(\lambda_\Gamma)) \, L_\Gamma$.

2.2.4 Boundary conditions

Let Γ_{BC} be an edge of a cell C_{BC} that belongs to the physical domain boundary. A numerical flux ϕ_{BC} has to be calculated trough Γ_{BC} in such a way to prescribe the boundary condition, following *Ghidaglia and Pascal* [33] :

- in the case of an *outlet* boundary condition, we impose a *Von Neumann* like condition on normal fluxes $\frac{\partial F}{\partial n} = 0$ as follows : $\phi_{BC} = F(C_{BC})$,
- in the case of a *wall/symmetry* condition, the flux ϕ_{BC} is calculated so that a zero normal velocity is imposed on Γ_{BC}. This is obtained by writing $u_{\Gamma_{BC}} \cdot n_{\Gamma_{BC}} = 0$. Therefore, the boundary flux reads as $\phi_{BC} = (0, p_{\Gamma_{BC}} n_{\Gamma_{BC}}, 0)$. The *wall/symmetry* condition is then prescribed by the calculation of an unique unknown which is the wall pressure $p_{\Gamma_{BC}}$. The fourth eigenvalue $\lambda^{(4)}_{\Gamma_{BC}} = u_{\Gamma_{BC}} \cdot n_{\Gamma_{BC}} + c_{\Gamma_{BC}} = c_{\Gamma_{BC}}$ is the sound speed on edge Γ_{BC}, therefore always positive, in direction of the outgoing normal. It corresponds to an outgoing wave from the domain. As in Section 2.2.2, the local Riemann invariant $\ell^{(4)}(C_{BC}) \cdot F$

for the linearized flux equation (2.11) corresponding to the eigenvalue $\lambda^{(4)}_{\Gamma_{BC}}$ is determined at the edge Γ_{BC} by following the characteristic curve. The result corresponds to the upwinding of this quantity : $\ell^{(4)}(C_{BC})\cdot\phi_{BC} = \ell^{(4)}(C_{BC})\cdot F(C_{BC})$. The wall pressure $p_{\Gamma_{BC}}$ is obtained by this equation and then the boundary flux $\phi_{BC} = (0, p_{\Gamma_{BC}} n_{\Gamma_{BC}}, 0)$.

Remark 7. *Note that the numerical flux ϕ_{BC} is computed in a homogeneous way with respect to internal cell fluxes. The flux $F(C_{BC})$ is calculated using variables values $V(C_{BC})$. But this flux should be calculated using reconstructed variable values on Γ_{BC} as done in the bulk cells of the domain, by the MUSCL method with slope limiting.*

2.2.5 Perturbation filtering

Even for order one and for any time step, a pathology is appearing in simulations where a strong plane shock wave is aligned with grid lines in *2D/3D*. This have been described as odd-even decoupling and analyzed by *Quirk* [64] or *Moschetta* [41]. This is a common failing of most of eulerian schemes [52] in this situation.
To cure this pathology, a physical point of view has been adopted. In fact, when a plane shock is aligned with grid lines, the instability is growing when even very small perturbations appear in the shock plane. It seems that sound speeds are slightly perturbated, then the shock plane is perturbated and the instability grows by this manner. This is a very similar behavior from hydrodynamic instabilities growing that leads to turbulence. The idea is the following : in Large Eddy Simulation (LES) of turbulence, the small scales of the flow are approximated by a turbulent diffusion. Actually, small perturbations are diffused and then only large scales of turbulence are really computed. We need exactly the same process to stop the growth of plane shock perturbations, i.e. diffusing them when they are very small. The simplest LES model is the *Smagorinsky* model of turbulence [74], in which the turbulent diffusion coefficient reads as :

$$\nu_t = C_f L^2 \sqrt{\overline{S} : \overline{S}} \tag{2.21}$$

with $L = \sqrt{dx\ dy}$, dx and dy the x and y space step, the dimension of space D and

$$\overline{S}_{ij} = \frac{1}{2}\left(\frac{\partial u_i}{\partial x_j} + \frac{\partial u_j}{\partial x_i}\right) - \frac{div(u)\delta_{ij}}{D}.$$

The value $C_f = 0.07$ is given by the experiment and seems well adapted for a wide range of flow regimes. This value is in the same range with physical values ($0.003 \leq C_{f\ exp} \leq 0.09$) used in similar models [70]. Of course, the form of this filtering is close from a tensorial artificial viscosity. The big difference is that the scheme does not need an artificial viscosity to be stable. In particular $\nu_t = 0$ in *1D* in our case. It is just a perturbation filtering to cut off small shears in the flow. Moreover, the value $C_f = 0.07$ used here is very small compare to the usual value for the equivalent constant for artificial viscosity $C_q = 2$.
This filtering is performed applying a splitted Navier-Stockes diffusion term, at the end of a time step :

$$\begin{aligned} \frac{V^{filter} - V^{n+1}}{dt} &= \begin{pmatrix} 0 \\ \text{div}\ \left(2\mu\overline{D} + \lambda div(u)\overline{I}\right) \\ \text{div}\ \left((2\mu\overline{D} + \lambda div(u)\overline{I})\ u\right) \end{pmatrix} \\ &= \begin{pmatrix} 0 \\ \text{div}\,(2\rho\nu_t\overline{S}) \\ \text{div}\,(2\rho\nu_t\overline{S}\ u) \end{pmatrix} \end{aligned} \tag{2.22}$$

with

$$Trace(2\mu\overline{D} + \lambda div(u)\overline{I}) = Trace(2\rho\nu_t\overline{S}) = 0$$

and $\mu = \rho\nu_t$.
The discretization of this diffusion operator is explicit and uses, in this context, the known values at time t^{n+1}. We use a finite volume scheme discretization, integrating equation (2.22) on the volume Vol_C of a cell C bounded by faces A_f :

$$Vol_C \frac{V^{filter} - V^{n+1}}{dt} = \begin{pmatrix} 0 \\ 2\sum_f A_f \rho_f (\nu_t)_f \overline{S}_f\ n_f \\ 2\sum_f A_f \rho_f (\nu_t)_f \overline{S}_f\ u_f \cdot n_f \end{pmatrix} \tag{2.23}$$

where values $\overline{S}_f$, ρ_f, $(\nu_t)_f$ and u_f are basically discretized on faces A_f using averages, as in a standard BBC scheme [21].

It can be easily proved that the explicit CFL condition for this diffusion filtering is satisfied when the eulerian CFL condition (2.17) is satisfied.

Remark 8. *This filtering is a post-treatment of the solution at each time step. This process should not lead to a diffusion of materials. Therefore, diffusion fluxes are only calculated for faces of the mesh between pure cells, and set to zero on faces of mixed cells.*

Remark 9. *This post-processing is only designed to cure this so called "odd-even decoupling" pathology of the scheme. If the system one wants to simulate does not contain strong shocks aligned with grid lignes, this is not needed at all.*

2.3 Multi-material extension : *NIP algorithm*

The purpose of this section is to extend a single phase finite volume scheme, with cell centered variables, to interface capturing in multi-material fluid flows. This new method introduced by the authors of this report is named *NIP* for *Natural Interface Positioning* and explicitly computes variables in partial volumes and the interfaces motion, without any diffusion between materials. The method is locally conservative in mass, momentum and total energy, and allows a perfect sliding of materials on each others.

2.3.1 1D Integration of the system

First, we consider the following *1D* system of conservation laws :

$$\partial_t V + \partial_x F(V) = 0. \tag{2.24}$$

- Let be $F(V)\cdot n$ the flux in direction n of conservative variables in *1D* :

$$\begin{array}{rcl} F(V)\cdot n & = & (\rho(u\cdot n), \rho u(u\cdot n)+pn, (\rho E+p)(u\cdot n)) \\ & = & V(u\cdot n)+pN \end{array} \tag{2.25}$$

  with $V=(\rho,\rho u,\rho E)^t$ and $N=(0,n,u\cdot n)$.
- Let A be the transverse section area and Vol the volume of a cell in *1D*.
- For given materials $i=1,2$, let ρ_i be the density, u_i the velocity vector, e_i the specific internal energy, p_i the pressure, $E_i = e_i + (u_i)^2/2$ the total specific energy, and V_i the variable vector associated with material i in the partial volume Vol_i inside a mixed cell. Of course, one has $Vol_1 + Vol_2 = Vol$.

Let $\Omega(t)$ be a volume and its surface boundary $\Gamma(t) = \Gamma_{u_{int}=0} \bigcup \Gamma_{u_{int}\neq 0}$, with $\Gamma_{u_{int}=0}$ time independent edges and $\Gamma_{u_{int}\neq 0}$ moving edges with local velocity u_{int} on $\Gamma_{u_{int}\neq 0}$ depending on time. Then, system (2.24) is integrated over $\Omega(t)$, taking into account volume evolution with time :

$$\int_{\Omega(t)} (\partial_t V + \partial_x F(V))\, d\tau = \frac{d}{dt}\int_{\Omega(t)} V d\tau - \int_{\Gamma_{u_{int}\neq 0}} V(u_{int}\cdot n_{int}) ds + \int_{\Gamma_{u_{int}\neq 0}} F(V)(e_x \cdot n_{int}) ds + \int_{\Gamma_{u_{int}=0}} F(V)(e_x \cdot n_{int}) ds. \quad (2.26)$$

Moreover, using the notation $N(u_{int}, n_{int}) = (0, n_{int}, u_{int}\cdot n_{int})^t$:

$$\int_{\Gamma_{u_{int}\neq 0}} F(V)\cdot n\, ds = \int_{\Gamma_{u_{int}\neq 0}} V(u_{int}\cdot n_{int})\, ds + \int_{\Gamma_{u_{int}\neq 0}} p_{int} N(u_{int}, n_{int})\, ds. \quad (2.27)$$

Finally simplifying the common advection terms in (2.26) and (2.27), the integrated system reads :

$$\frac{d}{dt}\int_{\Omega(t)} V d\tau + \int_{\Gamma_{u_{int}\neq 0}} p_{int} N(u_{int}, n_{int})\, ds + \int_{\Gamma_{u_{int}=0}} F(V)\cdot n\, ds = 0, \quad (2.28)$$

The finite volume scheme then reads as :

$$\frac{|\Omega^{n+1}|V^{n+1} - |\Omega^n|V^n}{dt} + A\phi_{u_{int}=0} + A p_{int} N(u_{int}, n_{int}) = 0 \quad (2.29)$$

with

$$V^n = \frac{1}{|\Omega^n|}\int_{\Omega^n} V^n d\tau$$

the average value in Ω^n at time t^n, dt the time step, A the transverse section of the *1D* cell (or face area in *2D/3D* in the direction n),

$$\phi_{u_{int}=0} = \frac{1}{A}\int_\Gamma F\cdot n_f\, ds$$

the flux trough the edge Γ given by the single phase scheme. The flux through a moving interface is $p_{int}N(u_{int}, n_{int})$. The determination of interface pressure p_{int} and velocity u_{int} will be discussed hereafter.

Strategy to deal with partial volumes

Two difficulties appear when dealing with partial volumes :

- the above scheme is constrained with the same *CFL* condition as the single phase scheme in Section 2.2.2 :

$$dt < \min_i \left(\frac{Vol_i}{A \ \max |(\lambda_i)_k|} \right)$$

  Here, control volumes Vol_i are the partial volumes in mixed cells that may be arbitrarily small, and then lead to tiny time steps.
- when an interface moves from a cell C_1 to a neighboring cell C_2, the scheme cannot be written because the topology of these cells is changing during the time step.

These difficulties are artificially induced by the interface motion in an Eulerian mesh. As an example, let us consider a system composed of two identical materials, same variable values and same equations of state : the interface is obviously artificial. We want this two material system to have the same behavior as the identical one material system, in particular no restriction on the time step due to mixed cells.

Remark 10. *In this method, the time step is calculated only considering pure cells. We do not want small volumes in mixed cells to restrict dramatically the course of the computation.*

Our method consists in removing cell edges when an interface potentially goes through it. Therefore each partial volume is merged with the neighboring pure cell that is filled with the same material. Variables in these enlarged partial volumes are obtained by writing the conservation laws :

$$\begin{aligned} \overline{Vol_1} &= Vol_1 + Vol_{pure\ 1} \\ \overline{Vol_2} &= Vol_2 + Vol_{pure\ 2} \\ \overline{V}_1 &= \frac{Vol_1\ V_1 + Vol_{pure\ 1}\ V_{pure\ 1}}{\overline{Vol_1}} \\ \overline{V}_2 &= \frac{Vol_2\ V_2 + Vol_{pure\ 2}\ V_{pure\ 2}}{\overline{Vol_2}} \end{aligned} \tag{2.30}$$

The 1D three cell system constituted with one mixed cell between two pure cells, is associated with its left and right single phase fluxes ϕ_ℓ and ϕ_r. Internal cells edges are forgotten, considering only enlarged volumes $\overline{Vol_1}$ and $\overline{Vol_2}$

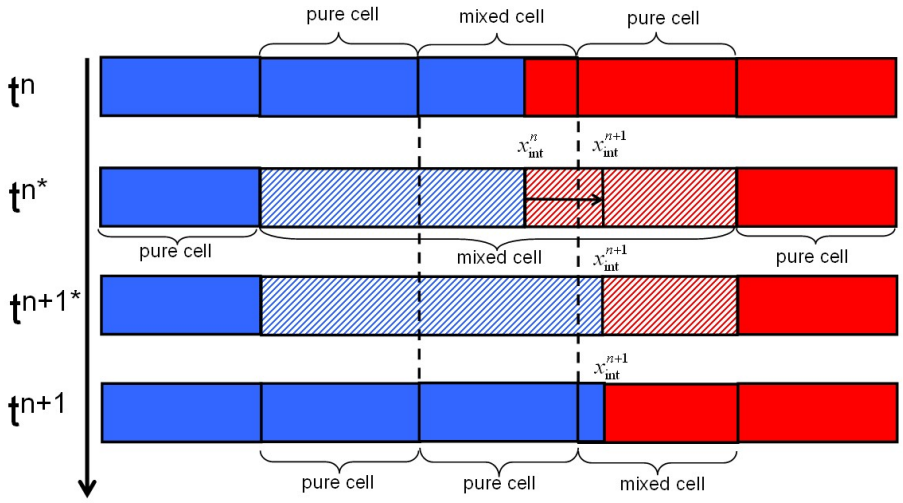

FIG. 2.1 – Evolution of an interface through a cell face.

and averaged variables $\overline{V}_1$ *and* $\overline{V}_2$*, separated by an interface. This system is a data structure called* condensate *that will be defined more generally in Section 2.3.2.*

The *CFL* condition is then taken as its value calculated on pure cells, because waves that were evolving in the mixed cells are diffused by the conservative average in the *condensate*. We assume that their velocity values stay close from those in pure cells. Thus the interface should not go through a cell edge during the time step, thanks to the *CFL* constraint on time step in pure cells. The new values of condensate volumes and variables are then remapped on the Eulerian mesh. The interface might have moved from one cell to another during the *condensate* evolution.

Explicit scheme in a *condensate*

The scheme is written for the *condensate* defined in the previous section, using enlarged volumes defined in equations (2.30). The interface is moving along x axis and conservation laws are written for materials 1, on the left side, and 2, on the right side, using the flux expression (2.29) for a moving

interface in Section 2.3.1 :

$$\begin{cases} \dfrac{Vol_1^{n+1}V_1^{n+1} - Vol_1^nV_1^n}{dt} + A\left(\phi_\ell + p_{int}N(u_{int}, n_{int,1})\right) = 0 \\ \dfrac{Vol_2^{n+1}V_2^{n+1} - Vol_2^nV_2^n}{dt} + A\left(\phi_r + p_{int}N(u_{int}, n_{int,2})\right) = 0 \end{cases} \tag{2.31}$$

with

$$\begin{aligned} Vol_1^{n+1} &= Vol_1^n + dtA(u_{int} \cdot n_{int,1}), \\ Vol_2^{n+1} &= Vol_2^n + dtA(u_{int} \cdot n_{int,2}), \end{aligned}$$

$n_{int,1}$ and $n_{int,2}$ denoting the outgoing normal vectors at the interface for volumes Vol_1^n and Vol_2^n respectively, dt the time step.
The scheme is then written for each quantity explicitly :

$$\begin{cases} m_1^{n+1} &= m_1^n - dtA \;\; \phi_\ell(1) \\ m_2^{n+1} &= m_2^n - dtA \;\; \phi_r(1) \\ m_1^{n+1}u_1^{n+1} &= m_1^nu_1^n - dtA\left(\phi_\ell(2) + p_{int}\right) \\ m_2^{n+1}u_2^{n+1} &= m_2^nu_2^n - dtA\left(\phi_r(2) - p_{int}\right) \\ m_1^{n+1}v_1^{n+1} &= m_1^nv_1^n - dtA\left(\phi_\ell(3)\right) \\ m_2^{n+1}v_2^{n+1} &= m_2^nv_2^n - dtA\left(\phi_r(3)\right) \\ m_1^{n+1}E_1^{n+1} &= m_1^nE_1^n - dtA\left(\phi_\ell(4) + p_{int}u_{int}\right) \\ m_2^{n+1}E_2^{n+1} &= m_2^nE_2^n - dtA\left(\phi_r(4) - p_{int}u_{int}\right) \end{cases} \tag{2.32}$$

with $n_{int,1} = 1$ and $n_{int,2} = -1$, $\phi(i)$ the i coordinate of the FVCF numerical flux in $2D$.
Variable values at time t^{n+1} are then obtained following these steps :

$$\begin{array}{ll} m_1^n = \rho_1^nVol_1^n & m_2^n = \rho_2^nVol_2^n \\ m_1^{n+1} = m_1^n - dtA\phi_\ell(1) & m_2^{n+1} = m_2^n - dtA\phi_r(1) \\ \theta_1 = \dfrac{m_1^n}{m_1^{n+1}} & \theta_2 = \dfrac{m_2^n}{m_2^{n+1}} \\ \kappa_1 = \dfrac{Vol_1^n}{dtA} & \kappa_2 = \dfrac{Vol_2^n}{dtA} \end{array} \tag{2.33}$$

These last values are independent of the pressure p_{int} and the velocity u_{int} at the interface.

$$\begin{array}{ll}
Vol_1^{n+1} = Vol_1^n + dtA\ u_{int} & Vol_2^{n+1} = Vol_2^n - dtA\ u_{int} \\
\rho_1^{n+1} = \dfrac{m_1^{n+1}}{Vol_1^{n+1}} & \rho_2^{n+1} = \dfrac{m_2^{n+1}}{Vol_2^{n+1}} \\
u_1^{n+1} = \theta_1 \left(u_1^n - \dfrac{\phi_\ell(2) + p_{int}}{\rho_1^n \kappa_1} \right) & u_2^{n+1} = \theta_2 \left(u_2^n - \dfrac{\phi_r(2) - p_{int}}{\rho_2^n \kappa_2} \right) \\
v_1^{n+1} = \theta_1 \left(v_1^n - \dfrac{\phi_\ell(3)}{\rho_1^n \kappa_1} \right) & v_2^{n+1} = \theta_2 \left(v_2^n - \dfrac{\phi_r(3)}{\rho_2^n \kappa_2} \right) \\
E_1^{n+1} = \theta_1 \left(E_1^n - \dfrac{\phi_\ell(4) + p_{int} u_{int}}{\rho_1^n \kappa_1} \right) & E_2^{n+1} = \theta_2 \left(E_2^n - \dfrac{\phi_r(4) - p_{int} u_{int}}{\rho_2^n \kappa_2} \right)
\end{array} \tag{2.34}$$

The interface position x_{int}^{n+1} at time t^{n+1} is given by :

$$x_{int}^{n+1} = x_{int}^n + dt\ u_{int} \tag{2.35}$$

Remaining unknowns are the pressure p_{int} and the velocity u_{int} at the interface. Their calculation is the purpose of the next section.

Pressure and velocity at the interface

The *1D* system of conservation laws (2.24) is written in Lagrangian coordinates :

$$\partial_t V_{lag} + \partial_m F_{lag} = 0, \tag{2.36}$$

with $\partial_m(.) = 1/\rho\ \partial_x(.)$, the specific total energy E, $V_{lag} = (m, u, E)^t$ and $F_{lag} = p\ (0, n, u \cdot n)^t$.
As in Section 2.2.2 for the Eulerian *FVCF* scheme, this system may be diagonalized. It follows that local Riemann invariants $\pi^+ = p + \rho c u$ and $\pi^- = p - \rho c u$ are advected with the sound speed $\pm c$:

$$\partial_t \pi^+ + c\, \partial_x \pi^+ = 0, \qquad \text{and} \qquad \partial_t \pi^- - c\, \partial_x \pi^- = 0. \tag{2.37}$$

As for the single phase system in Section 2.2.2, advection velocities in the numerical scheme are linearized around interface values. Then the equations are solved following characteristic curves. Here, the advection velocity c (resp. $-c$) is sound velocity that is always positive (resp. negative). Therefore, upwinding leads to :

$$\begin{array}{lll}
\pi_{int}^+ = \pi_\ell^+ & \Leftrightarrow & p_{int} + \rho_{int} c_{int} u_{int} = p_\ell + \rho_\ell c_\ell u_\ell, \\
\pi_{int}^- = \pi_r^- & \Leftrightarrow & p_{int} - \rho_{int} c_{int} u_{int} = p_r - \rho_r c_r u_r.
\end{array} \tag{2.38}$$

Values of p_{int} and u_{int} are then given by :

$$\left\{ \begin{array}{l} p_{int} = \dfrac{\rho_r c_r p_\ell + \rho_\ell c_\ell p_r}{\rho_\ell c_\ell + \rho_r c_r} + \rho_\ell c_\ell \rho_r c_r \dfrac{u_\ell - u_r}{\rho_\ell c_\ell + \rho_r c_r} \\ u_{int} = \dfrac{\rho_\ell c_\ell u_\ell + \rho_r c_r u_r}{\rho_\ell c_\ell + \rho_r c_r} + \dfrac{p_\ell - p_r}{\rho_\ell c_\ell + \rho_r c_r} \end{array} \right. \tag{2.39}$$

Note that these formulae are the same as Godunov's acoustic solver [66].

As in the eulerian case, the time step dt is given by the *CFL* stability condition for this lagrangian scheme :

$$dt < \min_i \left(\frac{Vol_i}{A\ c_i} \right) \tag{2.40}$$

with Vol the volume and A the transverse section of the cell.

Proposition 11. *Let us set the following approximation for sound speeds :*

$$\tilde{c}_i = \min(c_i, \kappa_i)$$

in cell i and $\kappa_i = Vol_i^n/(dt\, A)$.
Equations (2.39) for p_{int} and u_{int} are then modified in :

$$\left\{ \begin{array}{l} p_{int} = \dfrac{\rho_r \tilde{c}_r p_\ell + \rho_\ell \tilde{c}_\ell p_r}{\rho_\ell \tilde{c}_\ell + \rho_r \tilde{c}_r} + \rho_\ell \tilde{c}_\ell \rho_r \tilde{c}_r \dfrac{u_\ell - u_r}{\rho_\ell \tilde{c}_\ell + \rho_r \tilde{c}_r} \\ u_{int} = \dfrac{\rho_\ell \tilde{c}_\ell u_\ell + \rho_r \tilde{c}_r u_r}{\rho_\ell \tilde{c}_\ell + \rho_r \tilde{c}_r} + \dfrac{p_\ell - p_r}{\rho_\ell \tilde{c}_\ell + \rho_r \tilde{c}_r} \end{array} \right. \tag{2.41}$$

Let us consider the case of a layer i between two moving interfaces where the fluxes are computed using formulae (2.41).
The layer evolution between t^n and t^{n+1} is "entropic" in the sense of the following discrete entropy inequality :

$$T^n(s^{n+1} - s^n) = e^{n+1} - e^n + p^n \left(\frac{1}{\rho^{n+1}} - \frac{1}{\rho^n} \right) \geq 0. \tag{2.42}$$

Proof :
1) When the CFL condition (2.40) $dt < Vol_i^n/(A\, c_i)$ for the evolution of the Lagrangian quantities is fulfilled, that is equivalent to write $c_i < \kappa_i$, thus $\tilde{c}_i = \min(c_i, \kappa_i) = c_i$. The important case is when the layer i is thin and does not fulfill the CFL condition (2.40). In this case, we have $c_i > \kappa_i$ and thus

$\tilde{c}_i = \min(c_i, \kappa_i) = \kappa_i$. Note that no constraint has been made on the time step to satisfy the CFL condition (2.40) in mixed cells. The time step is only calculated according to pure cells with eulerian CFL condition (2.17).
2) Besides, the discrete entropy inequality (2.42) is deduced from the continuous entropy inequality :

$$\rho T \frac{Ds}{Dt} = \rho \left(\frac{De}{Dt} + p \frac{D}{Dt} \left(\frac{1}{\rho} \right) \right) \geq 0, \quad \text{where} \quad \frac{D}{Dt} = \partial_t + u\, \partial_x,$$

so that integrating on the Lagrangian cell $\Omega_{lag}(t)$ and choosing an explicit approximation in time for temperature T and pressure p yields :

$$mT^n \int_{t^n}^{t^{n+1}} \frac{d}{dt} \left(\int_{\Omega_{lag}(t)} s\, d\tau \right) dt$$

$$= m \left(\int_{t^n}^{t^{n+1}} \frac{d}{dt} \left(\int_{\Omega_{lag}(t)} e\, d\tau \right) dt + p^n \int_{t^n}^{t^{n+1}} \frac{d}{dt} \left(\int_{\Omega_{lag}(t)} \frac{d\tau}{\rho} \right) dt \right) \geq 0.$$

Therefore, we obtain the discrete entropy inequality (2.42) :

$$T^n (s^{n+1} - s^n) = e^{n+1} - e^n + p^n \left(\frac{1}{\rho^{n+1}} - \frac{1}{\rho^n} \right) \geq 0.$$

3) The variable vector V^{n+1} at time t^{n+1} in layer i, dropping the subscript i, reads as :

$$\frac{Vol^{n+1} V^{n+1} - Vol^n V^n}{dt} + A \left(\phi^+_{int} + \phi^-_{int} \right) = 0,$$

with the flux $\phi^\pm_{int} = (0, p^\pm_{int} n^\pm_{int}, p^\pm_{int} (u^\pm_{int} \cdot n^\pm_{int}))^t$ where $+$ and $-$ denotes respectively right and left interfaces.
Explicitly, for each quantity :

$$\begin{aligned}
Vol^{n+1} &= Vol^n + dtA\, (u^+_{int} - u^-_{int}) \\
m^{n+1} &= m^n \\
\rho^{n+1} &= \frac{\rho^n}{1 + \dfrac{u^+_{int} - u^-_{int}}{\kappa}} \\
u^{n+1} &= u^n - \frac{p^+_{int} - p^-_{int}}{\rho^n \kappa} \\
v^{n+1} &= v^n \\
E^{n+1} &= E^n - \frac{p^+_{int} u^+_{int} - p^-_{int} u^-_{int}}{\rho^n \kappa} \\
e^{n+1} &= E^{n+1} - \frac{1}{2} \left((u^{n+1})^2 + (v^{n+1})^2 \right).
\end{aligned}$$

Thus we obtain :

$$\begin{aligned} T^n(s^{n+1}-s^n) &= e^{n+1}-e^n+p^n\left(\frac{1}{\rho^{n+1}}-\frac{1}{\rho^n}\right) \\ &= -\frac{p_{int}^+u_{int}^+-p_{int}^-u_{int}^--u^n(p_{int}^+-p_{int}^-)-p^n(u_{int}^+-u_{int}^-)}{\rho^n\kappa} \\ &\quad -\frac{1}{2}\left(\frac{p_{int}^+-p_{int}^-}{\rho^n\kappa}\right)^2 \\ &= -\frac{(p_{int}^+-p^n)(u_{int}^+-u^n)-(p^n-p_{int}^-)(u^n-u_{int}^-)}{\rho^n\kappa} \\ &\quad -\frac{1}{2}\left(\frac{p_{int}^+-p_{int}^-}{\rho^n\kappa}\right)^2. \end{aligned}$$

By using (2.41) and with the notations :

$$\delta p^+ = p_{int}^+ - p^n, \qquad \delta p^- = p^n - p_{int}^-,$$
$$\delta u^+ = u_{int}^+ - u^n, \qquad \delta u^- = u^n - u_{int}^-,$$

we obtain :

$$\delta p^+ + \rho^n\ \tilde{c}\ \delta u^+ = 0, \qquad \text{and} \qquad \delta p^- - \rho^n\ \tilde{c}\ \delta u^- = 0,$$

with $\tilde{c} = \min(c^n, \kappa)$. Introducing this result in the entropy inequality :

$$\begin{aligned} T^n(s^{n+1}-s^n) &= -\frac{\delta p^+\delta u^+-\delta p^-\delta u^-}{\rho^n\kappa}-\frac{1}{2}\left(\frac{\delta p^++\delta p^-}{\rho^n\kappa}\right)^2 \\ &= \frac{(\delta p^+)^2+(\delta p^-)^2}{\rho^n\kappa\rho^n\tilde{c}}-\frac{1}{2}\left(\frac{\delta p^++\delta p^-}{\rho^n\kappa}\right)^2 \\ &= \frac{(\delta p^+)^2+(\delta p^-)^2}{(\rho^n\kappa)^2}\left(\frac{\kappa}{\tilde{c}}-1\right)+\frac{1}{2}\left(\frac{\delta p^+-\delta p^-}{\rho^n\kappa}\right)^2. \end{aligned}$$

- When the CFL condition (2.40) is satisfied in the moving cell, we have $\tilde{c} = \min(c, \kappa) = c < \kappa$, thus :

$$T^n(s^{n+1}-s^n) = \frac{(\delta p^+)^2+(\delta p^-)^2}{(\rho^n\kappa)^2}\left(\frac{\kappa}{c}-1\right)+\frac{1}{2}\left(\frac{\delta p^+-\delta p^-}{\rho^n\kappa}\right)^2 \geq 0,$$

- When the CFL condition (2.40) is not satisfied, we have $\tilde{c} = \min(c, \kappa) = \kappa$, thus :

$$T^n(s^{n+1}-s^n) = \frac{1}{2}\left(\frac{\delta p^+-\delta p^-}{\rho^n\kappa}\right)^2 \geq 0.$$

Therefore, Proposition (11) is proven.

Remark 12. *In the* $1D$ *case, thin layers cannot exist because we merge small volumes in mixed cell with volumes of pure neighboring cells in such a way that the CFL condition (2.40) is satisfied. However, thin layers can appear in* $2D/3D$ *when dealing with a juxtaposition of several mixed cells, as we will see in Section 2.3.2.*

Remark 13. *Since Proposition (11) is proven, the second Principle of Thermodynamics is satisfied in thin layers in the sense of the discrete entropy inequality (2.42). However, this good property does not imply the positivity of volumes, since the advection based CFL condition* $udt < dx$ *is not guaranteed for thin layers. This will be the purpose of Section 2.4.*

Proposition 14. *Let us consider the case of a layer* i *between a moving interface on the right side and a cell edge on the left side. The flux* ϕ^ℓ *in the direction of the outgoing normal vector is defined on the left side of the cell. Let us settle the left flux as :*

$$\phi^\ell = -\phi_i^n \cdot e_x = -\left(\rho_i^n u_i^n, \rho_i^n (u_i^n)^2 + p_i^n, \rho_i^n u_i^n v_i^n, \rho_i^n E_i^n u_i^n + p_i^n u_i^n\right)^t,$$

with ϕ_i^n *the layer* i *centered flux at time* t^n*.*

Then, the layer evolution between t^n *and* t^{n+1} *is entropic in the sense of the following discrete entropy inequality :*

$$T^n(s^{n+1} - s^n) = e^{n+1} - e^n + p^n\left(\frac{1}{\rho^{n+1}} - \frac{1}{\rho^n}\right) \geq 0. \tag{2.43}$$

Proof : the quantities at time t^{n+1} in layer i, dropping the subscript i, read as :

$$\frac{Vol^{n+1}V^{n+1} - Vol^n V^n}{dt} + A\left(\phi^\ell + \phi_{int}^+\right) = 0,$$

with the flux $\phi_{int}^+ = (0, p_{int}^+ n_{int}^+, p_{int}^+ (u_{int}^+ \cdot n_{int}^+))^t$ where $+$ denotes the right interface.

$$
\begin{aligned}
Vol^{n+1} &= Vol^n + dtA\ (u^+_{int}) \\
m^{n+1} &= m^n - dtA\ \phi^\ell(1) \\
\theta &= \frac{m^n}{m^{n+1}} = \frac{1}{1+\dfrac{u^n}{\kappa}} \\
\rho^{n+1} &= \frac{\rho^n}{\theta(1+\dfrac{u^+_{int}}{\kappa})} \\
u^{n+1} &= \theta\left(u^n - \frac{p^+_{int}+\phi^\ell(2)}{\rho^n\kappa}\right) = u^n - \theta\frac{p^+_{int}-p^n}{\rho^n\kappa} \\
v^{n+1} &= \theta\left(v^n - \frac{\phi^\ell(3)}{\rho^n\kappa}\right) = v^n \\
E^{n+1} &= \theta\left(E^n - \frac{p^+_{int}u^+_{int}+\phi^\ell(4)}{\rho^n\kappa}\right) = E^n - \theta\frac{p^+_{int}u^+_{int}-p^nu^n}{\rho^n\kappa} \\
e^{n+1} &= E^{n+1} - \frac{1}{2}\left((u^{n+1})^2+(v^{n+1})^2\right)
\end{aligned}
$$

with u^+_{int} the right interface velocity, as well the interface pressure p^+_{int}. Substituting into (2.43) yields :

$$
\begin{aligned}
T^n(s^{n+1}-s^n) &= e^{n+1}-e^n+p^n\left(\frac{1}{\rho^{n+1}}-\frac{1}{\rho^n}\right) \\
&= -\frac{\theta}{\rho^n\kappa}(p^+_{int}-p^n)(u^+_{int}-u^n) - \frac{1}{2}\left(\frac{\theta}{\rho^n\kappa}\right)^2(p^+_{int}-p^n)^2
\end{aligned}
$$

By using (2.41) and with the notations :

$$\delta p^+ = p^+_{int}-p^n, \qquad \delta u^+ = u^+_{int}-u^n,$$

leading to

$$\delta p^+ + \rho^n\ \tilde{c}\ \delta u^+ = 0, \quad \text{with} \quad \tilde{c} = \min(c,\kappa).$$

Introducing this result in the entropy inequality, one gets :

$$T^n(s^{n+1}-s^n) = \frac{\theta}{\rho^n\tilde{c}}(\delta p^+)^2\left(\frac{1}{\rho^n\tilde{c}} - \frac{1}{2}\frac{\theta}{\rho^n\kappa}\right) \geq 0.$$

This condition is obtained if $\theta < 2$, equivalent to the time step restriction

$$dt < \frac{Vol^n}{(2A|u^n|)}.$$

From a practical point of view, this condition is satisfied using a single fluid CFL condition (2.17) with a coefficient less than 1/2.
Therefore, Proposition (14) is proven.

Proposition 15. *Let us finally consider the case of a layer i between a moving interface on the left side and a cell edge on the right side, where a flux ϕ^r goes through, in the direction of the outgoing normal vector. Let us define the left flux*

$$\phi^r = \phi_i^n \cdot e_x = \left(\rho^n u^n, \rho^n (u^n)^2 + p^n, \rho^n u^n v^n, \rho^n E^n u^n + p^n u^n\right)^t,$$

with ϕ_i^n the layer centered flux at time t^n.

The layer evolution between t^n and t^{n+1} is entropic in the sense of the following discrete entropy inequality, :

$$T^n(s^{n+1} - s^n) = e^{n+1} - e^n + p^n \left(\frac{1}{\rho^{n+1}} - \frac{1}{\rho^n}\right) \geq 0, \tag{2.44}$$

The proof follows the lines of that of Proposition (14).

Remark 16. *Situations of Propositions (14) and (15) are not the standard cases of the method, because the flux ϕ given for the proof is the layer centered flux instead of the one given by the single fluid finite volume scheme. This result only shows that when the eulerian flux through the cell face has good properties, the flux through the moving interfaces still provides a correct entropy behavior in the layer.*

Boundary conditions for a mixed cell

The physical flux is calculated for materials 1 and 2, namely $F_1(C_{BC}) = F(V_1(C_{BC}))$ and $F_2(C_{BC}) = F(V_2(C_{BC}))$ as described in Section 2.2.4. The flux $\phi(\Gamma_{BC})$ prescribed through the edge Γ_{BC} is given by :

$$\phi(\Gamma_{BC}) = \frac{\rho_2 \widetilde{c}_2 F_1(C_{BC}) + \rho_1 \widetilde{c}_1 F_2(C_{BC})}{\rho_1 c_1 + \rho_2 c_2} \tag{2.45}$$

with the density ρ_i, $\tilde{c}_i = \min(c_i, \kappa_i)$ and $\kappa_i = Vol_i^n/(dt\, A)$.
The considered averaging is homogeneous with the flux calculation through a moving interface described in Section 2.3.1.

2.3.2 *NIP* Algorithm

The extension of the single phase *FVCF* scheme to multi-material fluid flows in *2D* is the purpose of this section, using *1D* results. The next sections describe the interface capturing method *NIP*, based on a directional splitting on cartesian structured mesh. The method is detailed for only one direction generically termed x for each direction x, y or z. In d dimensions of space, the algorithm described in x direction has to be repeated on d steps, one for each direction. In *2D* :

- variables and interface positions at t^{nx} are calculated from those at t^n by the x direction step,
- variables and interfaces positions at t^{n+1} are calculated from those at t^{nx} by the y direction step.

For symmetry reasons, successive steps x and y have to be alternated at each time step, (xy), then (yx), and so on.
The method is described here in *2D*, but is easily extended and with no restriction in *3D* by alternating at each time step any combination of x, y, z steps : (xyz), then (xzy), then (yxz), then (yzx), then (zxy), then (zyx) and so on.

Variables evolution in pure cells

The variables calculation at t^{n+1} from those at t^n is achieved in *2D* by a two step directional splitting, first in x direction and second in y direction :

$$\begin{aligned} V^{nx} &= V^n - \frac{dt}{Vol} Area_x(\phi_\ell^n + \phi_r^n), \\ V^{n+1} &= V^{nx} - \frac{dt}{Vol} Area_y(\phi_d^n + \phi_u^n), \end{aligned} \tag{2.46}$$

with time step dt, cell volume Vol, $Area_x$ and $Area_y$ denoting the cell transverse section respectively in x and y direction, ϕ_u^n, ϕ_d^n, ϕ_r^n, ϕ_ℓ^n up, down, right and left direction fluxes, calculated using variables at time t^n.
Moreover, the standard single phase scheme writes in one step :

$$V^{n+1} = V^n - \frac{dt}{Vol} \left(Area_x(\phi_\ell^n + \phi_r^n) + Area_y(\phi_d^n + \phi_u^n) \right). \tag{2.47}$$

Of course, the result obtained using two steps (2.46) and one step (2.47) equations is strictly identical, when fluxes are calculated using variables at same time t^n.

Remark 17. *The NIP method is based on this result that permits the calculation of 2D/3D single phase flows by directional splitting which exactly reproduces the same result as the one step calculation. Therefore we can conveniently calculate mixed cells evolution by a real directional splitting, without loosing the scheme accuracy in pure cells.*

Definition of a *condensate*

The multi-material treatment in *2D/3D* with interface reconstruction on an Eulerian mesh requires to take into account three main constraints :

- to write conservation laws in a robust way without any restriction on the time step from mixed cells,
- to allow an interface motion from one cell to another,
- to allow two or more neighboring mixed cells.

The method described here creates a *1D* data structure named *condensate*.

Definition : *A condensate is a 1D data structure constituted of nc layers of different materials, separated by nc-1 Lagrangian interfaces. The boundaries of the condensate are Eulerian edges, where a flux go through, see figure (2.3) third row. Each layer is associated with layer centered variables and each interface is associated with a 2D/3D normal vector.*

Actually, this is a condensation of neighboring mixed cells in one direction of the cartesian mesh, in which interfaces between different materials are considered *1D*, namely they are considered vertical in x direction step. They move independently from the Eulerian mesh.
A *condensate* then contains layers of successive different materials that are separated by interfaces and the thickness of these layers is calculated by volume conservation. The ordering of material layers is known by the *2D/3D* description at the previous time step. It is determined by volume fractions in neighboring cells, as it is described in Section 2.3.5. Their evolution is calculated in a Lagrangian point of view and the scheme is written as described in Section 2.3.1. Obviously, layers can be as thin as partial volumes are small. Once quantities and interface positions inside the *condensate* are known at time t^{n+1}, they are remapped on the original Eulerian mesh.

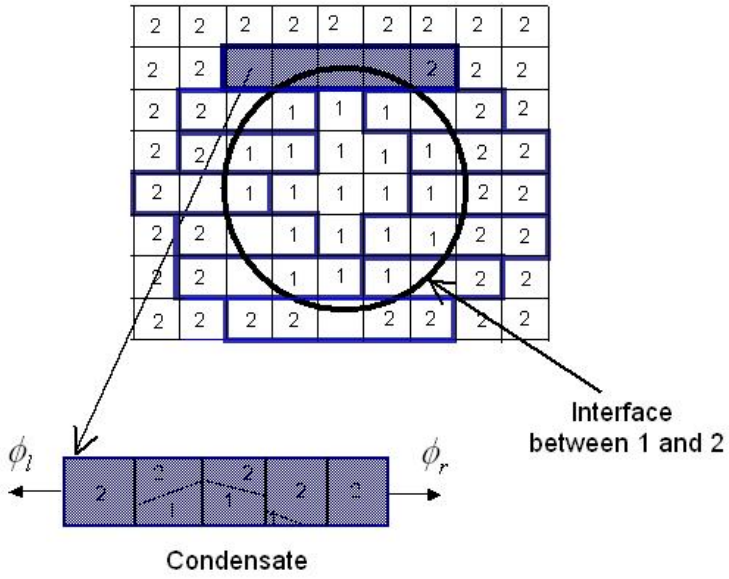

FIG. 2.2 – Extraction of neighboring mixed cells from the grid to become a *condensate* during x direction step.

Construction of a *condensate*

The mesh is covered line by line in x direction step and a *condensate* is created if a mixed cell is detected. The number of successive mixed cells is then determined, and they are associated with the previous and next pure cells of these mixed cells. The evolution of this set of cells is calculated independently of the Eulerian mesh as a *condensate*. The *condensate* is described by the following variables :

- each volume in these mixed and pure cells becomes a layer of the *condensate*, separated by a vertical interface, in x direction step, which the abscissa is determined by volume conservation. The materials ordering in each direction is known in each mixed cell. If two successive layers are filled of the same material, then these two are merged in one layer and variables are averaged in a conservative way. Thus the *condensate* is constituted of nc layers of different successive materials,
- variables such as volume, density, velocity, internal energy, pressure are volume centered for partial volumes in mixed cells, thus they are known for each layer,
- border interfaces abscissas are known for each layer by construction,
- the interface normal vector is calculated in *2D/3D* and is associated with each *1D* interface of the *condensate*. If a *1D* interface of the *condensate* is created from a cell edge and not from an interface in a mixed cell, then the *2D/3D* normal vector associated with is naturally taken as the cell edge normal vector,
- the *condensate* description is completed by two outgoing fluxes, on the left and right side. These fluxes are single phase *FVCF* fluxes calculated before the *condensate* creation. At this stage, informations concerning the Eulerian mesh are no longer necessary to update *condensate* variables values at time t^{nx}.

Remark 18. *This approach is not restricted to two materials flows. This can be easily extended to $nm > 2$ materials flows, because the scheme only uses physical variables of each material, as density, velocity, internal energy, sound speed, pressure, but never an average of these variables.*

2.3.3 Evolution in a *condensate*

The evolution of *condensate* variables is *1D*, but using *2D/3D* information. Three types of layers exist in the *condensate* :

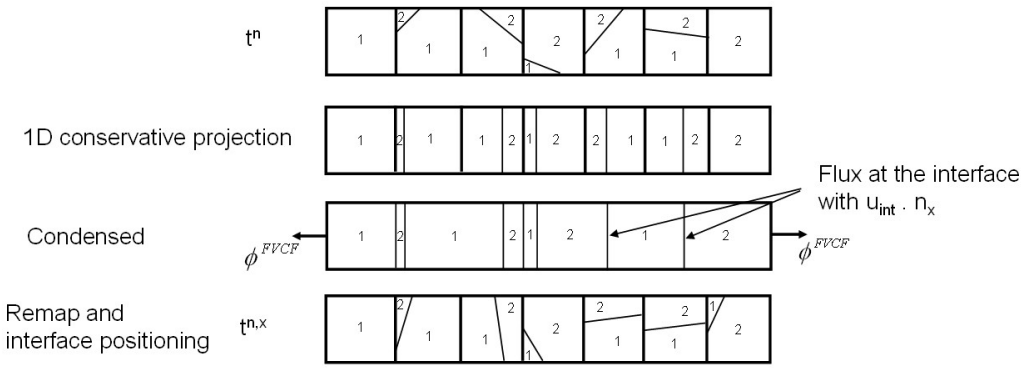

FIG. 2.3 – Treatment of neighboring mixed cells by using a *condensate*.

- the first layer ($k = 1$) has an interface on the left side that does not move and where a single phase outgoing flux is imposed. The interface on the right side is moving,
- internal layers ($1 < k < nc$) have moving interfaces on the left and right sides,
- the last layer ($k = nc$) has an interface on the right side that does not move and where a single phase outgoing flux is imposed. The interface on the left side is moving.

Let us describe the calculation of *condensate* variables at time t^{nx} from those at time t^n in x direction phase. Superscript $n+1$ denotes generically the result at the end of each directional step :

- first layer $k = 1$:

$$\frac{Vol_1^{n+1}V_1^{n+1} - Vol_1^n V_1^n}{dt} + A\left(\phi_\ell + \phi_{int}^{1,2}\right) = 0, \tag{2.48}$$

- internal layers $1 < k < nc$:

$$\frac{Vol_k^{n+1}V_k^{n+1} - Vol_k^n V_k^n}{dt} + A\left(\phi_{int}^{k,k-1} + \phi_{int}^{k,k+1}\right) = 0, \tag{2.49}$$

- last layer $k = nc$:

$$\frac{Vol_{nc}^{n+1}V_{nc}^{n+1} - Vol_{nc}^n V_{nc}^n}{dt} + A\left(\phi_{int}^{nc,nc-1} + \phi_r\right) = 0, \tag{2.50}$$

where Vol_k^n denotes the volume, $V_k^n = (\rho_k^n, \rho_k^n\ u_k^n, \rho_k^n\ E_k^n)^t$ the variable vector in layer k at time t^n obtained in section 2.3.2 by conservative averaging of merged layer variables, see equations (2.30). Fluxes ϕ_ℓ and ϕ_r are the prescribed outgoing fluxes at the *condensate* boundaries, $\phi_{int}^{i,j} = p_{int}^{i,j}\ (0, n_{1D}^{i,j}, u_{int}^{i,j} \cdot n_{1D}^{i,j})^t$ the flux through the moving interface between layers i and j, with $n_{1D}^{i,j}$ the x axis unit vector in x direction step, from layer i to layer j. In next sections, detailed calculations are provided for each variable.

Calculation of layer masses

Masses m^{n+1} at time t^{n+1} are known independently of layers volumes. They only depend on mass fluxes at the left and the right boundary of the *condensate* :

$$\begin{aligned} m_1^{n+1} &= m_1^n - dtA\phi_\ell(1), \\ m_k^{n+1} &= m_k^n, \\ m_{nc}^{n+1} &= m_{nc}^n - dtA\phi_r(1). \end{aligned}$$

with ϕ the $FVCF$ numerical flux, which components stands for $(\rho u, \rho u \otimes u + p, (\rho E + p)u)$. These masses are positive if the CFL condition is fulfilled. This is satisfied because the first and last layer contain at least a pure cell.

Calculation of layer volumes

Layer volume evolution in the *condensate* is given by interface velocities :

$$\left\{ \begin{array}{rcl} Vol_1^{n+1} &=& Vol_1^n + dt\ A\ (u_{int,x}^{1,2}), \\ Vol_k^{n+1} &=& Vol_k^n + dt\ A\ (u_{int,x}^{k,k+1} - u_{int,x}^{k-1,k}), \\ Vol_{nc}^{n+1} &=& Vol_{nc}^n + dt\ A\ (-u_{int,x}^{nc-1,nc}). \end{array} \right. \tag{2.51}$$

Calculation of layer velocities and total energies

Let us introduce two notations for each layer k :

$$\theta_k = \frac{m_k^n}{m_k^{n+1}}, \quad \text{and} \quad \kappa_k = \frac{Vol_k^n}{dtA} \tag{2.52}$$

Extracting equations for the velocity u_k in x direction, for the velocity v_k in y direction and for the total energy E_k in equations (2.48), (2.49) and (2.50),

we obtain :

$$\left\{\begin{array}{rcl} u_1^{n+1} &=& \theta_1\left(u_1^n - \dfrac{p_{int,x}^{1,2}+\phi_\ell(2)}{\rho_1^n\kappa_1}\right)\\ u_k^{n+1} &=& u_k^n - \dfrac{p_{int,x}^{k,k+1}-p_{int,x}^{k-1,k}}{\rho_k^n\kappa_k}\\ u_{nc}^{n+1} &=& \theta_{nc}\left(u_{nc}^n - \dfrac{\phi_r(2)-p_{int,x}^{nc,nc-1}}{\rho_{nc}^n\kappa_{nc}}\right)\end{array}\right. \tag{2.53}$$

$$\left\{\begin{array}{rcl} v_1^{n+1} &=& \theta_1\left(v_1^n - \dfrac{\phi_\ell(3)}{\rho_1^n\kappa_1}\right)\\ v_k^{n+1} &=& v_k^n\\ v_{nc}^{n+1} &=& \theta_{nc}\left(v_{nc}^n - \dfrac{\phi_r(3)}{\rho_{nc}^n\kappa_{nc}}\right)\end{array}\right. \tag{2.54}$$

$$\left\{\begin{array}{rcl} E_1^{n+1} &=& \theta_1\left(E_1^n - \dfrac{p_{int,x}^{1,2}u_{int,x}^{1,2}+\phi_\ell(4)}{\rho_1^n\kappa_1}\right)\\ E_k^{n+1} &=& E_k^n - \dfrac{p_{int,x}^{k,k+1}u_{int,x}^{k,k+1}-p_{int,x}^{k-1,k}u_{int,x}^{k-1,k}}{\rho_k^n\kappa_k}\\ E_{nc}^{n+1} &=& \theta_{nc}\left(E_{nc}^n - \dfrac{\phi_r(4)-p_{int,x}^{nc,nc-1}u_{int,x}^{nc-1,nc}}{\rho_{nc}^n\kappa_{nc}}\right)\end{array}\right. \tag{2.55}$$

Calculation of interface pressure and velocity in 2D

Interface pressure and velocity in $1D$ are given in Section 2.3.1 :

$$\left\{\begin{array}{ll} p_{int}^{\ell,r} = \dfrac{\rho_r\tilde{c}_r p_\ell + \rho_\ell\tilde{c}_\ell p_r}{\rho_\ell\tilde{c}_\ell+\rho_r\tilde{c}_r} & +\rho_\ell\tilde{c}_\ell\rho_r\tilde{c}_r\dfrac{u_\ell-u_r}{\rho_\ell\tilde{c}_\ell+\rho_r\tilde{c}_r}\\ u_{int}^{\ell,r} = \dfrac{\rho_\ell\tilde{c}_\ell u_\ell + \rho_r\tilde{c}_r u_r}{\rho_\ell\tilde{c}_\ell+\rho_r\tilde{c}_r} & +\dfrac{p_\ell-p_r}{\rho_\ell\tilde{c}_\ell+\rho_r\tilde{c}_r},\end{array}\right. \tag{2.56}$$

with $\tilde{c}_i = \min(c_i, \kappa_i)$ in layer i and $\kappa_i = \dfrac{Vol_i^n}{dt\_A}$. The *2D/3D* interface is in general not parallel with mesh directions. *1D* formulae are then written in the *2D/3D* direction of the interface normal vector $n^{\ell,r}$ as follows :

$$n^{\ell,r}\cdot n_{1D}^{\ell,r} \geq 0, \tag{2.57}$$

with $n_{1D}^{\ell,r}$ the x axis unit vector in x direction step, from layer ℓ to layer r. In the next definition, the perfect sliding of materials is settled.

Definition : In *2D/3D*, when contact condition between two materials is perfect sliding, the pressure gradient $\nabla p_{int}^{\ell,r}$ and the velocity $u_{int}^{\ell,r}$ at the interface have only a normal component and no tangential components.
Therefore, we define the pressure gradient and the velocity at the interface as follows using (2.3.1) :

$$\left\{ \begin{array}{ll} \nabla p_{int}^{\ell,r} = & \left(p_{int}^{\ell r} - \dfrac{\rho_r \tilde{c}_r p_\ell + \rho_\ell \tilde{c}_\ell p_r}{\rho_\ell \tilde{c}_\ell + \rho_r \tilde{c}_r} \right) n^{\ell r}, \\ u_{int}^{\ell r} = & (u_{int}^{\ell r} \cdot n^{\ell r})\ n^{\ell r}. \end{array} \right. \tag{2.58}$$

Then $1D$ formulae (2.41) can be rewritten along the interface normal vector as follows :

$$\left\{ \begin{array}{ll} \nabla p_{int}^{\ell r} \cdot n^{\ell r} & = \rho_\ell \tilde{c}_\ell \rho_r \tilde{c}_r \dfrac{u_\ell - u_r}{\rho_\ell \tilde{c}_\ell + \rho_r \tilde{c}_r} \cdot n^{\ell r}, \\ u_{int}^{\ell r} \cdot n^{\ell r} & = \dfrac{\rho_\ell \tilde{c}_\ell u_\ell + \rho_r \tilde{c}_r u_r}{\rho_\ell \tilde{c}_\ell + \rho_r \tilde{c}_r} \cdot n^{\ell r} + \dfrac{p_\ell - p_r}{\rho_\ell \tilde{c}_\ell + \rho_r \tilde{c}_r}. \end{array} \right. \tag{2.59}$$

with $u_{int}^{\ell r}$ the *2D/3D* interface velocity, $n^{\ell r} = (n_x^{\ell r}, n_y^{\ell r}, n_z^{\ell r})^t$ the *2D/3D* interface normal unit vector, p^ℓ and p^r pressures, u^ℓ and u^r velocity vectors in left and right layers.

This result is fully *2D/3D*. The hypothesis taken for the multidimensional approach consists in writing the scheme in such a way that the interface evolves direction by direction. Therefore, in x direction step, the interface motion is *1D* only along x axis. The *2D/3D* interface pressure gradient $\nabla p_{int}^{\ell r}$ and velocity $u_{int}^{\ell r}$ are projected on the x axis to obtain the interface pressure and velocity in x direction step :

$$\left\{ \begin{array}{ll} p_{int,x}^{\ell r} = & \dfrac{\rho_r \tilde{c}_r p_\ell + \rho_\ell \tilde{c}_\ell p_r}{\rho_\ell \tilde{c}_\ell + \rho_r \tilde{c}_r} + \left(\rho_\ell \tilde{c}_\ell \rho_r \tilde{c}_r \dfrac{u_\ell - u_r}{\rho_\ell \tilde{c}_\ell + \rho_r \tilde{c}_r} \cdot n^{\ell r} \right)\ n_x^{\ell r}, \\ u_{int,x}^{\ell r} = & \left(\dfrac{\rho_\ell \tilde{c}_\ell u_\ell + \rho_r \tilde{c}_r u_r}{\rho_\ell \tilde{c}_\ell + \rho_r \tilde{c}_r} \cdot n^{\ell r} + \dfrac{p_\ell - p_r}{\rho_\ell \tilde{c}_\ell + \rho_r \tilde{c}_r} \right)\ n_x^{\ell r}. \end{array} \right. \tag{2.60}$$

Unfortunately, these formulae do not satisfy contact discontinuity conditions for the velocity. Considering an uniform velocity field u_0 along the x axis and an uniform field of pressure p_0, interface velocity and pressure are :

$$\left\{ \begin{array}{l} p_{int,x}^{\ell r} = p_0, \\ u_{int,x}^{\ell r} = u_0\ (n_x^{\ell r})^2. \end{array} \right. \tag{2.61}$$

To cure this problem, we will use an alternative formulation for the $1D$ step interface motion, which preserves contact discontinuity and provides the same result, considering all steps of the directional splitting.

Proposition 19. *Let us assume that the normal unit vector at the interface does not change during the time step dt. Therefore interfaces at time t^n and t^{n+1} are parallel. Let us consider a point M_0 on the interface at time t^n. The position of the point M_1 on the interface at time t^{n+1} is obtained using (2.60) by :*

$$\overrightarrow{M_0M_1} = dt \ \left(\left(\frac{\rho_\ell \tilde{c}_\ell u_\ell + \rho_r \tilde{c}_r u_r}{\rho_\ell \tilde{c}_\ell + \rho_r \tilde{c}_r} \cdot n^{\ell r} \right) \ n^{\ell r} + \frac{p_\ell - p_r}{\rho_\ell \tilde{c}_\ell + \rho_r \tilde{c}_r} \ n^{\ell r} \right) \tag{2.62}$$

Let us consider the point M_2 defined by :

$$\overrightarrow{M_0M_2} = dt \ \left(\frac{\rho_\ell \tilde{c}_\ell u_\ell + \rho_r \tilde{c}_r u_r}{\rho_\ell \tilde{c}_\ell + \rho_r \tilde{c}_r} + \frac{p_\ell - p_r}{\rho_\ell \tilde{c}_\ell + \rho_r \tilde{c}_r} \ n^{\ell r} \right) \tag{2.63}$$

For each point M_0 on the interface at time t^n, the line defined by M_1 and the normal vector n and the line defined by M_2 and the normal vector n are the same line defining the interface at time t^{n+1}. M_1 and M_2 have the same projection on the normal. Therefore, interface position at time t^{n+1} obtained using $1D$ steps is the same as if using the following $1D$ interface pressure and velocity formulation in the generic x direction step :

$$\left\{ \begin{array}{rcl} p^{\ell r}_{int,x} = & \dfrac{\rho_r \tilde{c}_r p_\ell + \rho_\ell \tilde{c}_\ell p_r}{\rho_\ell \tilde{c}_\ell + \rho_r \tilde{c}_r} + \left(\rho_\ell \tilde{c}_\ell \rho_r \tilde{c}_r \dfrac{u_\ell - u_r}{\rho_\ell \tilde{c}_\ell + \rho_r \tilde{c}_r} \cdot n^{\ell r} \right) \ n^{\ell r}_x \\ u^{\ell r}_{int,x} = & \dfrac{\rho_\ell \tilde{c}_\ell u_{\ell,x} + \rho_r \tilde{c}_r u_{r,x}}{\rho_\ell \tilde{c}_\ell + \rho_r \tilde{c}_r} + \dfrac{p_\ell - p_r}{\rho_\ell \tilde{c}_\ell + \rho_r \tilde{c}_r} \ n^{\ell r}_x . \end{array} \right. \tag{2.64}$$

Proof :
Since normal unit vectors $n^{\ell r}$ at the interface are the same at time t^n and t^{n+1}, we will show that vector $\overrightarrow{M_1M_2}$ is orthogonal with vector $n^{\ell r}$. Thus M_1 and M_2 are on the same line.

$$\begin{array}{rcl} \overrightarrow{M_1M_2} \cdot n^{\ell r} & = & -\overrightarrow{M_0M_1} \cdot n^{\ell r} + \overrightarrow{M_0M_2} \cdot n^{\ell r} \\ & = & -\left(\dfrac{\rho_\ell \tilde{c}_\ell u_\ell + \rho_r \tilde{c}_r u_r}{\rho_\ell \tilde{c}_\ell + \rho_r \tilde{c}_r} \cdot n^{\ell r} \right) \ n^{\ell r} \cdot n^{\ell r} - \dfrac{p_\ell - p_r}{\rho_\ell \tilde{c}_\ell + \rho_r \tilde{c}_r} \ n^{\ell r} \cdot n^{\ell r} \\ & & + \dfrac{\rho_\ell \tilde{c}_\ell u_\ell + \rho_r \tilde{c}_r u_r}{\rho_\ell \tilde{c}_\ell + \rho_r \tilde{c}_r} \cdot n^{\ell r} + \dfrac{p_\ell - p_r}{\rho_\ell \tilde{c}_\ell + \rho_r \tilde{c}_r} \ n^{\ell r} \cdot n^{\ell r} \\ & = & 0 \end{array}$$

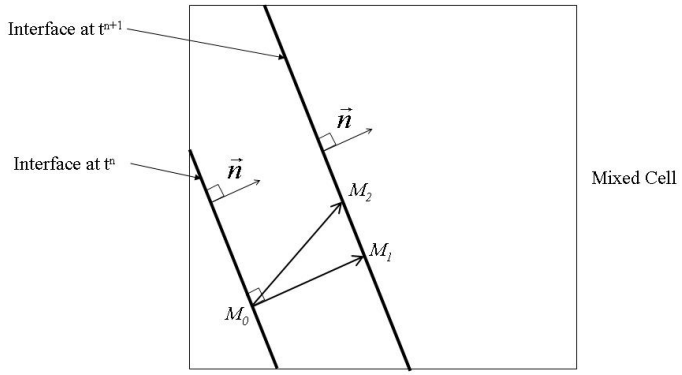

FIG. 2.4 – Equivalence between formulations (2.60) and (2.64) for interface velocity.

because $\|n^{\ell r}\| = 1$.

Therefore, one can use formulation (2.64) that preserves contact discontinuity in $1D$ steps, instead of formulation (2.60) which does not.

Remark 20. *We assume that normal unit vector does not change between the directional steps. This is not restrictive, because with both formulae, normal vectors are calculated at the end of each directional step and potentially change. The important points are to preserve contact discontinuities and to be consistant.*

2.3.4 Entropy condition in 2D

We first introduce a formal condition on the time step which guarantees entropy growth.

Proposition 21. *Let us define a closure law for p_{int} and u_{int} at an interface, as a function of layer pressure, velocity, sound speed, interface normal or whatever. We suggest a closure in (2.64).*

Let us consider the case of a layer i between two moving interfaces, with $+$ and $-$ respectively denotes right and left interface. The layer evolution between t^n and t^{n+1} will be "entropic" meaning that the discrete entropy inequality (2.42) holds :

$$T_i^n(s_i^{n+1} - s_i^n) = e_i^{n+1} - e_i^n + p_i^n \left(\frac{1}{\rho_i^{n+1}} - \frac{1}{\rho_i^n} \right) \geq 0,$$

when

$$dt \leq \frac{dx_i}{c_i^{\pm}}$$

with notations :

$$dx_i = \frac{Vol_i^n}{A},$$
$$c_i^+ = -\frac{\delta p^+}{\rho_i^n \delta u^+}, \qquad c_i^- = \frac{\delta p^-}{\rho_i^n \delta u^-},$$
$$\delta p^+ = p_{int}^+ - p_i^n, \qquad \delta p^- = p_i^n - p_{int}^-,$$
$$\delta u^+ = u_{int}^+ - u_i^n, \qquad \delta u^- = u_i^n - u_{int}^-.$$

Proof : The variable vector V^{n+1} at time t^{n+1} in layer i, dropping the subscript i, reads as :

$$\frac{Vol^{n+1}V^{n+1} - Vol^n V^n}{dt} + A\left(\phi_{int}^+ + \phi_{int}^-\right) = 0,$$

with the flux $\phi_{int}^{\pm} = (0, p_{int}^{\pm} n_{int}^{\pm}, p_{int}^{\pm}(u_{int}^{\pm} \cdot n_{int}^{\pm}))^t$ where $+$ and $-$ denotes respectively right and left interfaces.
Explicitly, for each quantity, we have :

$$\begin{aligned}
Vol_i^{n+1} &= Vol_i^n + dtA\ (u_{int}^+ - u_{int}^-) \\
m_i^{n+1} &= m_i^n \\
\rho_i^{n+1} &= \frac{\rho_i^n}{1 + \dfrac{u_{int}^+ - u_{int}^-}{\kappa_i}} \\
u_i^{n+1} &= u_i^n - \frac{p_{int}^+ - p_{int}^-}{\rho_i^n \kappa_i} \\
v_i^{n+1} &= v_i^n \\
E_i^{n+1} &= E_i^n - \frac{p_{int}^+ u_{int}^+ - p_{int}^- u_{int}^-}{\rho_i^n \kappa_i} \\
e_i^{n+1} &= E_i^{n+1} - \frac{1}{2}\left((u_i^{n+1})^2 + (v_i^{n+1})^2\right)
\end{aligned}$$

with respectively u^+_{int} and u^-_{int} interface velocity at right and at left of layer i, interface pressures p^+_{int} and p^-_{int}.
Following proposition (11) :

$$\begin{aligned} T^n_i(s^{n+1}_i - s^n_i) &= e^{n+1}_i - e^n_i + p^n_i \left(\frac{1}{\rho^{n+1}_i} - \frac{1}{\rho^n_i} \right) \\ &= -\frac{\delta p^+ \delta u^+ - \delta p^- \delta u^-}{\rho^n_i \kappa_i} - \frac{1}{2} \left(\frac{\delta p^+ + \delta p^-}{\rho^n_i \kappa_i} \right)^2 \end{aligned}$$

with the notation :

$$\delta p^+ = p^+_{int} - p^n_i, \qquad \delta p^- = p^n_i - p^-_{int},$$

$$\delta u^+ = u^+_{int} - u^n_i, \qquad \delta u^- = u^n_i - u^-_{int}.$$

Let us change the set of variables $(\delta p^+, \delta u^+)$ and $(\delta p^-, \delta u^-)$ to the following :

$$x = \frac{\delta p^+}{\rho^n_i \kappa_i}, \qquad \xi^+ = -\frac{\delta p^+}{\rho^n_i \kappa_i \delta u^+},$$

$$y = \frac{\delta p^-}{\rho^n_i \kappa_i}, \qquad \xi^- = \frac{\delta p^-}{\rho^n_i \kappa_i \delta u^-},$$

yielding $\delta p^+ + \xi^+ \rho^n_i \kappa_i \delta u^+ = 0$ and $\delta p^- - \xi^- \rho^n_i \kappa_i \delta u^- = 0$.
Therefore we can write :

$$\begin{aligned} T^n_i(s^{n+1}_i - s^n_i) &= \frac{x^2}{\xi^+} + \frac{y^2}{\xi^-} - \frac{1}{2}(x-y)^2 \\ &= \frac{1}{2}(x\ y) \begin{pmatrix} \frac{2}{\xi^+} - 1 & 1 \\ 1 & \frac{2}{\xi^-} - 1 \end{pmatrix} \begin{pmatrix} x \\ y \end{pmatrix} \end{aligned} \tag{2.65}$$

If we can diagonalize the matrix, calculating eigenvalues λ^+ and λ^-, thus we obtain the result :

$$\begin{aligned} T^n_i(s^{n+1}_i - s^n_i) &= \frac{1}{2}(X\ Y) \begin{pmatrix} \lambda^+ & 0 \\ 0 & \lambda^- \end{pmatrix} \begin{pmatrix} X \\ Y \end{pmatrix} \\ &= \frac{1}{2}\left(\lambda^+ X^2 + \lambda^- Y^2\right) \end{aligned} \tag{2.66}$$

A direct calculation yields :

$$\begin{aligned} \Delta &= \left(\frac{1}{\xi^+} - \frac{1}{\xi^-}\right)^2 + 1 \geq 0 \\ \lambda^+ &= \left(\frac{1}{\xi^+} + \frac{1}{\xi^-} - 1\right) + \sqrt{\Delta} \\ \lambda^- &= \left(\frac{1}{\xi^+} + \frac{1}{\xi^-} - 1\right) - \sqrt{\Delta} \end{aligned} \tag{2.67}$$

Both eigenvalues have to be positive and we have $\lambda^+ \geq \lambda^-$.

If we can guarantee that :

$$1 \geq \xi^{\pm} \geq 0 \tag{2.68}$$

Then :

$$\left(\frac{1}{\xi^+} + \frac{1}{\xi^-} - 1\right) \geq 0.$$

Moreover, considering that :

$$\begin{aligned} & \left(\frac{1}{\xi^+} + \frac{1}{\xi^-} - 1\right)^2 \geq \Delta \\ \Leftrightarrow \quad & \frac{2 - \xi^+ - \xi^-}{\xi^+ \, \xi^-} \geq 0 \end{aligned}$$

thus the condition $\lambda^+ \geq \lambda^- \geq 0$ is fulfilled.

Condition (2.68) is equivalent to the lagrangian CFL condition (2.40) on something we could call "effective" sound speeds $c_i^{\pm}$ by direction of the splitting. Whatever the model to calculate pressures and velocities at interfaces, one can calculate :

$$c_i^+ = -\frac{\delta p^+}{\rho_i^n \delta u^+}, \; c_i^- = \frac{\delta p^-}{\rho_i^n \delta u^-}, \tag{2.69}$$

Note that $\xi_i^{\pm} = \dfrac{c_i^{\pm}}{\kappa_i}$.
Entropy condition (2.68) can be written in this form :

$$0 \leq c_i^{\pm} \leq \kappa_i \tag{2.70}$$

equivalent to

$$dt \leq \frac{dx_i}{c_i^{\pm}}$$

with $\kappa_i = \dfrac{Vol_i^n}{dt\ A}$ and $dx_i = \dfrac{Vol_i^n}{A}$.

Entropy dissipation rate condition

We now try to apply Proposition (21) to two basic situations

In the $1D$ case, interface pressure and velocity were given in section (2.3.1) by :

$$\begin{array}{l} \delta p^+ + \rho_i \tilde{c}_i \delta u^+ = 0, \\ \delta p^- - \rho_i \tilde{c}_i \delta u^- = 0, \end{array} \tag{2.71}$$

with $\tilde{c}_i = \min(c_i, \kappa_i)$, c_i the sound speed in layer i and $\kappa_i = dx_i/dt$.
In this case, $c_i^+ = c_i^- = \tilde{c}_i$, thus the entropy condition (2.70) is satisfied for any time step dt :

$$0 \leq c_i^{\pm} = \min(c_i, \kappa_i) \leq \kappa_i.$$

We recognize the result of Proposition (11) in section 2.3.1, that entropy is increasing for any time step dt in $1D$.

In the $2D/3D$ case, let us investigate the properties of equations (2.64) on entropy during one step of the directional splitting, generically x. We will simplify these equations omitting transversal velocity terms. This is still relevant for this study, because the pathology is related to the projection of the $2D/3D$ problem on one axis.
With this, (2.64) writes :

$$\left\{ \begin{array}{rl} p_{int,x}^{\ell r} = & \dfrac{\rho_r \tilde{c}_r p_\ell + \rho_\ell \tilde{c}_\ell p_r}{\rho_\ell \tilde{c}_\ell + \rho_r \tilde{c}_r} + \rho_\ell \tilde{c}_\ell \rho_r \tilde{c}_r \dfrac{u_{\ell,x} - u_{r,x}}{\rho_\ell \tilde{c}_\ell + \rho_r \tilde{c}_r} \ (n_x^{\ell r})^2 \\ u_{int,x}^{\ell r} = & \dfrac{\rho_\ell \tilde{c}_\ell u_{\ell,x} + \rho_r \tilde{c}_r u_{r,x}}{\rho_\ell \tilde{c}_\ell + \rho_r \tilde{c}_r} + \dfrac{p_\ell - p_r}{\rho_\ell \tilde{c}_\ell + \rho_r \tilde{c}_r} \ n^{\ell r}. \end{array} \right. \tag{2.72}$$

for an interface between left and right layers ℓ and r. Subscript x will be dropped hereafter.

Let us introduce the expression of (p^+_{int}, u^+_{int}) between layers i and $i+1$ and (p^-_{int}, u^-_{int}) between layers $i-1$ and i using equations (2.72), without the subscript x for velocities component and superscript n for all magnitudes at time t^n :

$$\left\{\begin{array}{rcl} p^+_{int} = & \dfrac{\rho_{i+1}\tilde{c}_{i+1}p_i + \rho_i\tilde{c}_i p_{i+1}}{\rho_i\tilde{c}_i + \rho_{i+1}\tilde{c}_{i+1}} + \rho_i\tilde{c}_i\rho_{i+1}\tilde{c}_{i+1}\dfrac{u_i - u_{i+1}}{\rho_i\tilde{c}_i + \rho_{i+1}\tilde{c}_{i+1}}\ (n^{i\,i+1})^2, \\ u^+_{int} = & \dfrac{\rho_i\tilde{c}_i u_i + \rho_{i+1}\tilde{c}_{i+1}u_{i+1}}{\rho_i\tilde{c}_i + \rho_{i+1}\tilde{c}_{i+1}} + \dfrac{p_i - p_{i+1}}{\rho_i\tilde{c}_i + \rho_{i+1}\tilde{c}_{i+1}}\ n^{i\,i+1}, \end{array}\right.$$

and

$$\left\{\begin{array}{rcl} p^-_{int} = & \dfrac{\rho_i\tilde{c}_i p_{i-1} + \rho_{i-1}\tilde{c}_{i-1}p_i}{\rho_{i-1}\tilde{c}_{i-1} + \rho_i\tilde{c}_i} + \rho_{i-1}\tilde{c}_{i-1}\rho_i\tilde{c}_i\dfrac{u_{i-1} - u_i}{\rho_{i-1}\tilde{c}_{i-1} + \rho_i\tilde{c}_i}\ (n^{i-1\,i})^2, \\ u^-_{int} = & \dfrac{\rho_{i-1}\tilde{c}_{i-1}u_{i-1} + \rho_i\tilde{c}_i u_i}{\rho_{i-1}\tilde{c}_{i-1} + \rho_i\tilde{c}_i} + \dfrac{p_{i-1} - p_i}{\rho_{i-1}\tilde{c}_{i-1} + \rho_i\tilde{c}_i}\ n^{i-1\,i}. \end{array}\right.$$

By using notations :

$$\delta p^+ = p^+_{int} - p_i, \qquad \delta p^- = p_i - p^-_{int},$$
$$\delta u^+ = u^+_{int} - u_i, \qquad \delta u^- = u_i - u^-_{int},$$

we can calculate $c_i^\pm$ corresponding to the entropy condition (2.70) :

$$\begin{array}{l} c_i^+ = -\dfrac{\delta p^+}{\rho_i^n \delta u^+}, \\ c_i^- = \dfrac{\delta p^-}{\rho_i^n \delta u^-}. \end{array} \tag{2.73}$$

We obtain the following expressions :

$$\begin{array}{rcl} c_i^+ & = & \tilde{c}_i\dfrac{(p_{i+1} - p_i) - \rho_{i+1}\tilde{c}_{i+1}(u_{i+1} - u_i)\ (n^{i\,i+1})^2}{(p_{i+1} - p_i)\ n^{i\,i+1} - \rho_{i+1}\tilde{c}_{i+1}(u_{i+1} - u_i)}, \\ c_i^- & = & \tilde{c}_i\dfrac{(p_i - p_{i-1}) + \rho_{i-1}\tilde{c}_{i-1}(u_i - u_{i-1})\ (n^{i-1\,i})^2}{(p_i - p_{i-1})\ n^{i-1\,i} + \rho_{i-1}\tilde{c}_{i-1}(u_i - u_{i-1})}. \end{array} \tag{2.74}$$

with $\tilde{c}_i = \min(c_i, \kappa_i)$, c_i the sound speed in layer i and $\kappa_i = dx_i/dt$.

- In the case of $n^{i\,i+1} = n^{i-1\,i} = 1$, then we have $0 \leq c_i^{\pm} = \tilde{c}_i \leq \kappa_i$, thus entropy conditions (2.70) are satisfied.
- In the case of $n^{i\,i+1} = 0$ and $n^{i-1\,i} = 0$, we have

$$\begin{aligned} c_i^+ &= \tilde{c}_i \frac{(p_{i+1} - p_i)}{-\rho_{i+1}\tilde{c}_{i+1}(u_{i+1} - u_i)}, \\ c_i^- &= \tilde{c}_i \frac{(p_i - p_{i-1})}{\rho_{i-1}\tilde{c}_{i-1}(u_i - u_{i-1})}. \end{aligned} \tag{2.75}$$

  Entropy condition (2.70) is then not satisfied in general in this case.
- In the case of $\tilde{c}_i = \kappa_i \approx 0$ in very small layers, we have

$$\begin{aligned} c_i^+ &= \frac{\tilde{c}_i}{n^{i\,i+1}}, \\ c_i^- &= \frac{\tilde{c}_i}{n^{i-1\,i}}. \end{aligned} \tag{2.76}$$

  Entropy condition (2.70) is then not satisfied in general in this case.

Remark 22. *Unfortunately, we could not find a 2D expression for interface pressure and velocity that always satisfies this entropy condition. Even if we had found an expression with this property, it would not have ensured a good behavior of all quantities when in small layers the CFL condition (2.40) is not fulfilled. This will be discussed later while revisiting the CFL condition in section 2.4.*

2.3.5 Remapping of a *condensate*

Condensate variables calculated during x direction step are remapped, that is to say variables in cells at time t^n that were extracted from the Eulerian mesh to constitute the *condensate* are updated with values calculated in the condensate at time t^{nx}, end time of the x direction step. Interface positions in the *condensate* give the nature of cells, mixed or pure, at time t^{nx}. Partial volumes in each mixed cell is determined according to *1D* interface positions at time t^{nx}. The ordering of materials in the mixed cell is obvious in x direction by construction of the *condensate* successive layers. The ordering in y direction could have changed during x direction step. In a mixed cell C, it is given at t^{nx} by volume fractions in neighboring cells, C_{up} up and C_{down} down in y direction :

- if the volume fraction of material 1 in cell C_{up} is larger than the one in C_{down}, then the material 1 is on the upper part of the mixed cell,
- if the volume fraction of material 1 in cell C_{down} is larger than the one in C_{up}, then the material 1 is on the lower part of the mixed cell.

2.3.6 Interface reconstruction in *2D/3D*

At time t^{nx}, mixed cells, partial volumes and materials ordering in each direction are known. The *2D/3D* normal is calculated with *Youngs* formulation [85]. It is based on an approximation of the volume fraction gradient ∇f in mixed cells, which gives the normal direction in cell i :

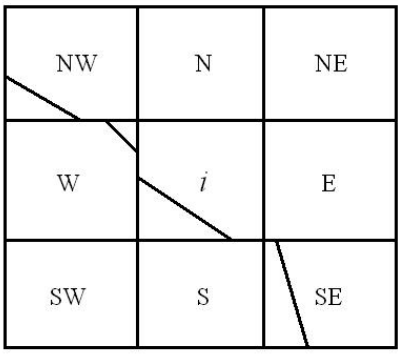

FIG. 2.5 – Neighboring of cell i in $2D$.

$$n_i = -\frac{\nabla f_i}{\|\nabla f_i\|}, \tag{2.77}$$

with $\nabla f_i = (\frac{\partial f_i}{\partial x}, \frac{\partial f_i}{\partial y})^t$ the *2D/3D* gradient of volume fraction. It is approximated by :

$$\partial_x f_i = \frac{f_E - f_W}{2 \triangle x} \quad \text{and} \quad \partial_y f_i = \frac{f_N - f_S}{2 \triangle y}, \tag{2.78}$$

where $\triangle x$ and $\triangle y$ respectively denote the x and y space steps, and

$$\begin{array}{ll} f_E = \dfrac{f_{NE} + 2f_E + f_{SE}}{4} & f_W = \dfrac{f_{NW} + 2f_W + f_{SW}}{4} \\ f_N = \dfrac{f_{NW} + 2f_N + f_{NE}}{4} & f_S = \dfrac{f_{SW} + 2f_S + f_{SE}}{4} \end{array} \tag{2.79}$$

Remark 23. *In the NIP algorithm, the explicit location of points defining the interface in a mixed cell is not required : the algorithm just needs partial volumes, materials ordering and 2D interface normal vectors.*

2.4 CFL condition

When CFL condition (2.40) is not satisfied in small layers of a condensate, the scheme cannot give an acceptable solution. The time step is computed using pure cells only, in order to avoid small time steps implied by small volumes in mixed cells. We then cannot obtain an accurate solution in very small volumes in mixed cells. However, the solution has to be controled in mixed cells in such a way that the pressure in particular, behaves as if the CFL condition was fulfilled. We mean that pressure cannot increase or decrease too much during one time step, in a sense we will describe in this section.
For this purpose, let us write the upwind scheme for the $1D$ linear advection equation

$$\frac{\partial f}{\partial t} + a\frac{\partial f}{\partial x} = 0$$

of a quantity f at constant velocity $a > 0$:

$$\begin{array}{l} \dfrac{f_i^{n+1} - f_i^n}{dt} + a\dfrac{f_i^n - f_{i-1}^n}{dx} = 0 \\ \Leftrightarrow f_i^{n+1} = \left(1 - \dfrac{a\ dt}{dx}\right) f_i^n + \left(\dfrac{a\ dt}{dx}\right) f_{i-1}^n \\ \Leftrightarrow \dfrac{f_i^{n+1} - f_i^n}{f_i^n} = -\dfrac{a\ dt}{dx} + \dfrac{a\ dt}{dx}\dfrac{f_{i-1}^n}{f_i^n} \end{array} \tag{2.80}$$

The second line shows that, when CFL condition is fulfilled, namely $dt < dx/a$, the scheme is positive and monotonic. The third line shows another aspect of the CFL condition, namely that the variation during a time step

of quantity f_i is controled. Another way of saying that is : derivatives are linearized for one time step, but the evolution of the discrete solution (f_i) of linearized equations should not go too far from the exact solution f of the continuous equation.
This is the way we choose in order to control the solution evolution when layer volumes are small and then CFL condition (2.40) is not satisfied. In this situation, we will control the evolution of quantities like pressure, density or entropy. This will couple neighboring layers and may give a way to stabilize the system even when (2.40) is violated.

2.4.1 Control of pressure evolution

Pressure is the quantity we have to control the most. Experimentally, we see that when pressure has monotonic variations, other quantities as density, velocity or internal energy are also monotonic. When using an equation of state of the form $p = P(\rho, e)$, with ρ the density and e the specific internal energy, we have no equation for p to work on. Pressure evolution in time must then be controled through the evolution of variables ρ and e :

$$dp = \left(\frac{\partial p}{\partial e}\right)_\rho de + \left(\frac{\partial p}{\partial \rho}\right)_e d\rho \tag{2.81}$$

Let us introduce the Grüneisen coefficient $\Gamma = \frac{1}{\rho}\left(\frac{\partial p}{\partial e}\right)_\rho$ and the sound speed $c^2 = \left(\frac{\partial p}{\partial \rho}\right)_s$, with s the specific entropy. Let us set $\beta = \left(\frac{\partial p}{\partial \rho}\right)_e$.
For reversible thermodynamic evolutions we have $Tds = de + pd(1/\rho)$.
Therefore

$$dp = \rho\Gamma T ds + \left(\frac{\Gamma p}{\rho} + \beta\right) d\rho,$$

and then

$$c^2 = \left(\frac{\partial p}{\partial \rho}\right)_s = \frac{\Gamma p}{\rho} + \beta.$$

Hence $\beta = c^2 - \frac{\Gamma p}{\rho}$ and then the evolution of p as a function of the evolution of ρ and e is given by :

$$\frac{dp}{p} = \left(\frac{\rho e \Gamma}{p}\right)\frac{de}{e} + \left(\frac{\rho c^2}{p} - \Gamma\right)\frac{d\rho}{\rho}. \tag{2.82}$$

The evolution of p as a function of the evolutions of ρ and s reads :

$$\frac{dp}{p} = \left(\frac{\rho\Gamma}{p}\right) Tds + \left(\frac{\rho c^2}{p}\right) \frac{d\rho}{\rho}. \tag{2.83}$$

Remark 24. *For perfect gases, $p = (\gamma - 1)\rho e$, $c^2 = \gamma p/\rho$, $\Gamma = \gamma - 1$, the relevant coefficients are :*

$$\frac{\rho e\Gamma}{p} = 1, \qquad \frac{\rho c^2}{p} - \Gamma = 1.$$

These coefficients can be very different from 1 when the material is weakly compressible for instance.

2.4.2 Discrete control of pressure evolution

At the discrete level, the only variables of the scheme we can change, without loosing conservation of layers Eulerian quantities, are interfaces pressure and velocity. The purpose of this section is to find constraints on these variables that ensure a "reasonable" evolution of p, that we define as :

$$\left|\frac{p^{n+1} - p^n}{p^n}\right| \leq 2\varepsilon \tag{2.84}$$

with $\varepsilon = 0.1$ for instance. This approach is very usual in compressible hydrodynamics computation, in particular to control density's evolution in such a way that pressure evolution is controled. Another way of saying that is to set a control of the compression rate between one step to another.
For computational efficiency, the discrete control of pressure p between t^n and t^{n+1} will be achieved with explicit values at time t^n, using expression (2.83) :

$$\frac{p^{n+1} - p^n}{p^n} \approx \left(\frac{\rho^n\Gamma^n}{p^n}\right) T^n(s^{n+1} - s^n) + \left(\frac{\rho^n(c^n)^2}{p^n}\right) \frac{\rho^{n+1} - \rho^n}{\rho^n} \tag{2.85}$$

We will exhibit the dependency of each term of this equation to interfaces pressure and velocity and control each one.

In next sections, we consider the case of a layer i between two moving interfaces, $+$ denotes the right one and $-$ denotes the left one. The case of first and last layer of the condensate will be treated in section 2.4.5.

2.4.3 Control of density's evolution

First, let us control the density's evolution in equation (2.83) as follows :

$$\left| \left(\frac{\rho^n (c^n)^2}{p^n} \right) \frac{\rho^{n+1} - \rho^n}{\rho^n} \right| \leq \varepsilon. \tag{2.86}$$

Let us write the expression of density :

$$\begin{aligned} m_i^{n+1} &= m_i^n \\ \rho_i^{n+1} &= m_i^{n+1} / Vol_i^{n+1} \\ Vol_i^{n+1} &= Vol_i^n \left(1 + \frac{\Delta(u)_i}{\kappa_i} \right) \end{aligned}$$

with m_i the mass of layer i, $\Delta(u)_i = u^+ - u^-$, $\kappa_i = Vol_i^n / dtA$.
The constraint (2.86) then writes :

$$\left| \frac{-\frac{\Delta(u)_i}{\kappa_i}}{1 + \frac{\Delta(u)_i}{\kappa_i}} \right| \leq \frac{\varepsilon p_i^n}{\rho_i^n (c_i^n)^2}.$$

Assuming that $\left| \frac{\Delta(u)_i}{\kappa_i} \right| < \varepsilon < 1$ because layer volume must be also positive, we obtain the following constraint :

$$\left| \frac{\Delta(u)_i}{\kappa_i} \right| \leq \frac{\varepsilon p_i^n}{\rho_i^n (c_i^n)^2}. \tag{2.87}$$

When this constraint is satisfied, density's evolution is controled as defined in (2.86).

We have assumed $\left| \frac{\Delta(u)_i}{\kappa_i} \right| < \varepsilon$, what is generally ensured by this constraint, because for perfect gases $\rho_i^n (c_i^n)^2 / p_i^n = \gamma_i^n > 1$. For general equations of state, we have to verify that $\rho_i^n (c_i^n)^2 / p_i^n > 1$. If this is not satisfied, we have to choose ε in such a way that $\frac{\varepsilon p_i^n}{\rho_i^n (c_i^n)^2} < 1$.

2.4.4 Control of entropy's evolution

Second, let us control entropy's evolution in equation (2.83) as follows :

$$\left| \left(\frac{\rho_i^n \Gamma_i^n}{p_i^n} \right) T_i^n (s_i^{n+1} - s_i^n) \right| \leq \varepsilon. \tag{2.88}$$

Considering the discrete expression for entropy's evolution as defined in section 2.3.1, we have :

$$T^n(s^{n+1} - s^n) = -\frac{\Delta(pu)_i - p_i^n \Delta(u)_i - u_i^n \Delta(p)_i}{\rho_i^n \kappa_i} - \frac{1}{2} \left(\frac{\Delta(p)_i}{\rho_i^n \kappa_i} \right)^2$$

and thus (2.88) is equivalent to :

$$\left(\frac{\rho_i^n \Gamma_i^n}{p_i^n} \right) \left| -\frac{\Delta(pu)_i - p_i^n \Delta(u)_i - u_i^n \Delta(p)_i}{\rho_i^n \kappa_i} - \frac{1}{2} \left(\frac{\Delta(p)_i}{\rho_i^n \kappa_i} \right)^2 \right| \leq \varepsilon \tag{2.89}$$

with the operator $\Delta(x)_i = x_i^+ - x_i^-$ and $\kappa_i = Vol_i^n / dtA$.
Let us define a velocity with an expression close from sound speed for perfect gases :

$$(\overline{c}_i^n)^2 = \frac{p_i^n}{\rho_i^n \Gamma_i^n}. \tag{2.90}$$

With this notation, (2.89) writes :

$$\left| -\frac{\Delta(pu)_i - p_i^n \Delta(u)_i - u_i^n \Delta(p)_i}{\rho_i^n \kappa_i (\overline{c}_i^n)^2} - \frac{1}{2} \left(\frac{\Delta p}{\rho_i^n \kappa_i \overline{c}_i^n} \right)^2 \right| \leq \varepsilon. \tag{2.91}$$

Both terms in this equation are second order when $\dfrac{\Delta(p)_i}{\rho_i^n \kappa_i \overline{c}_i^n}$ and $\dfrac{\Delta(u)_i}{\overline{c}_i^n}$ are small. In particular, the first term is second order :

$$\Delta(pu)_i - p_i^n \Delta(u)_i - u_i^n \Delta(p)_i = (u_i^- - u_i^n)\Delta(p)_i + (p_i^- - p_i^n)\Delta(u)_i + \Delta(p)_i \Delta(u)_i, \tag{2.92}$$

considering that $|u_i^- - u_i^n| \approx |\Delta(u)_i|$ and $|p_i^- - p_i^n| \approx |\Delta(p)_i|$ when pressure and velocity are monotonic.
The second term $\left(\dfrac{\Delta(p)_i}{\rho_i^n \kappa_i \overline{c}_i^n} \right)^2$ is obviously second order in $\dfrac{\Delta(p)_i}{\rho_i^n \kappa_i \overline{c}_i^n}$.
Nevertheless, when the Lagrangian CFL condition (2.40) in the layer i is not

fulfilled anymore, i.e. $\kappa_i = Vol_i^n/dtA \leq (c_i^n)$, the second term is dominating because it is divided by $(\kappa_i)^2$. Moreover, this term leads to a non entropic behavior, because it has always a negative sign in the entropy equation. Therefore, it is the one we choose to control by a constraint on $\Delta(p)_i$ which reads :

$$\left| -\frac{1}{2} \left(\frac{\Delta(p)_i}{\rho_i^n \kappa_i \overline{c}_i^n} \right)^2 \right| \leq \varepsilon, \tag{2.93}$$

that is

$$|\Delta(p)_i| \leq \rho_i^n \kappa_i \sqrt{\frac{2\varepsilon p_i^n}{\rho_i^n \Gamma_i^n}}. \tag{2.94}$$

With the constraint (2.94), we control in equation (2.91) the value of the second term

$$T_2 = -\frac{1}{2} \left(\frac{\Delta(p)_i}{\rho_i^n \kappa_i \overline{c}_i^n} \right)^2. \tag{2.95}$$

We have to verify that in equation (2.91), the first term

$$T_1 = -\frac{\Delta(pu)_i - p_i^n \Delta(u)_i - u_i^n \Delta(p)_i}{\rho_i^n \kappa_i (\overline{c}_i^n)^2} \tag{2.96}$$

is controled equivalently when constraint (2.94) and (2.87) are satisfied.

Using equation (2.92), let us set the following assumption :

$$\Delta(pu)_i - p_i^n \Delta(u)_i - u_i^n \Delta(p)_i \approx 3\Delta(p)_i \Delta(u)_i$$

Using constraint (2.94) on $\Delta(p)_i$ and constraint (2.87) on $\Delta(u)_i$, we obtain a control of the first term :

$$|T_1| \approx \left| 3 \frac{\Delta(p)_i \Delta(u)_i}{\rho_i^n \kappa_i (\overline{c}_i^n)^2} \right| \leq 3\ \varepsilon \frac{\kappa_i}{(c_i^n)^2} \sqrt{\frac{2\varepsilon \Gamma_i^n p_i^n}{\rho_i^n}} = 3\ \varepsilon \frac{\kappa_i}{c_i^n} \frac{\overline{c}_i^n}{c_i^n} \sqrt{2\varepsilon} \tag{2.97}$$

In the case of perfect gases, we have $p = (\gamma - 1)\rho e$, $c^2 = \gamma p/\rho$, $\Gamma = \gamma - 1$ and thus inequality (2.97) reads :

$$|T_1| \leq 3\ \varepsilon \frac{\kappa_i}{c_i^n} \sqrt{2\varepsilon \frac{\gamma_i^n - 1}{\gamma_i^n}} \tag{2.98}$$

We see that in the case of perfect gases, the more the lagrangian CFL condition (2.40) in the layer i is violated, i.e. $\kappa_i = Vol_i^n/dtA \leq (c_i^n)$, the more this

term is controled. We suppose that this good property is kept for general equations of state, because the order of magnitudes of physical quantities should not change drastically.

We obtain that when constraints (2.94) and (2.87) are satisfied, thus both terms T_1 (2.96) and T_2 (2.95) are controled. We finally obtain a control of entropy evolution slightly different than the control initially aimed in (2.88) but sufficiently constraining to obtain a reasonable behavior of pressure in the sense of (2.84).

2.4.5 Extension to boundary layers

Conditions (2.87) and (2.94) to control density and entropy's evolution are established for internal layers, i.e. layers between two moving interfaces. We need to extend these conditions to first and last layers of the condensate where an Eulerian flux is prescribed through the condensate boundaries, which are cell faces.
Let us consider the first layer of a condensate in the x direction phase of the directional splitting. The left interface is a cell face with a flux ϕ^ℓ going through, defined with the outgoing normal vector, from right to left. The left interface is a moving interface at velocity $u^+_{int,x}$ and with pressure $p^+_{int,x}$ defined by equations (2.64), with a flux $\phi^+_{int,x} = (0, p^+_{int}, p^+_{int,x}\ u^+_{int,x}))^t$ going through, defined with the outgoing normal vector n^+_{int}, from left to right.

First layer variables evolution is given by the following relations :

$$\begin{aligned}
Vol_1^{n+1} &= Vol_1^n + dtA\ (u_{int,x}^+) \\
m_1^{n+1} &= m_1^n - dtA\ \phi^\ell(1) \\
\theta_1 &= \frac{m_1^n}{m_1^{n+1}} \\
\rho_1^{n+1} &= \frac{\rho_1^n}{\theta_1(1+\frac{u_{int,x}^+}{\kappa_1})} \\
u_1^{n+1} &= \theta_1\left(u_1^n - \frac{p_{int,x}^+ + \phi^\ell(2)}{\rho_1^n\kappa_1}\right) \\
v_1^{n+1} &= \theta_1\left(v_1^n - \frac{\phi^\ell(3)}{\rho_1^n\kappa_1}\right) \\
E_1^{n+1} &= \theta_1\left(E_1^n - \frac{p_{int,x}^+ u_{int,x}^+ + \phi^\ell(4)}{\rho_1^n\kappa_1}\right) \\
e_1^{n+1} &= E_1^{n+1} - \frac{1}{2}\left((u_1^{n+1})^2 + (v_1^{n+1})^2\right)
\end{aligned}$$

with A the transverse section of the condensate, $\kappa_1 = \dfrac{Vol_1^n}{dt\ A}$, $\phi^\ell(i)$ the coordinate i of the flux ϕ^ℓ.

Control of density's evolution

Let us define $\Delta(u)_1 = u_{int,x}^+$ the velocity difference in the first layer. Thus we can calculate density's relative evolution, which transforms (2.87) into :

$$\left|\frac{\rho_1^{n+1}-\rho_1^n}{\rho_1^n}\right| = \left|\frac{1-\theta_1-\theta_1\dfrac{\Delta(u)_1}{\kappa_1}}{\theta_1\left(1+\dfrac{\Delta(u)_1}{\kappa_1}\right)}\right| \leq \frac{\varepsilon p_1^n}{\rho_1^n(c_1^n)^2}.$$

Considering that $\left|\dfrac{\Delta(u)_1}{\kappa_1}\right| < \varepsilon << 1$, we obtain a constraint to be imposed on $\Delta(u)_1$ in order to control density's evolution taking into account the mass flux into the layer 1, that reads :

$$\left|\frac{1-\theta_1}{\theta_1} - \frac{\Delta(u)_1}{\kappa_1}\right| \leq \frac{\varepsilon p_1^n}{\rho_1^n(c_1^n)^2}.$$

We obtain the same formulae for the last layer of the condensate, where the Eulerian flux ϕ^r is going through the cell face at right of the layer and with a moving interface at left. For internal layers, i.e. a layer i between two moving interfaces, no mass fluxes are exchanged, thus $\theta_i = 1$. Therefore, for any layer i in the condensate, the density's evolution control by a constraint on $\Delta(u)_i$ reads generically :

$$\left| \frac{1-\theta_i}{\theta_i} - \frac{\Delta(u)_i}{\kappa_i} \right| \leq \frac{\varepsilon p_i^n}{\rho_i^n (c_i^n)^2}. \tag{2.99}$$

with $\theta_i = \dfrac{m_i^n}{m_i^{n+1}}$, $\kappa_i = \dfrac{Vol_i^n}{dt\ A}$ and for a condensate of nc layers :

$$\Delta(u)_1 = u_{int,x}^{1,2},$$

$$\Delta(u)_{nc} = -u_{int,x}^{nc-1,nc},$$

and for internal layers $1 < i < nc$:

$$\Delta(u)_i = u_{int,x}^{i,i+1} - u_{int,x}^{i-1,i},$$

with $u_{int,x}^{i,i+1}$ the velocity of the interface between layers i and $i+1$.

Control of entropy's evolution

As well as for density's evolution control, we have to take into account mass evolution into the constraint (2.94) obtained to control entropy's evolution. For an internal layer i, i.e. a layer between to moving interfaces, the condition takes the form (2.94) :

$$|\Delta(p)_i| \leq \rho_i^n \kappa_i \sqrt{\frac{2\varepsilon p_i^n}{\rho_i^n \Gamma_i^n}}.$$

For the first layer of the condensate, we have a flux ϕ^ℓ going through left interface which is a cell face. This flux of Eulerian variables is associated implicity with a flux of entropy that we cannot exhibit in general. The entropy control, as it is defined precedently, cannot be achieved.
However, the control of the pressure gradient which appears in the entropy condition (2.94) can be viewed as a control on the velocity increase :

$$\left| u_1^{n+1} - u_1^n \right| = \left| \frac{\Delta(p)_1}{\rho_1^n \kappa_1} \right| \leq \sqrt{\frac{2\varepsilon p_1^n}{\rho_1^n \Gamma_1^n}}. \tag{2.100}$$

A velocity increase is not physical within a contact discontinuity. However, it will create kinetic energy and therefore may excessively decrease the internal energy. Thus, controling this velocity increase in a boundary layer could be a good alternative in first and last layer to the control of entropy production. We therefore take as a new condition :

$$\left| \frac{u_1^{n+1} - u_1^n}{\theta_1} \right| \leq \sqrt{\frac{2\varepsilon p_1^n}{\rho_1^n \Gamma_1^n}}. \tag{2.101}$$

Using the x velocity formula, this is rewritten as :

$$\left| \frac{1-\theta_1}{\theta_1} u_1^n + \frac{\Delta(p)_1}{\rho_1^n \kappa_1} \right| \leq \sqrt{\frac{2\varepsilon p_1^n}{\rho_1^n \Gamma_1^n}}. \tag{2.102}$$

We obtain the same formulae for last layer of the condensate, where the Eulerian flux ϕ^r is going through the cell face at right of the layer and with a moving interface at left. For internal layers, i.e. a layer i between two moving interfaces, no mass fluxes are exchanged, thus $\theta_i = 1$. Therefore, for any layer i in the condensate, we control velocity's evolution with the constraint on $\Delta(p)_i$ that reads generically :

$$\left| \frac{1-\theta_i}{\theta_i} u_i^n + \frac{\Delta(p)_i}{\rho_i^n \kappa_i} \right| \leq \sqrt{\frac{2\varepsilon p_i^n}{\rho_i^n \Gamma_i^n}} \tag{2.103}$$

with $\theta_i = \dfrac{m_i^n}{m_i^{n+1}}$, $\kappa_i = \dfrac{Vol_i^n}{dt\ A}$ and for a condensate of nc layers :

$$\Delta(p)_1 = p_{int}^{1,2} + \phi^\ell(2),$$

$$\Delta(p)_{nc} = \phi^r(2) - p_{int}^{nc-1,nc},$$

and for internal layers $1 < i < nc$:

$$\Delta(p)_i = p_{int}^{i,i+1} - p_{int}^{i-1,i},$$

with $1 < i < nc$ and $p_{int}^{i,i+1}$ the pressure of the interface between layers i and $i+1$.

2.4.6 Control conditions

Let us summarize the results of the three preceding sections :
To obtain a "reasonable" behavior of the pressure in layer i between t^n and t^{n+1} when the CFL condition (2.40) is not fulfilled ($\kappa_i = Vol_i^n/dtA \leq (c_i^n)$), the values of $\Delta(p)_i$ and $\Delta(u)_i$ have to be controled as follows :

$$\begin{aligned} \left| \frac{1-\theta_i}{\theta_i} - \frac{\Delta(u)_i}{\kappa_i} \right| &\leq \frac{\varepsilon p_i^n}{\rho_i^n (c_i^n)^2} \\ \left| \frac{1-\theta_i}{\theta_i} u_i^n + \frac{\Delta(p)_i}{\rho_i^n \kappa_i} \right| &\leq \sqrt{\frac{2\varepsilon p_i^n}{\rho_i^n \Gamma_i^n}} \end{aligned} \tag{2.104}$$

Remark 25. *The initial goal was to achieve a strict control of the pressure as follows :*

$$\left| \frac{p^{n+1} - p^n}{p^n} \right| \leq 2\varepsilon.$$

These inequalities are established with some approximations compared to continuous relation (2.83) : first, the gap between continuous and discrete level in equation (2.85) and second, calculation approximations made to obtain these inequalities. However, they involve physical quantities of materials, as acoustic impedance $\rho_i^n (c_i^n)^2$ and Grüneisen coefficient Γ_i^n that are relevant to control flow evolution. Moreover, the effect of these constraints is to enforce the flow to degenerate in a contact discontinuity in layers where the CFL condition (2.40) is not satisfied, what seems to be the only reasonable choice.

2.4.7 Correction algorithm for interface pressure and velocity

The purpose of this section is to find a way to take the constraints (2.104) into account by a correction of the condensate solution obtained by the method described in chapter (2.3). This correction should keep local conservation of eulerian quantities in our method. The choice is then to correct only velocities and pressures at interfaces in order to satisfy constraints (2.104). Local conservation is then still ensured. Moreover, the correction couples the layers inside a condensate. Therefore we could expect that the relevant step size dx to be taken into account in the CFL condition (2.40) would be the

size of the condensate and not the size of the layer.
Therefore, in a condensate, we will find values $(u^*_{int}, p^*_{int})_i$ of velocities and pressures at interfaces obtained by a projection of values $(u_{int}, p_{int})_i$, obtained by the method described in chapter (2.3), on the space of solutions that satisfy constraints (2.104). Projected values must also be as close as possible from initial values to keep properties of sliding and entropy growing for instance.

Evolution's control

Section (2.4.6) gives constraints on $\Delta(u)_i$ and $\Delta(p)_i$ to obtain a correct evolution in each condensate layer i. We will use two conservative quantities, volume and momentum, which are respectively independent functions of $\Delta(u)_i$ and $\Delta(p)_i$:

$$\begin{aligned} Vol_i^{n+1} &= Vol_i^n \left(1 + \frac{\Delta(u)_i}{\kappa_i}\right) \\ m_i^{n+1} u_i^{n+1} &= m_i^n u_i^n - dtA\Delta(p)_i \end{aligned} \tag{2.105}$$

with $\kappa_i = Vol_i^n / dtA$, Vol_i^n volume of layer i, u_i^n the x velocity in x direction step, A the transverse section of the condensate.
On the other hand, considering a condensate of nc layers, the sum of volumes and momentums are known at time t^{n+1} :

$$\begin{aligned} \sum_{i=1}^{nc} Vol_i^{n+1} &= \sum_{i=1}^{nc} Vol_i^n \\ \sum_{i=1}^{nc} m_i^{n+1} u_i^{n+1} &= \sum_{i=1}^{nc} m_i^n u_i^n - dtA(\phi_g(2) + \phi_d(2)) \end{aligned} \tag{2.106}$$

with $\phi_g(2)$ the outgoing $FVCF$ flux of momentum at left side of the condensate and $\phi_d(2)$ the outgoing $FVCF$ flux of momentum at right side of the condensate.
Let us calculate $2D$ interface pressure and velocity between layer i and $i+1$ in the x step of the splitting as given by (2.64) :

$$\begin{cases} p_{int,x}^{i\ i+1} = \dfrac{\rho_{i+1}\tilde{c}_{i+1} p_i + \rho_i \tilde{c}_i p_{i+1}}{\rho_i \tilde{c}_i + \rho_{i+1}\tilde{c}_{i+1}} + \rho_i \tilde{c}_i \rho_{i+1} \tilde{c}_{i+1} \dfrac{(u_i - u_{i+1}) \cdot n^{i\ i+1}}{\rho_i \tilde{c}_i + \rho_{i+1}\tilde{c}_{i+1}}\ n_x^{i\ i+1} \\ u_{int,x}^{i\ i+1} = \dfrac{\rho_i \tilde{c}_i u_{i,x} + \rho_{i+1}\tilde{c}_{i+1} u_{i+1,x}}{\rho_i \tilde{c}_i + \rho_{i+1}\tilde{c}_{i+1}} + \dfrac{p_i - p_{i+1}}{\rho_i \tilde{c}_i + \rho_{i+1}\tilde{c}_{i+1}}\ n_x^{i\ i+1}. \end{cases}$$

with $\tilde{c}_i = \min(c_i, \kappa_i)$, $\kappa_i = Vol_i^n/dt\ A$, Vol_i^n the volume at time t^n, ρ_i^n the density at time t^n, c_i the sound speed in layer i, A the transverse section of the condensate, $n_x^{i\ i+1}$ the x coordinate of the normal vector of the interface between layers i and $i+1$.
Therefore $\Delta(u)_i = u_{int,x}^{i\ i+1} - u_{int,x}^{i-1\ i}$ and $\Delta(p)_i = p_{int,x}^{i\ i+1} - p_{int,x}^{i-1\ i}$, thus Vol_i^{n+1} and $m_i^{n+1}u_i^{n+1}$ can be calculated for each layer i of the condensate and conservation equations (2.106) are satisfied by construction.
Afterward, we restrict the values of $\Delta(u)_i$ and $\Delta(p)_i$ with constraints (2.104) given in section 2.4.6 :

$$\begin{array}{rcl} \left|\dfrac{1-\theta_i}{\theta_i} - \dfrac{\Delta(u)_i^*}{\kappa_i}\right| & \leq & \dfrac{\varepsilon p_i^n}{\rho_i^n (c_i^n)^2} \\ \left|\dfrac{1-\theta_i}{\theta_i} u_i^n + \dfrac{\Delta(p)_i^*}{\rho_i^n \kappa_i}\right| & \leq & \sqrt{\dfrac{2\varepsilon p_i^n}{\rho_i^n \Gamma_i^n}} \end{array}$$

with $\Delta(u)_i^* = \Delta(u)_i$ if the constraint is satisfied, or the maximum value allowed by the constraint if it is not. The same for $\Delta(p)^*$.
Therefore we obtain new values of volumes and velocities in the condensate, keeping masses unchanged because their values do not depend on interface pressure and velocity :

$$\begin{array}{rcl} Vol_i^* & = & Vol_i^n \left(1 + \dfrac{\Delta(u)_i^*}{\kappa_i}\right) \\ m_i^{n+1} u_i^* & = & m_i^n u_i^n - dtA\Delta(p)_i^*. \end{array}$$

Conservation of quantities after correction

Of course, the conservation equations (2.106) are no longer satisfied with corrected values Vol_i^* and u_i^* :

$$\begin{array}{rcl} \displaystyle\sum_{i=1}^{nc} Vol_i^* & \neq & \displaystyle\sum_{i=1}^{nc} Vol_i^n, \\ \displaystyle\sum_{i=1}^{nc} m_i^{n+1} u_i^* & \neq & \displaystyle\sum_{i=1}^{nc} m_i^n u_i^n - dtA(\phi_g(2) + \phi_d(2)). \end{array} \tag{2.107}$$

Considering conservation equation (2.106), there exists constants K_{ui} and K_{p_i} that satisfies :

$$\begin{aligned}
&\sum_{i=1}^{nc} K_{ui}(Vol_i^* - Vol_i^n) = 0, \\
&\sum_{i=1}^{nc} K_{p_i}(m_i^{n+1}u_i^* - m_i^n u_i^n) = -dtA(\phi_g(2) + \phi_d(2)).
\end{aligned} \tag{2.108}$$

For example

$$K_{ui} = \frac{Vol_i^{n+1} - Vol_i^n}{Vol_i^* - Vol_i^n}$$

and

$$K_{p_i} = \frac{m_i^{n+1}u_i^{n+1} - m_i^n u_i^n}{m_i^{n+1}u_i^* - m_i^n u_i^n}$$

satisfy these equations.

Our objective is now to find values $1 \geq K_{ui} \geq 0$ and $1 \geq K_{p_i} \geq 0$, defining updated variables Vol_i^{**} and u_i^{**}, which satisfy conservation equations, of the form :

$$\begin{array}{lll}
Vol_i^{**} - Vol_i^n & = K_{ui}(Vol_i^* - Vol_i^n) & = K_{ui}\dfrac{Vol_i^n \Delta(u)_i^*}{\kappa_i} \\
m_i^{n+1}u_i^{**} - m_i^n u_i^n & = K_{p_i}(m_i^{n+1}u_i^* - m_i^n u_i^n) & = K_{p_i}(-dt\ A\Delta(p)_i^*).
\end{array}$$

Both equations (2.108) are of the form :

$$\sum_{i=1}^{nc} K_i\ q_i = -\varphi.$$

with
$q_i = (Vol_i^* - Vol_i^n)$ and $\varphi = 0$, or
$q_i = m_i^{n+1}u_i^* - m_i^n u_i^n$ and $\varphi = dtA(\phi_g(2) + \phi_d(2))$.
Let us distinguish positive and negative terms in the sum with an obvious adaptation of notation for K_i :

$$\sum_{i=1(q_i \geq 0)}^{nc} K_i^+\ q_i + \sum_{i=1(q_i < 0)}^{nc} K_i^-\ q_i = -\varphi.$$

For all layers i in the condensate we will use $K_i^+ = K^+$ and $K_i^- = K^-$. It follows that we must solve

$$K^+ \, S^+ - K^- S^- = -\varphi \tag{2.109}$$

with $S^+ = \sum_{i=1(q_i \geq 0)}^{nc} q_i \geq 0$ and $S^- = -\sum_{i=1(q_i<0)}^{nc} q_i \geq 0$.
We need to find $1 \geq K^+ \geq 0$ and $1 \geq K^- \geq 0$ that satisfy equation (2.109), but with values as close as possible from 1 to modify as less as possible the values Vol_i^* and u_i^*. A simple analysis of this equation gives the following results :

(1) if $-\dfrac{\varphi}{S^+} \leq 1$ and $\dfrac{\varphi}{S^-} \leq 1$ then

if $\dfrac{S^- - \varphi}{S^+} \leq 1$ then

$$K^- = 1 \text{ and } K^+ = \frac{S^- - \varphi}{S^+}$$

else if $\dfrac{S^- - \varphi}{S^+} > 1$ then

$$K^+ = 1 \text{ and } K^- = \frac{S^+ + \varphi}{S^-}$$

(2) if $-\dfrac{\varphi}{S^+} > 1$ then

$$K^+ = -\frac{\varphi}{S^+} \text{ and } K^- = 0$$

(3) if $\dfrac{\varphi}{S^-} > 1$ then

$$K^- = \frac{\varphi}{S^-} \text{ and } K^+ = 0$$

Remark 26. *In cases (2) and (3), which can only occur in the momentum equation with $\varphi \neq 0$, we do not ensure $1 \geq K^+$ and $1 \geq K^-$. However, the conservation for momentum in (2.106) can be rewritten in the following form :*

$$\sum_{i=1(q_i^{n+1} \geq 0)}^{nc} q_i^{n+1} + \sum_{i=1(q_i^{n+1}<0)}^{nc} q_i^{n+1} = -\varphi$$

with $q_i^{n+1} = m_i^{n+1} u_i^{n+1} - m_i^n u_i^n$ and $\varphi = dtA(\phi_g(2) + \phi_d(2))$ as defined in

(2.106). Moreover, defining

$$S^{n+1,+} = \sum_{i=1(q_i^{n+1}\geq 0)}^{nc} q_i^{n+1},$$

and

$$S^{n+1,-} = -\sum_{i=1(q_i^{n+1}<0)}^{nc} q_i^{n+1}.$$

It follows that :

in case (2), $K^-S^- = 0$ *and* $S^+ \leq K^+S^+ = -\varphi \leq S^{n+1,+}$,

in case (3), $K^+S^+ = 0$ *and* $S^- \leq K^-S^- = \varphi \leq S^{n+1,-}$.

This shows that cases (2) and (3) are situations where values u_i^{n+1} *cannot be strictly controled by formulae (2.104). However, these situations should not be the general case, because this control algorithm only changes layers values where CFL condition (2.40) is not satisfied in small volume layers. If* S^+ *and* S^- *are too different from* $S^{n+1,+}$ *and* $S^{n+1,-}$*, it indicates that formulae (2.104) are too restrictive or that time step is too large for the calculation.*

Quantities after correction

The solutions of equation (2.109) $K_u^{\pm}$ and $K_p^{\pm}$ are calculated respectively for volume and momentum equations (2.108). The final result for Vol_i^{**} and u_i^{**} is then :

$$\begin{array}{lll} Vol_i^{**} & = Vol_i^n & +K_{ui}(Vol_i^* - Vol_i^n) \\ m_i^{n+1}u_i^{**} & = m_i^n u_i^n & +K_{p_i}(m_i^{n+1}u_i^* - m_i^n u_i^n) \end{array}$$

with

if $(Vol_i^* - Vol_i^n) \geq 0$ then
$K_{ui} = K_u^+$
elseif $(Vol_i^* - Vol_i^n) < 0$ then
$K_{ui} = K_u^-$,

if $(m_i^{n+1}u_i^* - m_i^n u_i^n) \geq 0$ then
$$K_{p_i} = K_p^+$$
elseif $(m_i^{n+1}u_i^* - m_i^n u_i^n) < 0$ then
$$K_{p_i} = K_p^-.$$

Corresponding densities can thus be calculated :

$$\rho_i^{**} = \frac{m_i^{n+1}}{Vol_i^{**}}.$$

At this point, Vol_i^{**} and u_i^{**} satisfy pressure control constraints (2.104) and conservation of volume and momentum :

$$\begin{array}{rcl} \sum_{i=1}^{nc} Vol_i^{**} & = & \sum_{i=1}^{nc} Vol_i^n \\ \sum_{i=1}^{nc} m_i^{n+1}u_i^{**} & = & \sum_{i=1}^{nc} m_i^n u_i^n - dtA(\phi_g(2) + \phi_d(2)). \end{array} \tag{2.110}$$

Let us finally observe that there exists unique values for interface pressure $p_{int,x}^{i\ i+1,**}$ and interface velocity $u_{int,x}^{i\ i+1,**}$ that realize values Vol_i^{**} and u_i^{**}. First we find $\Delta(u)_i^{**}$ and $\Delta(p)_i^{**}$ with relations :

$$\begin{array}{rcl} Vol_i^{**} & = & Vol_i^n \left(1 + \frac{\Delta(u)_i^{**}}{\kappa_i}\right) \\ m_i^{n+1}u_i^{**} & = & m_i^n u_i^n - dtA\Delta(p)_i^{**} \end{array}$$

Afterward, $p_{int,x}^{i\ i+1,**}$ and $u_{int,x}^{i\ i+1,**}$ are simply calculated recursively according to the relations :

$$\begin{array}{l} u_{int,x}^{i\ i+1,**} = u_{int,x}^{i-1\ i,**} + \Delta(u)_i^{**}, \\ p_{int,x}^{i\ i+1,**} = p_{int,x}^{i-1\ i,**} + \Delta(p)_i^{**}. \end{array}$$

Corresponding total energies E_i^{**} can thus be calculated :

$$m_i^{n+1}E_i^{**} = m_i^n E_i^n - dtA\Delta(pu)_i^{**}.$$

Values of layers internal energy is thus obtain by $e_i^{**} = E_i^{**} - 1/2((u_i^{**})^2 + (v_i^{n+1})^2)$ and layers pressures are finally derived from the equation of state for the fluid f in layer i $p_i^{**} = P_f(\rho_i^{**}, e_i^{**})$.

Remark 27. *This algorithm does not ensure monotonicity of solution* $(u)_i$ *and* $(p)_i$ *in the condensate, i.e. monotonicity of values* $u_{int,x}^{i\ i+1,**}$ *at interfaces compared with* u_i^{**} *within layers or of values* $p_{int,x}^{i\ i+1,**}$ *at interfaces compared with* p_i^{**} *within layers. Interfaces values and layers values are dual and nothing is explicitly made in this algorithm to couple these values. However, controlling the evolution in each layer and imposing global conservation of volume and momentum forbids any large differences between these dual values, unless a control relation in a layer is violated. In practice, this seems to work well.*

2.5 Numerical results

2.5.1 Equation of State

Air

In all the following benchmarks, air is supposed to follow a perfect gas type of equation of state :

$$\begin{aligned} p &= (\gamma_a - 1)\ \rho\ e, \\ T &= \frac{e}{c_v}, \\ s &= c_v\ log\left(\frac{p}{\rho^{\gamma_a}}\right), \end{aligned} \tag{2.111}$$

with the constant $\gamma_a = 1.4$, and values p $[Pa]$, ρ $[kg/m^3]$, e $[J/kg]$, T $[K]$, C_v $[J/K/kg]$, s $[J/K/kg]$ respectively associated to pressure, density, specific internal energy, temperature, specific heat at constant volume, specific entropy of air. Atmospheric conditions for air are supposed to be close from $(p = 10^5\ Pa, \rho = 1\ kg/m^3, T = 300\ K)$, sound speed is $c_a(300K) = \sqrt{\gamma_a p/\rho} = 374.16\ m/s$.

Water

In all the following benchmarks, water is supposed to follow a stiffened gas type of equation of state :

$$\begin{aligned} p &= (\gamma_w - 1)\ \rho\ e - \pi, \\ T &= \frac{1}{c_v}\left(e - \frac{\pi}{\gamma_w \rho}\right) \\ s &= c_v\ log\left(\frac{\frac{p+\pi}{\gamma_w - 1} - \frac{\pi}{\gamma_w}}{\rho^{\gamma_w}}\right), \end{aligned} \tag{2.112}$$

with constants $\gamma_w = 7$, $\pi = 21.\ 10^8$ $[Pa]$, and values p $[Pa]$, ρ $[kg/m^3]$, $e[J/kg]$, T $[K]$, $C_v[J/K/kg]$, s $[J/K/kg]$ respectively associated to pressure, density, specific internal energy, temperature, specific heat at constant volume, specific entropy of water. Atmospheric conditions for water are supposed to be close from $(p = 10^5\ Pa, \rho = 1000\ kg/m^3, T = 300\ K)$, sound speed is $c_w(300K) = \sqrt{(\gamma_w p + \pi)/\rho} = 1449.38\ m/s$.

Rankine-Hugoniot conditions for Stiffened Gas

Rankine-Hugoniot conditions are needed to determine the state of a compressible fluid in both sides of a shock wave. Let us denote the shocked state of the fluid by no subscript and the unshocked state by the subscript 0.
Rankine-Hugoniot jump relations for a shock wave discontinuity propagating at velocity D for a conservation law of the form $\partial_t V + \partial_x F(V) = 0$ (V a value, $F(V)$ the flux of V) can be written generically as :

$$F(V) - F(V_0) = D\ (V - V_0). \tag{2.113}$$

For *1D* Euler equations, conservation laws are :

$$\begin{array}{lll} \partial_t\ \rho & +\partial_x\ (\rho u) = 0 \\ \partial_t\ \rho u & +\partial_x\ (\rho u^2 + p) = 0 \\ \partial_t\ \rho E & +\partial_x\ (\rho E + p)u = 0. \end{array} \tag{2.114}$$

Thus we obtain the associated Rankine-Hugoniot jump relations :

$$\begin{array}{ll} \rho u - \rho_0 u_0 & = D(\rho - \rho_0) \\ (\rho u^2 + p) - (\rho_0 u_0^2 + p_0) & = D(\rho u - \rho_0 u_0) \\ (\rho E + p)u - (\rho_0 E_0 + p_0)u_0 & = D(\rho E - \rho_0 E_0). \end{array} \tag{2.115}$$

Let us set M the Mach number, the state ρ_0, p_0, the velocity $u_0 = 0$ and the sound speed $c_0^2 = (\gamma_w p_0 + \pi)/\rho_0$.
The solution of equations (2.115) reads :

$$\begin{array}{ll} D = & c_0\ M \\ K = & \rho_0\ D^2/p0 \\ X = & 2\ \dfrac{(\gamma_w - 1)\ (1 + K/2) + \pi/p_0 + 1}{(\gamma_w + 1)\ K} \\ Y = & 1 + K\ (1 - X) \\ p = & Y * p_0 \\ \rho = & \rho_0/X \\ U = & \dfrac{p - p_0}{\rho_0\ D} \end{array} \tag{2.116}$$

$$
\begin{aligned}
D &= c_0\ M \\
e &= \frac{p+\pi}{\rho\ (\gamma_w - 1)} \\
T &= \frac{1}{c_v}\left(e - \frac{\pi}{\gamma_w \rho}\right) \\
s &= c_v\ log\left(\frac{\frac{p+\pi}{\gamma_w - 1} - \frac{\pi}{\gamma_w}}{\rho^{\gamma_w}}\right)
\end{aligned}
$$

This result will be needed to calculate initial state in benchmarks containing a shock wave propagating in a fluid.

2.5.2 Shock/Rarefaction tubes

All shock tubes are computed using perfect gas equation of state $p = (\gamma - 1)\ \rho\ e$.

Sod

The *1D* domain has a length of 1. Material 1 at left and material 2 at right are separated by an interface at the abscissa 0.5 and are made of the same perfect gas of coefficient $\gamma = 1.4$. Material 1 initial state is $(\rho = 1,\ u = 0,\ p = 1)$. Material 2 initial state is $(\rho = 0.125,\ u = 0,\ p = 0.1)$. Final time is 0.2. For this normalized benchmark, units are dropped. The mesh is made of 400x1 cells.
Analytical result is known for this case, from left to right states :
- $x < 0.263$, left initial state $(\rho = 1,\ u = 0,\ p = 1)$,
- $0.263 < x < 0.486$, rarefaction waves,
- $0.486 < x < 0.685$ left state of contact discontinuity $(\rho = 0.426,\ u = 0.927,\ p = 0.303)$,
- $0.685 < x < 0.850$ right state of contact discontinuity $(\rho = 0.265,\ u = 0.927,\ p = 0.303)$,
- $0.850 < x$ right initial state $(\rho = 0.125,\ u = 0,\ p = 0.1)$.

Remark 28. *Levels and wave locations are in good agreement with analytic results. The interface is positioned on the contact discontinuity with perfect monotonicity of pressure and velocity. Nevertheless, some spurious overshoots on the solution around the interface exist for ρ and e, but one can see on the entropy graph that these errors increase the entropy . This error of computation is then compatible with second Principle of Thermodynamics. The similarity of density's behavior around the interface between this method and Loubere's method (Lagrange Discontinuous-Galerkin type) is striking [56].*

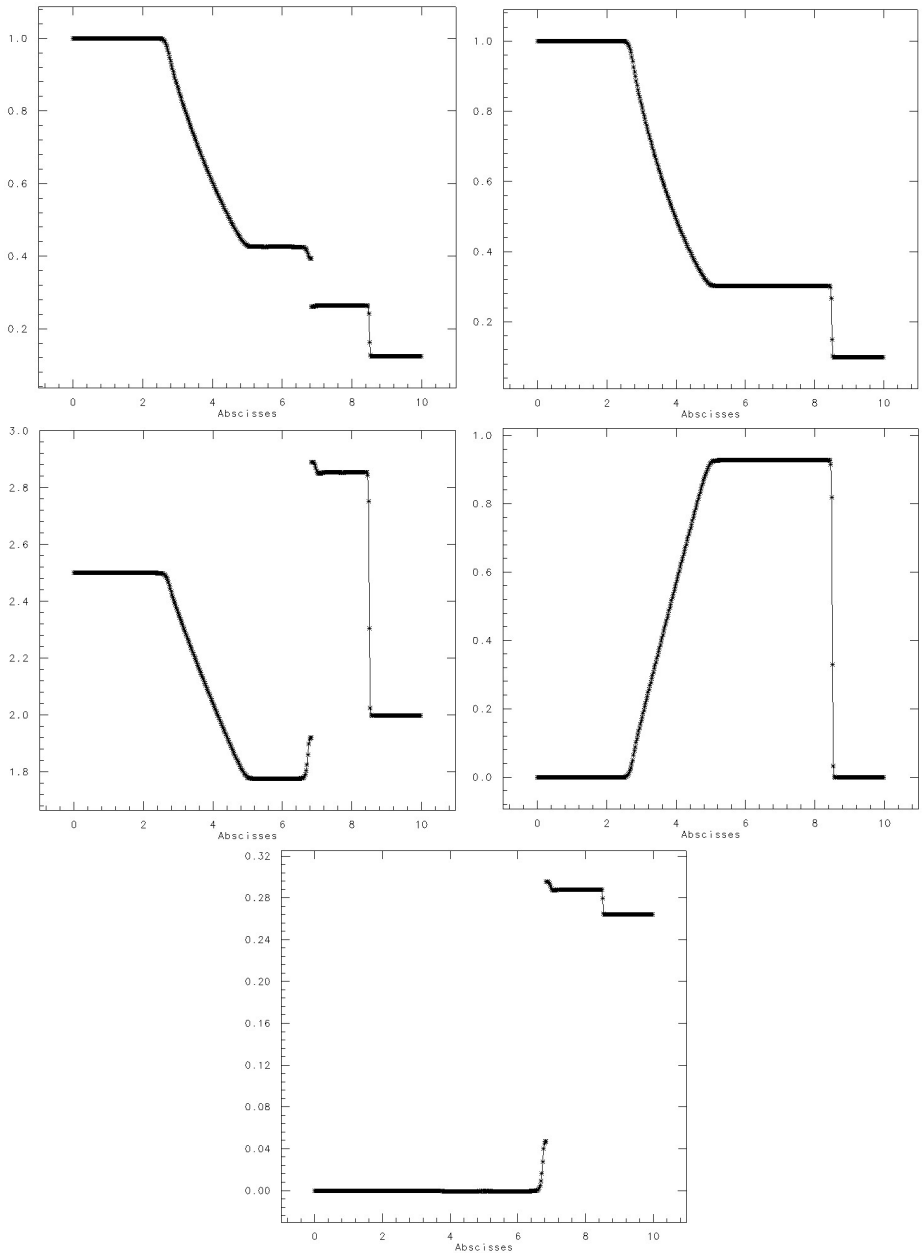

FIG. 2.6 – SOD shock tube, from left to right, from top to bottom : density, pressure, internal energy, velocity, entropy at final time 0.2.

Blastwave

The *1D* domain has a length of unity. Material 1 at left, material 2 at the center and material 3 at right, are separated by two interfaces respectively at abscissas 0.1 and 0.9. All materials are made of the same perfect gas of coefficient $\gamma = 1.4$. Material 1 initial state is $(\rho = 1.,\ p = 1000.,\ u = 0)$. Material 2 initial state is $(\rho = 1.,\ p = 0.01,\ u = 0)$. Material 3 initial state is $(\rho = 1.,\ p = 100.,\ u = 0)$. Final time is 0.038. For this normalized benchmark, units are dropped. The mesh is made of 400x1 cells.

Liska and Wendroff in [52] present compared results with several Eulerian schemes on this benchmark using 400 and 2000 cells : composite scheme CFLF, hybrid scheme CFLFh of Liska and Wendroff, centered scheme of Jiang-Nessyahu-Tadmor JT, Clawpack scheme of LeVeque, Weighted average flux scheme WAFT of Toro, schemes WENO5 and CWENO3 (C stands for conservative, 5 and 3 stand for theoretical order of precision) of Jiang and Shu and PPM of Woodward and Collela. All references and practical aspects of the use of these schemes can be found in the paper.

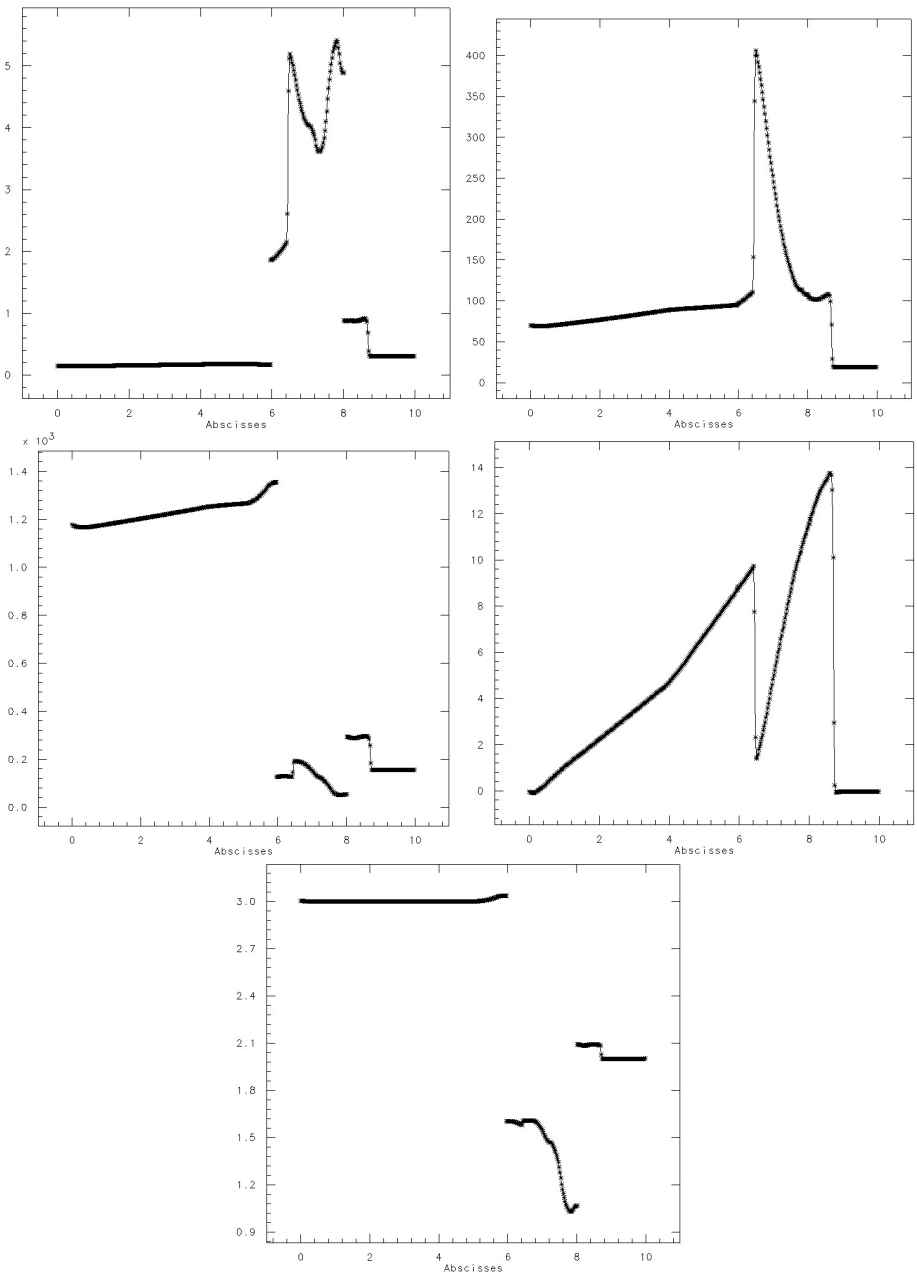

FIG. 2.7 – Blastwave shock tube, from left to right, from top to bottom : density, pressure, internal energy, velocity, entropy at final time 0.038.

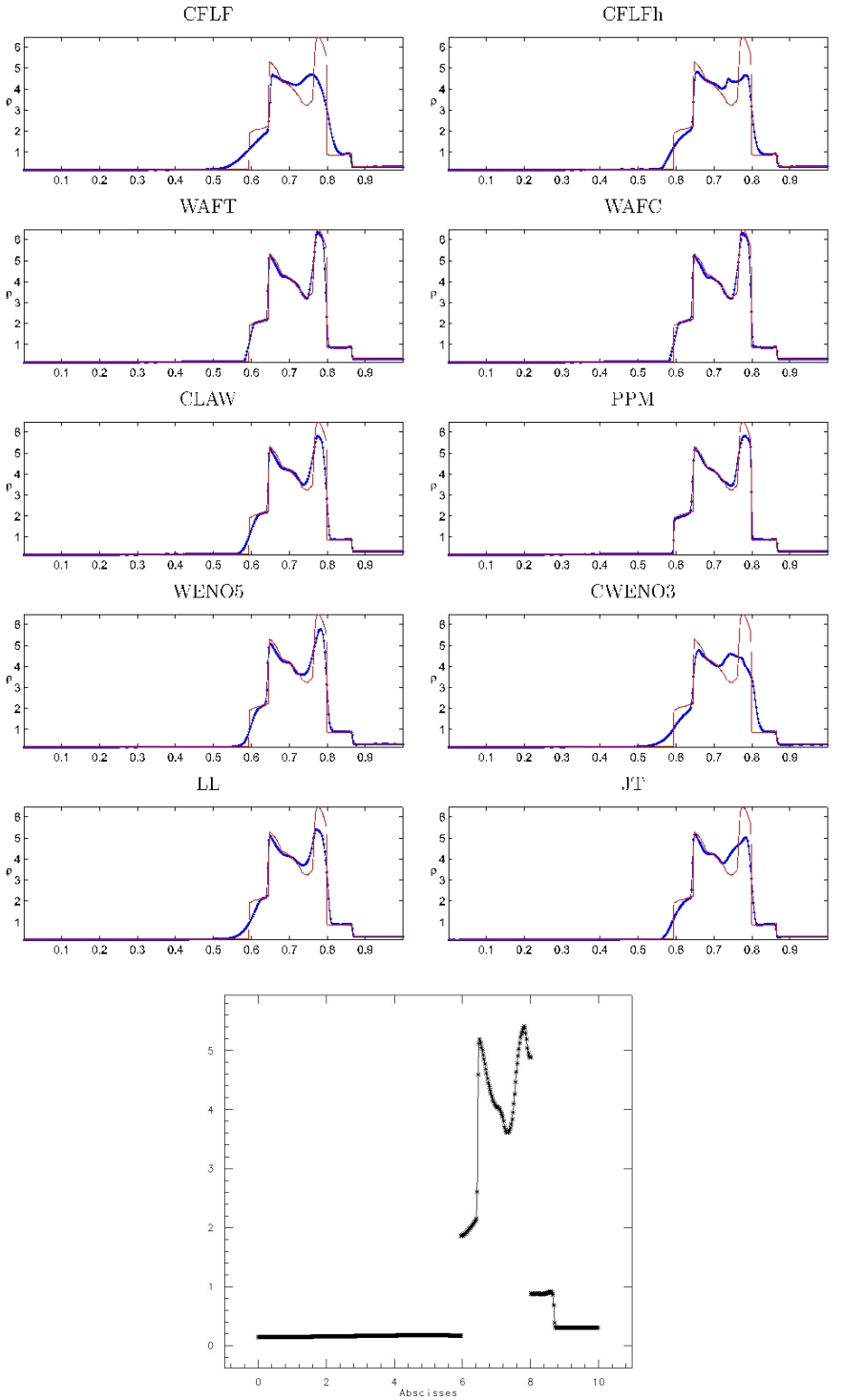

FIG. 2.8 – Results of several schemes using 400 cells by Liska and Wendroff [52] and below *VFFC-NIP* using 400 cells. Density at time $t = 0.038$.

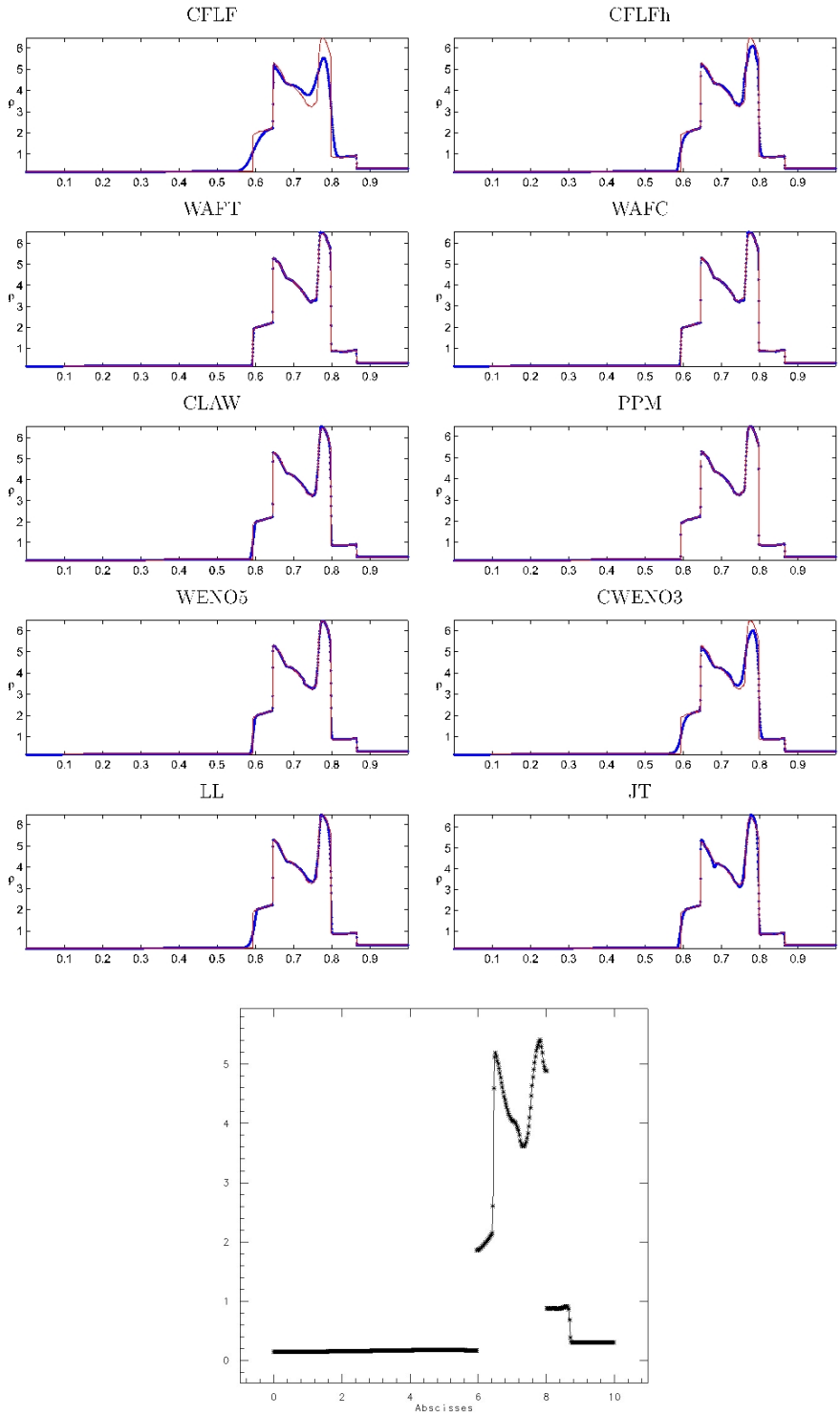

FIG. 2.9 – Results of several schemes using 2000 cells by Liska and Wendroff [52] and below *VFFC-NIP* using 400 cells. Density at time $t = 0.038$.

Double rarefaction waves

The *1D* domain has a length of 1. Material 1 at left and material 2 at right are separated by an interface at the abscissa 0.5 and are made of the same perfect gas of coefficient $\gamma = 1.4$. Material 1 initial state is ($\rho = 1.,\ p = 0.4,\ u = -2.$). Material 2 initial state is ($\rho = 1.,\ p = 0.4,\ u = 2.$). For this normalized benchmark, units are dropped. Final time is 0.16. The mesh is made of 401x1 cells.

Liska and Wendroff in [52] present compared results with several Eulerian schemes on this benchmark using 400 cells : composite scheme CFLF, hybrid scheme CFLFh of Liska and Wendroff, centered scheme of Jiang-Nessyahu-Tadmor JT, Clawpack scheme of LeVeque, Weighted average flux scheme WAFT of Toro, schemes WENO5 and CWENO3 (C stands for conservative, 5 and 3 stand for theoretical order of precision) of Jiang and Shu and PPM of Woodward and Collela. All references and practical aspects of the use of these schemes can be found in the paper.

Remark 29. *Opposite velocities at Mach number* 2.7 *make the pressure and the density at the center very close to zero. This case strongly challenges the behavior of entropy in rarefaction waves. One can see that entropy is unphysically growing at the center, but the error has the right sign with respect to second principle of thermodynamics.*

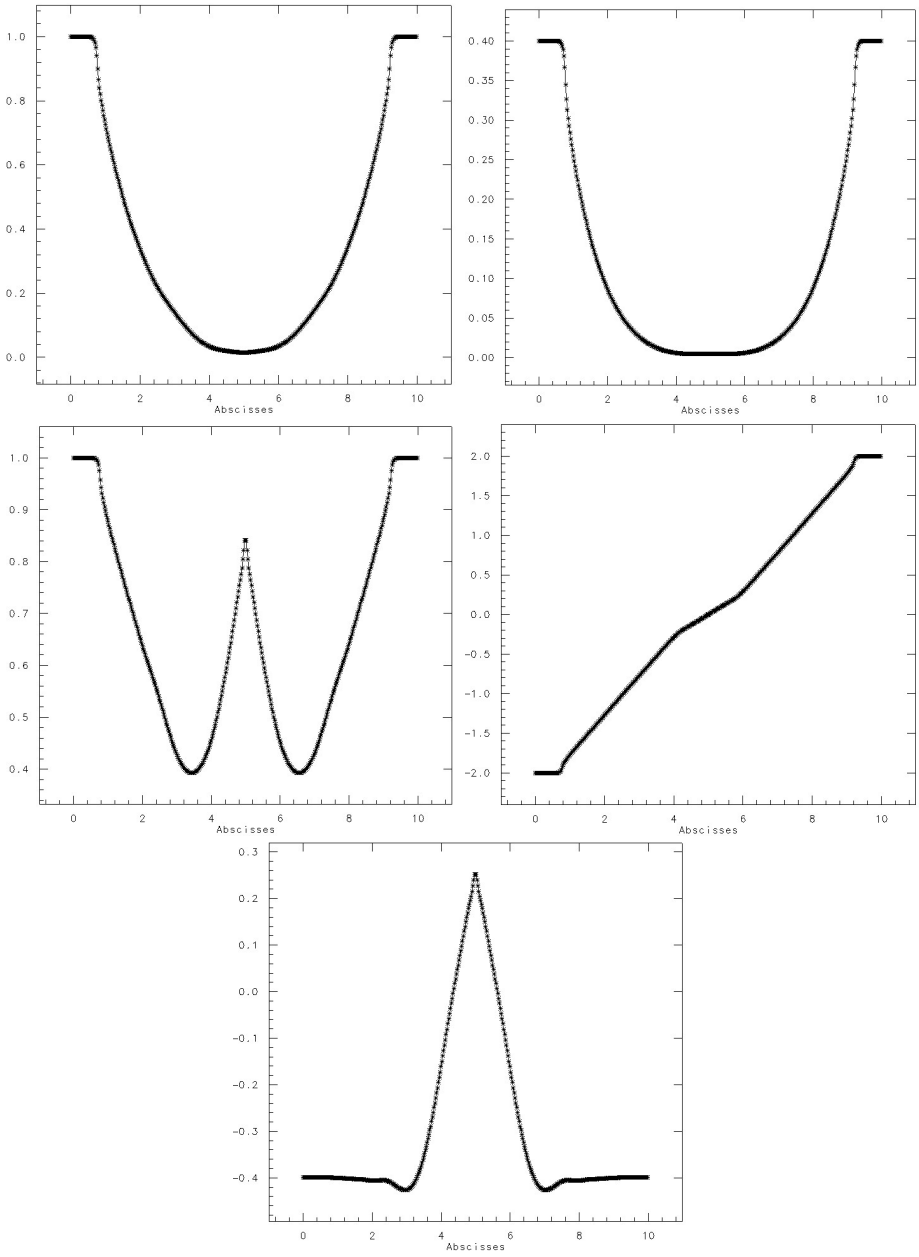

FIG. 2.10 – Double rarefaction waves, from left to right, from top to bottom : density, pressure, internal energy, velocity, entropy at final time $t = 0.16$.

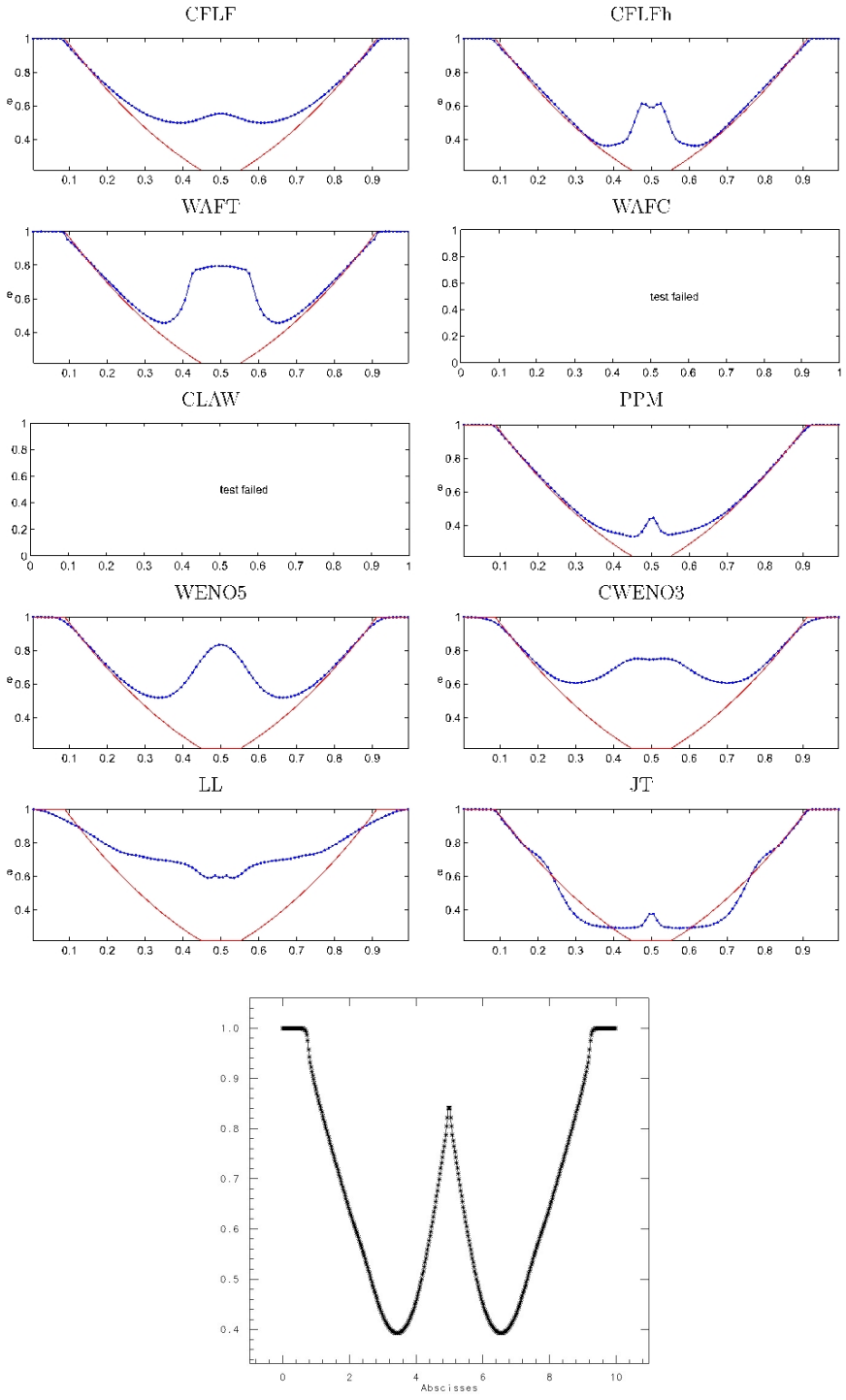

FIG. 2.11 – Results of several schemes using 400 cells by Liska and Wendroff [52] and below *VFFC-NIP* using 401 cells. Internal energy at time $t = 0.16$.

2.5.3 Pure sliding

We consider two materials separated by an oblic interface. Material 1 at left and material 2 at right are perfect gases of coefficient $\gamma = 1.4$. Material 1 initial state is ($\rho = 1.4,\ p = 0.25,\ u_x = 0.4,\ u_y = 1.$). Material 2 initial state is ($\rho = 2.8,\ p = 0.25,\ u_x = -0.4,\ u_y = -1.$). Initial velocities are parallel to the interface for both materials, but with opposite sign. For this normalized benchmark, units are dropped. Final time is 0.25. The domain is 1 long and 1 wide. The mesh is made of 50x50 cells.

Remark 30. *No boundary conditions are appropriate here, because in mixed cells on the domain boundary, the flow is inlet and outlet in the same cell. That cannot be properly managed by an inlet/oulet condition as we described. Therefore, this error generates a wave coming from the boundaries. Nevertheless, one can see that the velocity field at the center is almost still perfect sliding, with velocities in mixed cells with opposite signs. Density and pressure stay close from initial values with a little distortion of the interface due to a numerical adaptation on the mesh.*

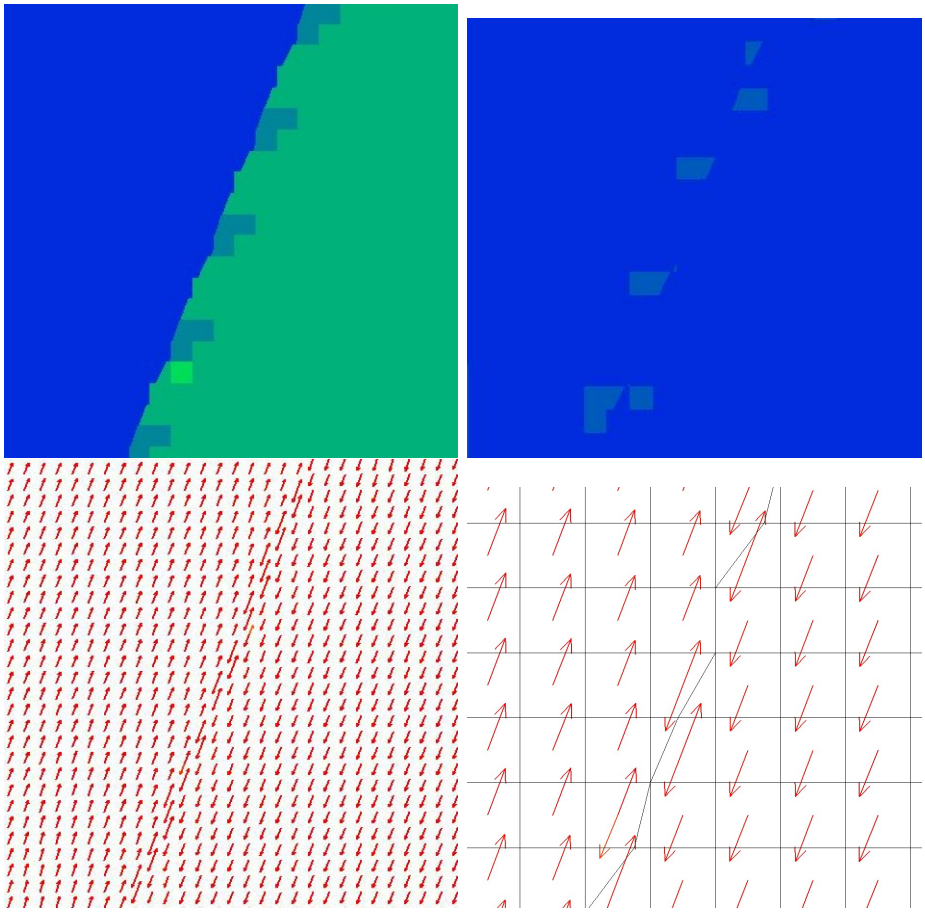

FIG. 2.12 – Pure sliding, from left to right, from top to bottom : density, pressure, velocity field, zoom at the velocity field center, at final time $t = 0.25$.

2.5.4 Pure advection of a bubble of air in water

We consider a cylindrical bubble of air in water. Velocity and pressure are homogeneous for both materials ($u_{x,a} = u_{x,w} = 4.53\ 10^4\ m/s,\ u_{y,a} = u_{y,w} = 1.\ 10^4\ m/s,\ p_a = p_w = 10^5\ Pa$), density for air is ($\rho_a = 1.\ kg/m^3$) and density for water is ($\rho_w = 1000.\ kg/m^3$). The bubble of air is then advected in a direction not aligned with grid lines. The shape of the bubble should obviously not change during the simulation. The domain is $1.8mm$ long and $0.8mm$ wide. The mesh is made of 180x80 cells.

Remark 31. *The spherical (hemispherical) bubble is becoming of square like shape, but the location of the bubble center is correct compare to analytic location and values are steady in each material. This is a point to be improved by a second order interface remap. However, numerical methods hardly preserve shape and conservation.*

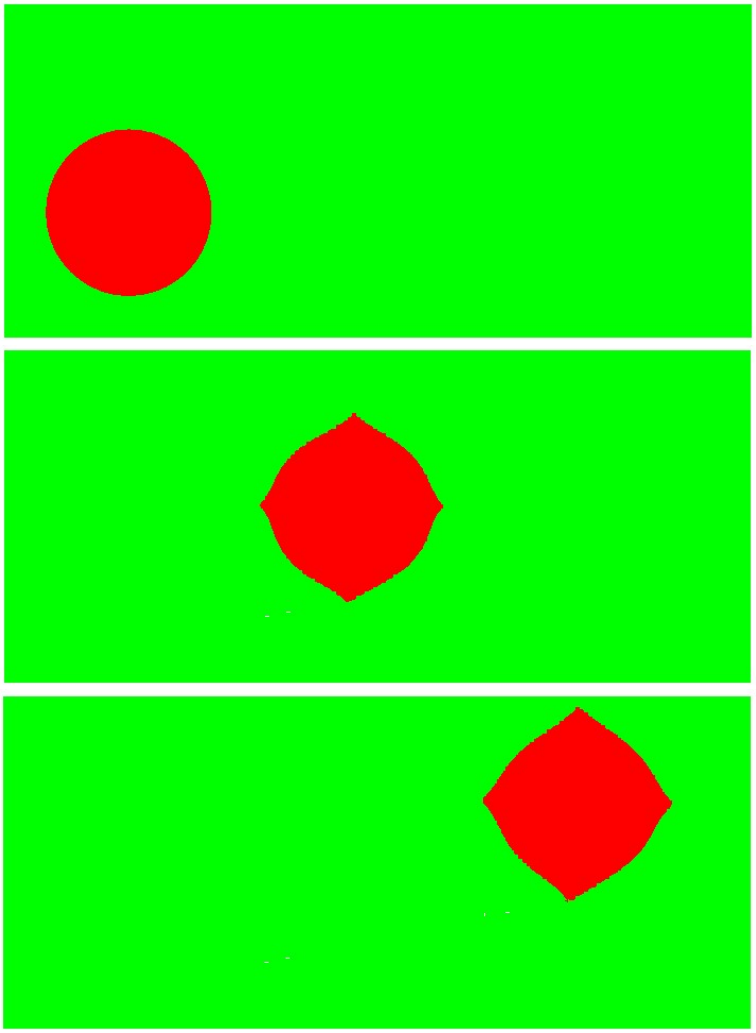

FIG. 2.13 – From top to bottom line : geometry of the bubble at time $t_0 = 0\ \mu s$, $t_1 = 1.2\ \mu s$, $t_2 = 2.4\ \mu s$.

2.5.5 Shock wave interaction with a bubble of air in water

We consider a half cylindrical bubble of air initially sticking to the wall inside water. A shock wave in the water is propagating from left to right. Initial state for air is ($\rho_a = 1.\ kg/m^3, p_a = 10^5 Pa, u_a = 0\ m/s$), for water is ($\rho_0 = 1000.\ kg/m^3, p_0 = 10^5 Pa, u_0 = 0\ m/s$), for shocked water is ($\rho = 1322.05\ kg/m^3, p = 200\ 000.\ 10^5\ Pa, u = 2206.68\ m/s$). Mach number is around $M = 6.25$. The domain is 10 cm long and 5 cm wide. The bubble has a radius of 2 cm. The mesh is made of 200x100 cells.

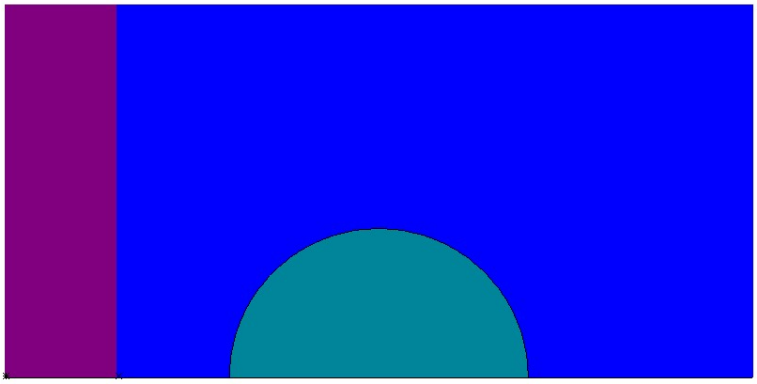

FIG. 2.14 – Initial geometry, a shock wave is propagating in the water from left to right. An air bubble sticks to the wall.

Remark 32. *This is a case where interface sliding between materials and own physical variables for each material in mixed cells seems obviously important. Any variable average in this computation, between such as different materials as water and air in term of density, sound speed or compressibility, leads to a strong error in term of physical modelling.*

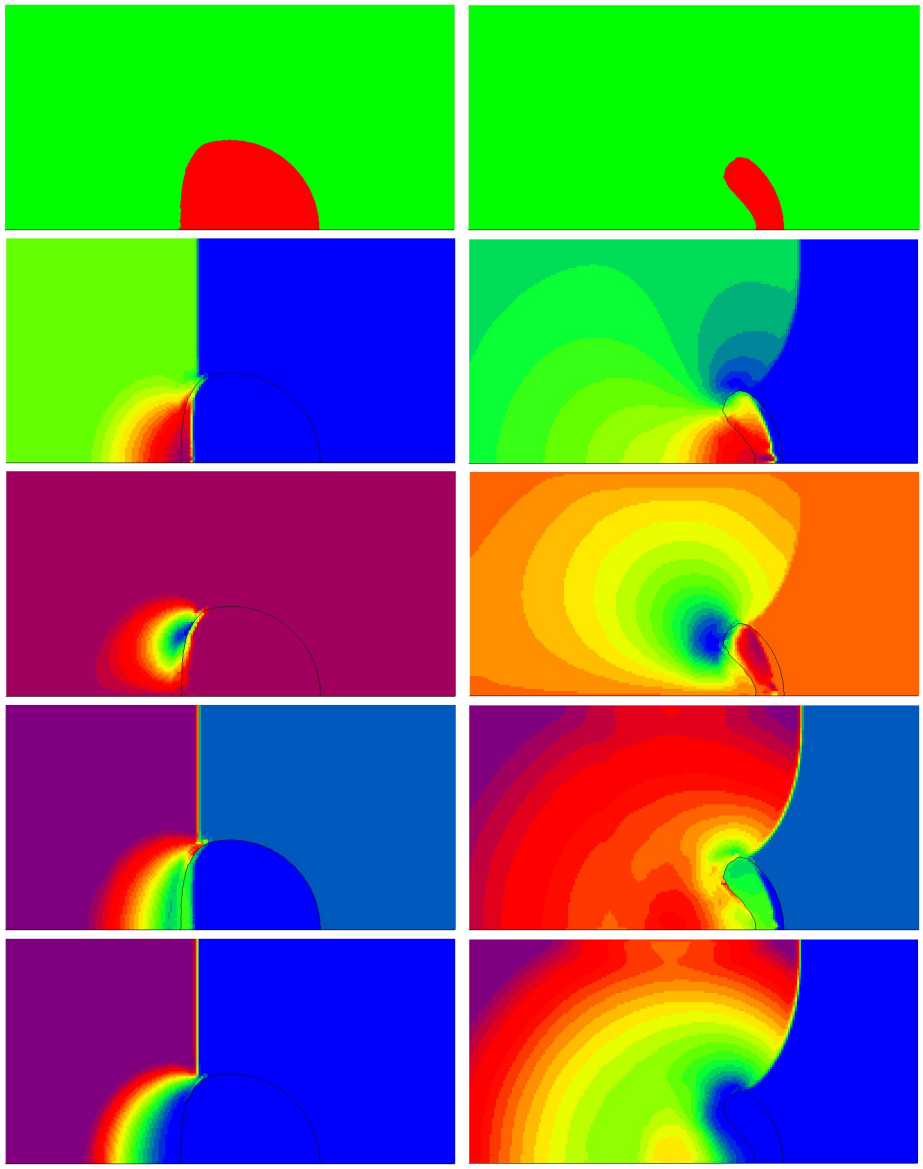

FIG. 2.15 – From top to bottom line : geometry of the bubble, horizontal component of the velocity, vertical component of the velocity, sound speed, pressure. Left row : time $t = 3\ \mu s$. Right row : time $t = 6.4\ \mu s$.

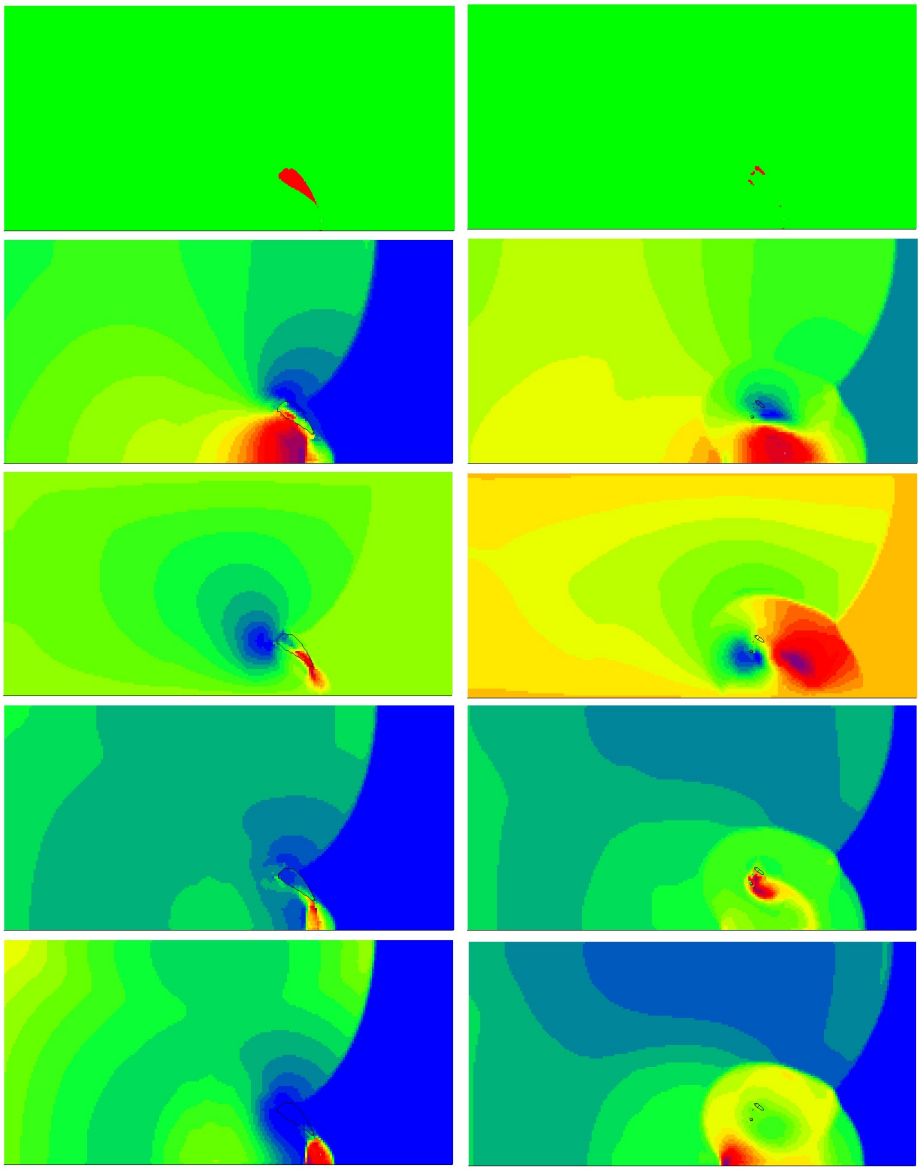

FIG. 2.16 – From top to bottom line : geometry of the bubble, horizontal component of the velocity, vertical component of the velocity, sound speed, pressure. Left row : time $t = 7.4\ \mu s$. Right row : time $t = 9\ \mu s$.

2.5.6 Spike of water in air

We consider a sinus shape interface between water and air. A shock wave in the water is propagating from right to left. Initial state for air is ($\rho_a = 1.\ kg/m^3, p_a = 10^5 Pa, u_a = 966.253\ m/s$), for water is ($\rho_0 = 1000.\ kg/m^3, p_0 = 10^5 Pa, u_0 = 966.253\ m/s$), for shocked water is ($\rho = 1285.71\ kg/m^3, p = 42\ 015.\ 10^5\ Pa, u = 0\ m/s$). Mach number is around $M = 3$. The domain is 39.6 cm long and 3.6 cm wide. Only the half geometry is computed. The mesh is made of 270x30 cells with geometric progression of aspect ratios in the grid, but preserving square cells on the spike.

FIG. 2.17 – Initial geometry, a shock wave is propagating in the water from right to left. A sinus shape interface between air at left and water at right.

Remark 33. *This case of Richtmyer-Meshkov instability, strongly tests the method robustness. Indeed, the spike is growing up occurring a very strong rarefaction in the water. In the air around the spike, an aerodynamical flow is developing, with a steady shock preceding the spike head. This case presents the same phenomenology, but much faster, as a bucket full of water dropped on the floor. When the bucket hits the floor, a shock wave is propagating upward in water, until it meets water/air interface at the bucket top. When this water surface is slightly perturbated by small wavelets, as the sinus shape in our case, the same kind of spikes are growing.*

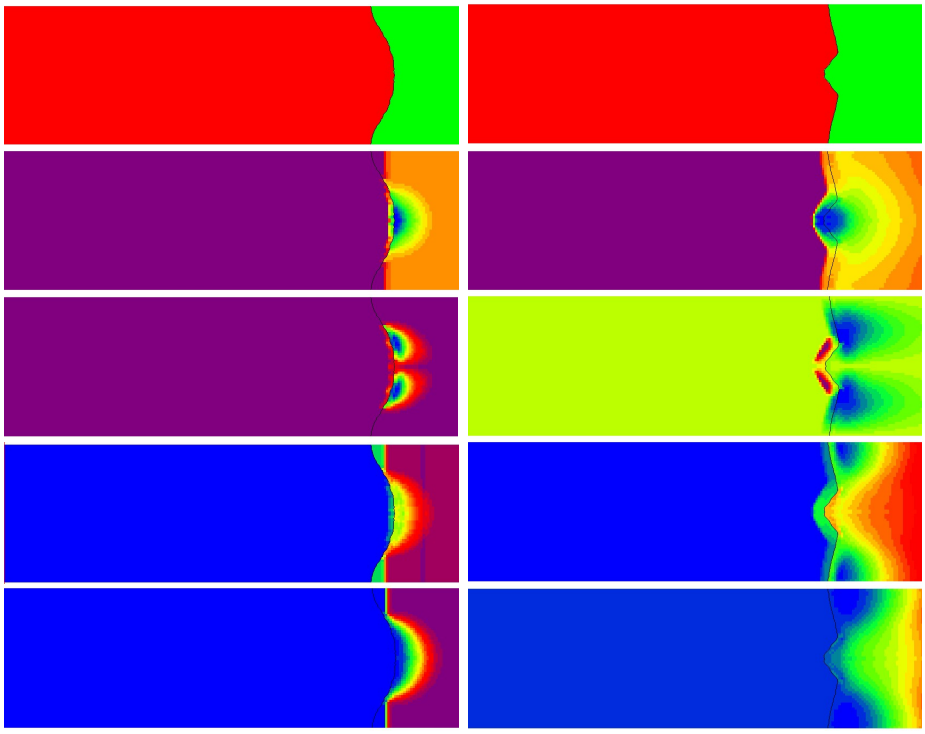

FIG. 2.18 – From top to bottom line : geometry of the spike, horizontal component of the velocity, vertical component of the velocity, sound speed, pressure. Left row : time $t = 3\ \mu s$. Right row : time $t = 7\ \mu s$.

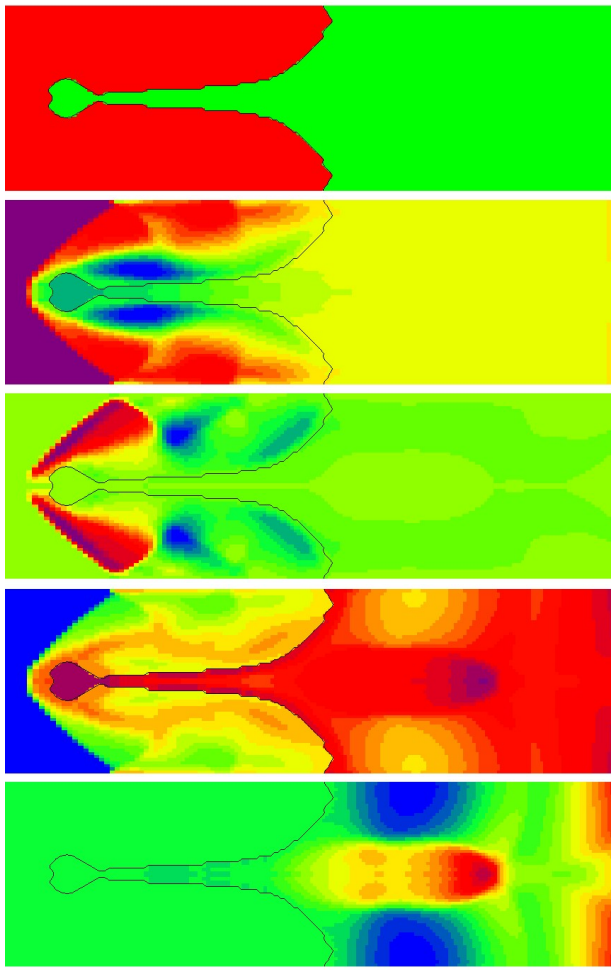

FIG. 2.19 – From top to bottom line : geometry of the spike, horizontal component of the velocity, vertical component of the velocity, sound speed, pressure. Time $t = 44\ \mu s$.

2.6 Conclusion

This method has been built step by step using severe benchmarks with very strong shocks, high sound speed ratios, high density ratios, high compressibility ratios and different equations of state for the fluids. This report describes the current result of the numerical studies we made to improve robustness. Of course, some points have to be further investigated. First concerning accuracy of the interface reconstruction considered yet to be of order one, that we will extend to order two by improvement of the remapping step of condensates. Second to investigate the possibility of free sliding of the materials in an Eulerian method with quantitative benchmarks and compare to other existing methods.

Chapitre 3

Chute d'un liquide sur une paroi

L'objet de ce chapitre est l'étude de la pression engendrée par la chute d'une masse d'eau sous l'effet de la gravité dans de l'air sur une paroi. L'objectif est d'étudier l'évolution de la pression maximale sur la paroi en fonction des paramètres du système. Les hypothèses de modélisation retenues pour l'eau et l'air sont communes à celles de la méthode, c'est-à-dire que les fluides sont non miscibles et séparés par une interface d'épaisseur nulle, que les fluides glissent parfaitement l'un sur l'autre, que le comportement de l'eau et de l'air est représenté par le modèle des équations d'Euler avec accélération par la gravité g :

$$\begin{cases} d_t\rho + \operatorname{div}(\rho u) = 0, \\ d_t(\rho u) + \operatorname{div}(\rho u \otimes u) + \nabla p = \rho\ g, \\ d_t(\rho E) + \operatorname{div}((\rho E + p)u) = \rho\ g \cdot u, \end{cases} \tag{3.1}$$

avec ρ la densité, $u \in \mathbb{R}^d$ le champ de vitesse, e l'énergie interne spécifique, p la pression et $E = e + |u|^2/2$ l'énergie totale spécifique.
De plus, le système est fermé par une équation d'état pour chacun des fluides :

- pour l'air, équation des gaz parfaits : la pression $p_{air} = (\gamma_{air} - 1)\rho_{air} e_{air}$, la vitesse du son $c^2_{air} = \gamma_{air} p_{air}/\rho_{air}$, le nombre de Grüneisen $\Gamma_{air} = \gamma_{air} - 1$. Le rapport des chaleurs spécifiques est $\gamma_{air} = 1.4$. Les conditons atmosphériques pour l'air sont alors supposées être proches de $(p_{air} = 10^5\ [Pa],\ \rho_{air} = 1\ [kg/m^3], T = 300\ [K])$, $c_{eau}(300K) = \sqrt{(\gamma_{air} p_{air})/\rho_{air}} = 374.16\ [m/s]$.

- pour l'eau, équation de Tate (ou Stiffened Gas) : la pression $p_{eau} = (\gamma_{eau} - 1)\rho_{eau}e_{eau} - \pi$, la vitesse du son $c^2_{eau} = (\gamma_{eau}p_{eau} + \pi)/\rho_{eau}$, le nombre de Grüneisen $\Gamma_{eau} = \gamma_{eau} - 1$. Les coefficients sont $\gamma_{eau} = 7$ et $\pi = 21\ 10^8\ Pa$. Les conditons atmosphériques pour l'eau sont alors supposées être proche de $(p_{eau} = 10^5\ [Pa], \rho_{eau} = 1000\ [kg/m^3], T_{eau} = 300\ [K])$, $c_{eau}(300K) = \sqrt{(\gamma_{eau}p_{eau} + \pi)/\rho_{eau}} = 1449.38\ [m/s]$.

3.1 Paramètres du système

La pression engendrée sur la paroi par la chute d'une masse d'eau dépend en particulier de la hauteur à partir de laquelle l'eau tombe et de la vitesse initiale de l'eau. En négligeant l'influence de l'air sur la chute de l'eau, le temps de chute et la vitesse de l'eau lors du choc sur la paroi est donnée par la relation fondamentale de la dynamique $m\ dv/dt = -m\ \overrightarrow{g}$:

$$\begin{aligned} t_c &= -\frac{v_0}{g} + \sqrt{\left(\frac{v_0}{g}\right)^2 + \frac{2\ h}{g}} \\ v_c &= g\ t_c + v_0 \end{aligned} \tag{3.2}$$

avec t_c la durée de la chute, v_c la vitesse du fluide au moment de l'impact sur la paroi, $g = 9.81 m/s^2$ l'accélération de la gravité, h la hauteur initiale de la face de l'eau entrant en contact avec la paroi, v_0 la vitesse initiale de l'eau au temps 0 supposée homogène dans tout le liquide.

En pratique, l'air est comprimé entre l'eau et la paroi et s'échappe de cette zone sous l'effet de l'augmentation de la pression. La pression de l'air s'opposant à la chute de l'eau dépend donc fortement de l'écoulement de l'air dans cette zone comprimée. La modélisation du glissement de l'air par rapport à la surface de l'eau et par rapport à la paroi est donc fondamentale dans ce cas test, car l'air doit pouvoir s'échapper de la zone comprimée jusqu'au moment de l'impact de l'eau sur la paroi.

3.2 Résultats numériques

Les dimensions du système $2D$ étudié sont : un bloc d'eau rectangulaire de 8 m x 5 m entouré d'air, dans une cuve de dimension 20 m x 15 m. La face basse du bloc d'eau est initiallement à 2 m du fond de la cuve. Le maillage

$v_0(m/s)$	$t_c(s)$	$v_{t_c}(m/s)$	$t_{c\ ca}(s)$	$p_{max\ ca}(bar)$
0	$0,638$	$6,264$	$0,636$	16
5	$0,307$	$8,014$	$0,316$	$16,6$
10	$0,183$	$11,8$	$0,191$	48
13	$0,145$	$14,430$	$0,15$	88
15	$0,127$	$16,255$	$0,133$	126
20	$0,097$	$20,958$	$0,101$	210

TAB. 3.1 – de gauche à droite : v_0 la vitesse initiale de l'eau vers le bas, t_c temps de chute théorique en l'absence d'air, v_{t_c} vitesse associée, $t_{c\ ca}$ temps correspondant à la pression maximale lors du calcul, $p_{max\ ca}$ pression maximale.

utilisé est 100x75 mailles et les conditions aux limites au bord du domaine sont de type mur. La gravité est verticale orientée vers le bas. La vitesse initiale de l'eau est verticale orientée vers le bas et de norme v_0, alors que la vitesse initiale de l'air est nulle.

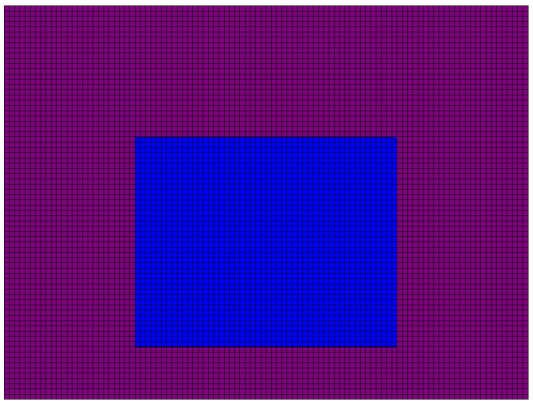

FIG. 3.1 – Géométrie initiale de l'eau dans la cuve.

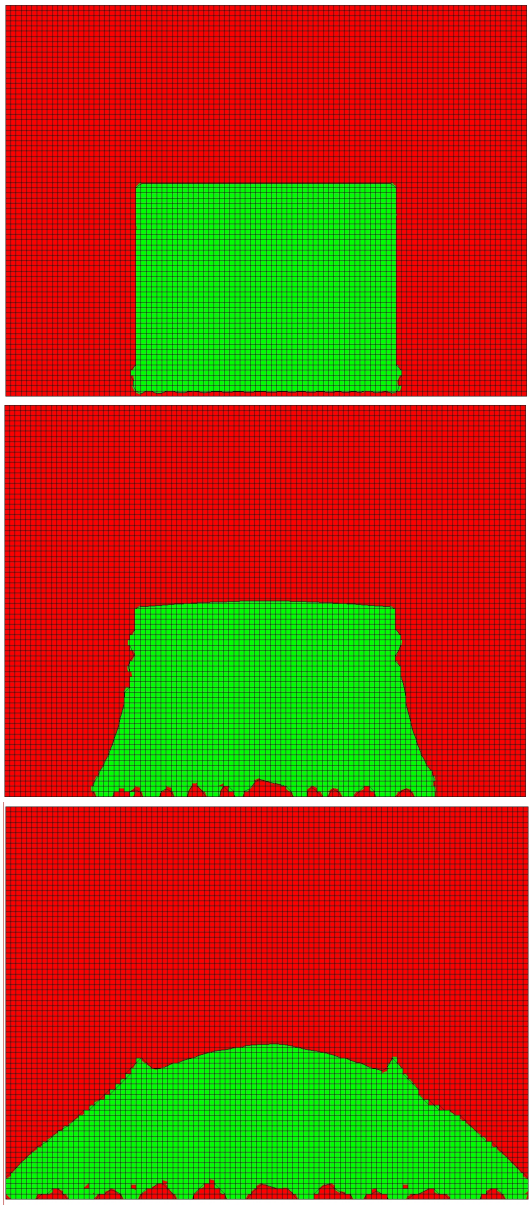

FIG. 3.2 – Géométrie de l'eau dans la cuve aux temps $t_1 = 0.12s$, $t_1 = 0.174s$, $t_1 = 0.35s$ pour une vitesse initiale de l'eau $v_0 = 15\ m/s$.

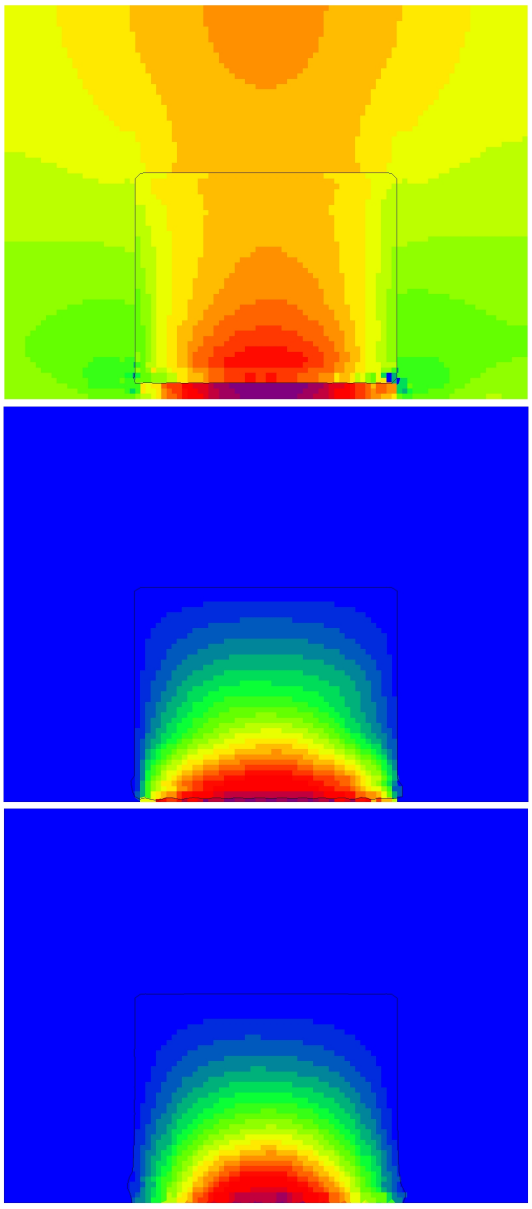

FIG. 3.3 – Pression aux temps $t_1 = 0.09s$, $t_1 = 0.12s$, $t_1 = 0.133s$ pour une vitesse initiale de l'eau $v_0 = 15\ m/s$.

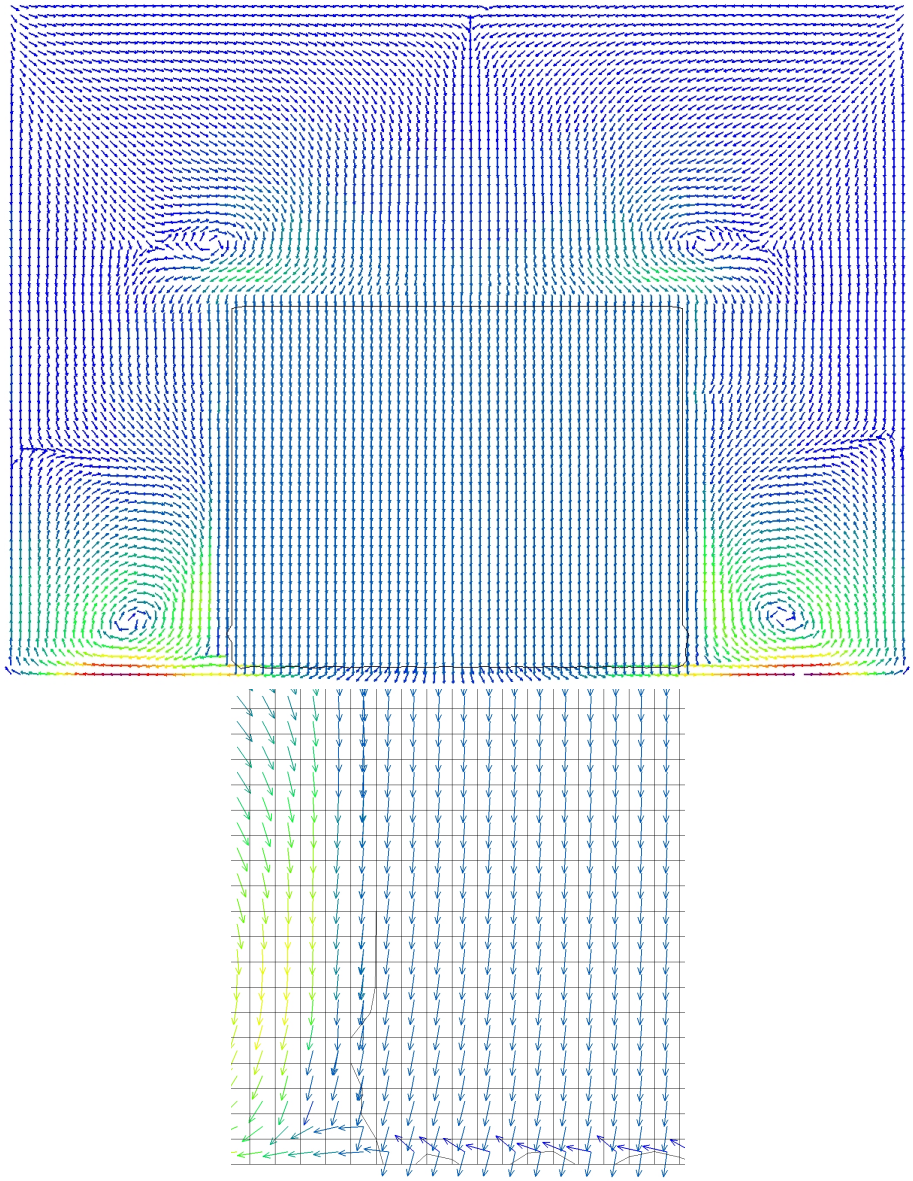

FIG. 3.4 – Champ de vitesse au temps $t = 0.12s$ et zoom sur la face avant de l'eau pour une vitesse initiale de l'eau $v_0 = 15\ m/s$.

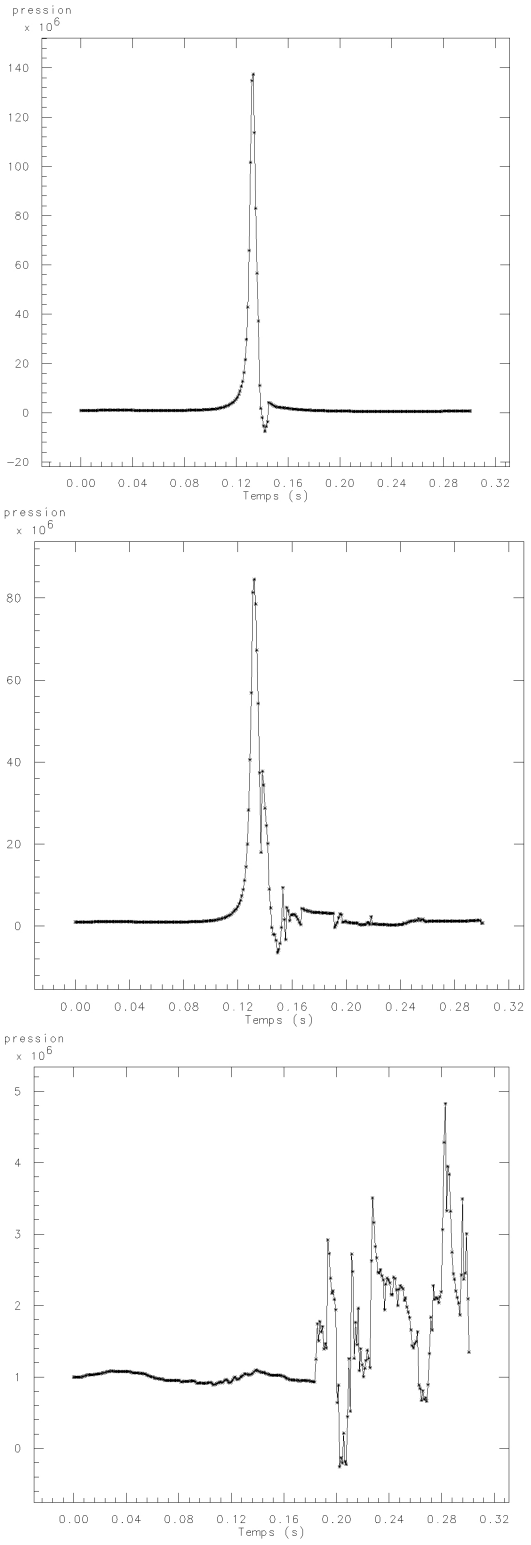

FIG. 3.5 – Historique de la pression sur la paroi aux abscisses $x = 10m$, $x = 12m$ et $x = 16m$ de l'eau pour une vitesse initiale de l'eau $v_0 = 15\ m/s$.

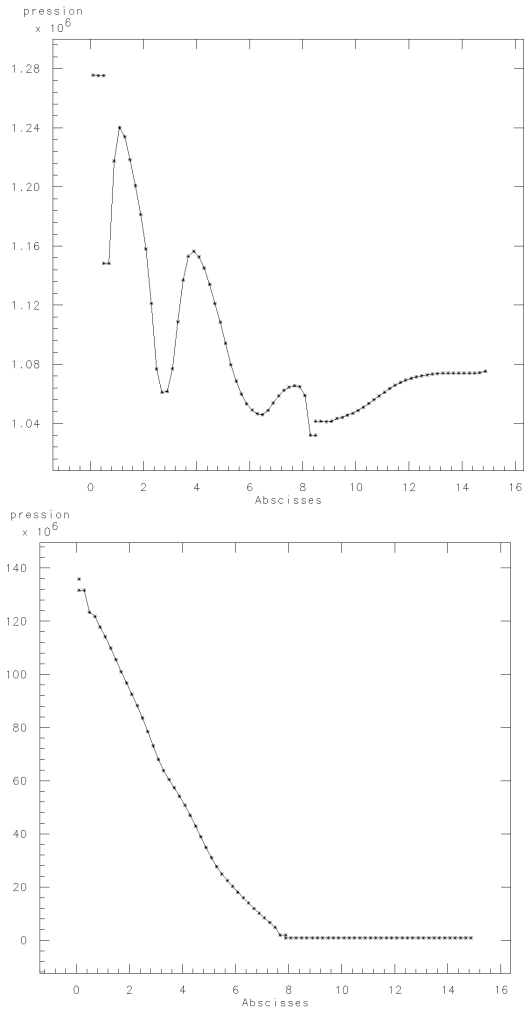

FIG. 3.6 – Coupe verticale de la pression à l'abscise $x = 10m$ aux temps $t = 0.09s$ et $t = 0.133s$ pour une vitesse initiale de l'eau $v_0 = 15\ m/s$.

Chapitre 4

Conclusion

Dans ce rapport, nous avons décrit la méthode *VFFC-NIP* (Natural Interface Positioning) qui permet de simuler les écoulements hydrodynamiques compressibles multi-matériaux avec reconstruction d'interfaces. Cette méthode est localement conservative pour les variables eulériennes (ρ, ρu, ρE) et permet un glissement parfait des matériaux aux interfaces. Nous avons proposé une méthode de contrôle de la solution pour pallier les difficultés liées au calcul de l'évolution des variables dans les très faibles volumes qui sont inévitablement créés lorsque une interface évolue dans un maillage eulérien. L'algorithme de contrôle met en jeu des contraintes sur l'évolution de la pression pour des équations d'état générales. Ceci est réalisé par le contrôle de l'évolution de la densité et de l'entropie. La méthode donne des résultats satisfaisants sur des cas-tests académiques et montre une très bonne robustesse, permettant de calculer des écoulements à fort gradients avec des équations d'état des matériaux très différentes. Cette modélisation du comportement des matériaux aux interfaces, glissement parfait, semble être bien adaptée aux matériaux aussi différents en terme de caractéristiques physiques que l'eau et l'air, comme nous avons pu le constater dans l'exemple de la chute d'un bloc d'eau dans de l'air au chapitre 3. Cette méthode reste cependant à améliorer par différents aspects.

La reconstruction d'interfaces pourrait être améliorée par une projection des condensats à l'ordre 2, considérant que la méthode décrite dans ce rapport est d'ordre 1. En effet, la projection d'une interface dans un condensat est aujourd'hui semblable à la description *SLIC* [58], à savoir que l'interface est considérée $1D$ (soit verticale, soit horizontale) lors de la projection et qu'elle

traverse entièrement la face d'une maille ou pas du tout. Une projection d'ordre 2 des condensats consisterait, de manière semblable à l'amélioration qu'a apporté *Youngs* dans les méthodes de type Lagrange-Projection [85], à prendre en compte l'inclinaison de l'interface lors de la projection. Dans un condensat, une interface chevauchant deux mailles serait alors projetée, créant des volumes partiels dans ces deux mailles. Cette amélioration pourrait diminuer l'affinité à 45 degrés des interfaces que semble montrer cette méthode.

D'autre part, il reste vraisemblablement des améliorations à apporter dans la résolution des condensats. Une implicitation de la méthode pourrait être envisagée, mais nos tests en la matière ont montré que cela conduit à des problèmes relativement raides à résoudre, notamment en présence de petits volumes. Une résolution explicite à l'ordre 2 des condensats, en un sens à définir, pourrait être envisageable pour obtenir une homogénéité de traitement entre les flux eulériens calculés à l'ordre 2 aux faces des mailles et les flux au travers des interfaces. De plus, il serait souhaitable d'améliorer l'algorithme de contrôle de la solution. D'une part, dans un condensat, les contraintes sur l'évolution des grandeurs dans les couches minces n'y assurent pas une croissance de l'entropie de la cas général. D'autre part, l'algorithme de projection de la solution pour satisfaire ces contraintes de manière globale sur le condensat pourrait être optimisé pour modifier le moins possible la solution initialement obtenue par le schéma. Enfin, l'utilisation de cette méthode pour la simulation d'écoulements en 3 dimensions pourrait nécessiter une programmation parallèle de l'algorithme.

Cependant, la démarche que nous avons proposée dans cette méthode semble prometteuse pour traiter des modèles physiques plus complexes. En effet, le centrement des variables, en particulier de la vitesse, dans les volumes partiels dans les mailles mixtes semble bien adapté à la discrétisation des contraintes dans les matériaux, ce qui pourrait s'avérer un avantage important dans le traitement de la tension de surface ou des écoulements élasto-plastiques par exemple. D'autre part, la formulation explicite des flux au travers des interfaces est un formalisme bien adapté au traitement du changement de phase d'un matériau où l'interface est le siège d'une transformation imposant la vitesse de l'interface et un flux de masse d'un matériau à l'autre. C'est le cas lorsque l'on traite des fronts de solidification ou la combustion de matériaux énergétiques tels que les propergols, par exemple.

D'autres modèles de fluides tels que le modèle de mélange turbulent *2SFK* de *Llor et al* [54] pourraient être traités à l'aide de cette méthode. En effet, d'une part, un travail important de *Ghidaglia et Pascal* [33] et de *Rovarch* [69] a permis de résoudre des modèles bifluides à 6 équations, qui sont la base du modèle *2SFK*, à l'aide du schéma *VFFC* en prenant en compte les termes non conservatifs qu'ils contiennent. D'autre part, la méthode avec reconstruction d'interfaces que nous proposons dans ce rapport semble très bien adaptée au traitement des flux turbulents entre les matériaux qui existent dans le modèle *2SFK*. Ce travail pourrait être mené lors d'une thèse à venir qui devrait s'avérer très enrichissante autant pour la compréhension de ces modèles turbulents que pour les outils numériques qui devront être développés.

Bibliographie

[1] R. Abgrall, How to prevent pressure oscillations in multicomponent flow calculations : a quasi conservative approach, *J. Comput. Phys.*, Vol. 125, p. 150–160, (1996).

[2] R. Abgrall, R. Loubère, J. Ovadia, A lagrangian Discontinuous Galerkin-type method on unstructured meshes to solve hydrodynamics problems, *Int. J. Numer. Meth. Fluids* 44, p. 645-663, (2004).

[3] R. Abgrall, J. Breil, P.-H. Maire, J. Ovadia, Un schéma centré pour l'hydrodynamique Lagrange bibimensionnelle, *Rapport Laboratoire de Recherche Correspondant du CEA* nM 03, LRC-04-10, (2004). `http://hal.inria.fr/inria-00113542`

[4] F. Alauzet, P.J. Frey, Estimateur d'erreur géométrique et métriques anisotropes pour l'adaptation de maillage. Partie 1 : aspects théoriques, *Rapport de recherche* RR-4759, INRIA, (2003).

[5] W.F. Ames, Numerical Method for Partial Differential Equations, Section 1.6 *Academic Press*, New York, (1977).

[6] D.M. Anderson, G.B. McFadden, A.A. Wheeler, A Diffuse-Interface Methods in Fluid Mechanics, *Ann. Rev. Fluid Mech.* Vol. 30, p. 139–165, (1998).

[7] I. Babuska, The finite element method with lagrange multipliers, *Numerische Mathematik*, 20, 179–192, (1973).

[8] R. Balian, Le temps macroscopique, Klein E., Spiro M. (eds.), Les Editions Frontières, (1994) ; Flammarion, Collection Champs, p. 155–211, (1995). `http://www-spht.cea.fr/articles/t94/009/`

[9] C. Baranger, Modeling of oscillations, breakup and collisions for droplets : the establishment of kernels for T.A.B. model, to appear, in *Math. Models Methods Appl. Sci.*

[10] T. Barth, Numerical Methods for Conservation Laws on Structured and Unstructured Meshes. VKI Lecture Series, (2003). `http://people.nas.nasa.gov/~barth/stanford_workshop/lecture_notes.pdf`

[11] D.J. Benson, Computational methods in Lagrangian and Eulerian hydrocodes. *Computer Methods in Applied Mechanics and Engineering*, 99, p. 235–394 (1992).

[12] D.J. Benson, An efficient, accurate, simple ALE method for nonlinear finite element programs, *Computer Methods in Applied Mechanics and Engineering*, vol.72 n.3, p.305–350, (1989).

[13] J.U. Brackbill, D. Jamet, D. Torres, On the theory and computation of surface tension : the elimination of parasitic currents through energy conservation in the second-gradient method, *J. Comput. Phys.* Vol. 182, Issue 1, p. 262–276, (2002).

[14] J.-P. Braeunig, B. Desjardins, J.-M. Ghidaglia, A pure eulerian scheme for multimaterial fluid flows, submitted *Eur. J. Mech. B–Fluids*, (2007).

[15] J.-P. Braeunig, B. Desjardins, C. Fochesato, J.-M. Ghidaglia. Interaction d'une onde de choc dans un liquide faiblement compressible avec une bulle de gaz sur une paroi, *Note CEA/DIF DO à paraître.*

[16] J.-P. Braeunig, J.-F. Bourgat, P. Charrier, F.Coatanea, B. Dubroca, G. Duffa, P. Le Tallec, L. Mieussens, B. Perthame, Comparison of discrete velociy and random particle methods for rarefied reentry flows, AIAA-2002-5180, (2002).

[17] F. Brezzi, M. Fortin, Mixed and Hybrid Finite Element Methods, *Springer-Verlag*, Heidelberg, (1991).

[18] L.J. Bridge, Computational Interface Capturing Methods for Phase Change in Porous Media, PhD Thesis, November 7, 2006. The University of British Columbia, Canada.

[19] C. Canuto, M. Y. Hussaini, A. Quarteroni, T.A. Zang, Spectral methods in fluid dynamics. *Springer-Verlag*, Berlin, (1988).

[20] K.A. Chang, W.B. Lindquist, Mass-Conserving Front Tracking for Miscible Two-Phase Flow, *SIAM Journal on Scientific Computing*, Vol. 18, 5, p. 1310–1327, (1997).

[21] P. Colella, P.R. Woodward, The piecewise parabolic method (PPM) for gas-dynamical simulations, *J. Comp. Phys.*, Vol. 54, p. 174–201, (1984).

[22] P. Colella, P.R. Woodward, The numerical simulation of two-dimensional fluid flow with strong shocks, *J. Comp. Phys.*, Vol. 54, p. 115–173, (1984).

[23] G.-H. Cottet, B. Rebourcet, L. Weynans, A multilevel adaptive particle-grid method for gas dynamics, ECCOMAS Thematic Conference on Meshless Methods, (2005).

[24] C.M. Dafermos, Polygonal approximations of solutions of the initial value problem for a conservation law, *J. Math. Anal. Appl.*, Vol. 38, p. 33–41, (1972).

[25] B. Desjardins, J. Francescatto, J.-M. Ghidaglia, A Multidimensional Multiphase Flow Finite Volume Solver using a Lagrangian Step and a Projection Technique, *Int. J. Finite Volumes*, (2007).

[26] B. Després, C. Mazeran, Symmetrization of Lagrangian gas dynamics in dimension two and multidimensional solvers, *C.R. Mécanique* 331, p. 475–480, (2003).

[27] B. Després, F. Lagoutière, La methode VoFiRe pour le transport bidimensionnel non dissipatif sur maillage quelconque. Rapport CEA, (2006).

[28] F. Dias, J.-M. Ghidaglia, G. Le Coq, On the fluid dynamics models for sloshing, *Rapport CMLA ENS Cachan* No 2007-1129, (2007).

[29] G. Dimonte, E. Frerking, M. Schneider, Richtmyer-Meshkov Instability in the Turbulent Regime, *Phys. Rev. Lett.* Vol. 74, p. 4855–4858 (1995).

[30] G. Dimonte et al, A comparative study of the turbulent Rayleigh-Taylor instability using high-resolution three-dimensional numerical simulations : The Alpha-Group collaboration, *Physics of Fluids* Vol. 16, 1668-1693 (2004).

[31] V. Dyadechko, M. Shashkov, Moment of fluid interface reconstruction, *Los Alamos report LA-UR-05-7571*, January 25, (2006).

[32] J.-M. Ghidaglia, Flux schemes for solving systems of conservation laws, `http://www.cmla.ens-cachan.fr/Cmla/Perfortmans/`, (1998).

[33] J.-M. Ghidaglia and F. Pascal. Flux boundary conditions for hyperbolic systems of conservations laws in the finite volume framework. In R. Herbin and D. Kroner, editors, *Finite volumes for complex applications* III, Problems and perspectives, p. 809–816, (2002).

[34] J.-M. Ghidaglia, A. Kumbaro, G. Le Coq, Une méthode volumes finis à flux caractéristiques pour la résolution numérique des systèmes hyperboliques de lois de conservation, *C.R. Acad. Sc. Paris*, Vol. 322, I, p. 981–988, (1996).

[35] J.-M. Ghidaglia, A. Kumbaro, G. Le Coq, On the numerical solution to two fluid models via a cell centered finite volume method, *Eur. J. Mech. B–Fluids*, Vol. 20, No 6, p.841–867, (2001).

[36] J. Glimm, J.W. Grove, X.L. Li, K.-M. Shyue, Y. Zeng, Q. Zhang, Three Dimensional Front Tracking, *SIAM Journal on Scientific Computing*,(1995).

[37] R. Glowinski, P. Le Tallec, M. Ravachol, V. Tsikkinis, Numerical solution of the Navier Stokes equations modelling the flow of two incompressible non miscible viscous fluids. *Finite Element in Fluids*, Vol. 8, p. 137–163, (1992).

[38] E. Godlewski, P. A. Raviart, Numerical approximation of hyperbolic systems of conservation laws, *Springer-Verlag*, (1996).

[39] S.K. Godunov, A finite difference method for the numerical computation and discontinuous solutions of the equations of fluid dynamics, Vol. 47, p. 271-306, (1959).

[40] F. Grasso, C. Speziale, Supersonic flow computations by two-equation turbulence modeling, AIAA 89-1951, (1989).

[41] J. Gressier, J.-M. Moschetta, Robustness versus accuracy in shock-wave computations, *Int. j. numer. methods fluids*, (1999).

[42] F. Grinstein, L.G. Margolin, W. Rider, Implicit Large Eddy Simulation, Computing turbulent fluid dynamics, *Cambridge University Press*, (2002).

[43] D. Gueyffier, J. Li, R. Scardovelli, S. Zaleski. Volume of fluid interface tracking with smoothed surface stress methods for three-dimensional flows, *J. Comp. Phys.*, Vol. 152, 423–456, (1999).

[44] H.Guillard, R.Abgrall, Modélisation numérique des fluides compressibles, Series in applied mathematics, P.-G. Ciarlet, P.-L. Lions, (2001).

[45] P. Hoch, Qualité de maillage et projection conservative en dynamique des fluides compressibles, Workshop "CEA-GAMNI", IHP Paris, 29-30 janvier 2007.

[46] D. Igra, K. Takayama, A high resolution upwind scheme for multicomponent flows, International journal for numerical methods in fluids *Int. j. numer. methods fluids* ISSN 0271-2091, vol. 38, No 10, p. 985–1007, (2002).

[47] A. Koniges, NIF-ALE-AMR : A Computational Tool for National Ignition Campaign Target Debris/Shrapnel Assessment, Workshop Numerical Methods for Multi-Material Fluid Flows, September 10th-14th, 2007. Czech Technical University, Prague, Czech Republic.
`http://www-troja.fjfi.cvut.cz/~multimat07/prezentace.html`

[48] B. Lafaurie C. Nardone, R. Scardovelli, S. Zaleski, G. Zanetti, Modelling merging and fragmentation in multiphase flows with SURFER. *J. Comput. Phys.*, Vol. 113, no. 1, p. 134–147, (1994).

[49] B.E. Launder, D.B. Spalding, Mathematical models of turbulence, *Academic Press*, (1972).

[50] A.-C. Lesage, A. Dervieux. A local mass conservation Method for the Level Set Method applied to twophase incompressible flow subjected to break-up Abstract submitted to ECCOMAS CFD 2006 *European Conference on Computational Fluid Dynamics*, The Netherlands, September 5-8 (2006).

[51] R.J. LeVeque, Numerical Methods for Conservation Laws, Birkhäuser, (1990).

[52] R. Liska, B. Wendroff, Comparision of several difference schemes on 1D and 2D test problems for the Euler equations, *SIAM J. Sci. Comput.* Vol. 25, No. 3, p. 995–1017, (2003).
Conservation Laws Preprint Server,
`http://www.math.ntnu.no/conservation/`, (2001).

[53] B. Liu, I. Lomov, Numerical modelling of explosions in underground chambers using interface tracking and material mixing, Workshop Numerical Methods for Multi-Material Fluid Flows September 5th-8th, 2005 St. Catherines College, Oxford, UK. `http://www.icfd.reading.ac.uk/Programme.htm`

[54] A. Llor, P. Bailly, O. Poujade, Derivation of a minimal 2-Fluid 2-Structure and 2-Turbulence (2SFK) model for gravitationally induced turbulent mixing layers, in : proceedings to be published of the 9th international workshop on compressible turbulent mixing, Cambridge, UK, 07/19-07/23/04.

[55] R. Loubère and M.J. Shashkov, A subcell remapping method on staggered polygonal grids for arbitrary-Lagrangian-Eulerian methods, *J. Comput. Phys.*, Vol. 209, 1, p. 105–138, (2005).

[56] R. Loubère, Une méthode particulaire Lagrangienne de type Galerkin Discontinu. Application à la Mécanique des Fluides et à l'Interaction Laser/Plasma, Thèse de Doctorat, Université Bordeaux 1, (2002).

[57] J. Mathiaud, Etude de systèmes de type Gaz-Particules, Thèse de Doctorat, Ecole Normale Supérieure de Cachan, (2006).

[58] W.F. Noh, P. Woodward, SLIC (Simple Line Interface Caculation), Lectures notes in Physics 59. *Editions Springer*, Berlin,(1976).

[59] S. Osher, F. Solomon, Upwind difference schemes for hyperbolic systems of conservation laws, *Math. Comp.* Vol. 38, p. 339–373, (1982).

[60] S. Osher, J. A. Sethian, Fronts propagating with curvature-dependent speed : Algorithms based on Hamilton-Jacobi formulations. *J. Comput. Phys.*, vol. 79, pages 12–49. (1988).

[61] O. Pironneau, Finite elements methods for fluids. Masson, (1989).

[62] S. Popinet, S. Zaleski, A front-tracking algorithm for accurate representation of surface tension. *Int. J. Num. Meth. Fluids*, Vol. 30, p. 775–793, (1999).

[63] E.G. Puckett, A.S. Almgren, J.B. Bell, D.L. Marcus, W.J. Rider, A high-order projection method for tracking fluid interfaces in variable density incompressible flows. *J. Comput. Phys.*, Vol. 130, p. 269–282, (1997).

[64] J.J. Quirk, A contribution to the great Riemann solver debate, *International Journal for Numerical Methods in Fluids*, Vol. 18, p. 555–574, (1994).

[65] P.-A. Raviart, J.-M. Thomas, Introduction à l'analyse numérique des équations aux dérivées partielles, Masson, (1983).

[66] R.D. Richtmyer, K.W. Morton, Difference methods for initial-value problems, John Wiley, (1967).

[67] P.L. Roe, Characteristic-based schemes for the Euler equations, *Ann. Rev. Fluid Mech.*, Vol. 18, p. 337, (1986).

[68] X. Rogue, Rodriguez, J.-F.Haas, and R. Saurel, Experimental and numerical investigation of the shock-induced fluidization of a particle bed, *Shock Waves*, Vol. 8, 29–45, (1998).

[69] J.-M. Rovarch, Solveurs tri–dimensionnels pour les écoulements de fluides diphasiques avec transferts d'énergie, Thèse de Doctorat, ENS de Cachan, (2003).

[70] P. Sagaut, Simulation numérique d'écoulements décollés avec des modèles de sous-mailles, Rapport de Thèse, Université de Paris VI, (1995).

[71] J. Serrin, J.E. Dunn, On the thermomechanics of interstitial working, *Arch. Rational Mech. Anal.* Vol. 88, p. 95–133,(1985).

[72] J.A. Sethian, Level Set methods, Cambridge University Press, Cambridge, (1996).

[73] C.W. Shu, S. Osher, Efficient implementation of essentially non-oscillatory shock-capturing schemes, *J. Comput. Phys.*, Vol. 2, p. 439–471, (1988).

[74] J. Smagorinsky, General circulation experiments with the primitive equations .I. The basic experiment, *Month. Weather Rev.* , 91–164, (1963).

[75] P. Smereka, J.A. Sethian, Level Set Methods for Fluid Interfaces, A*nnual Review of Fluid Mechanics* Vol. 35, p. 341–372 (2003).

[76] D. Stevens, Multiphase flow in ALE3D, Workshop Numerical Methods for Multi-Material Fluid Flows September 5th-8th, 2005 St. Catherines College, Oxford, UK. `http://www.icfd.reading.ac.uk/Programme.htm`

[77] M. Sussman, P. Smereka, S. Osher, A level set approach for computing solutions to incompressible two-phase flow, *Journal of Computational Physics*, Vol. 114, p. 146–159 (1994).

[78] E.F. Toro, Riemann solvers and numerical methods for fluid dynamics, *Springer*, Berlin (1999).

[79] B. Van Leer, Towards the ultimate conservative difference scheme : IV. A new approach to numerical convection, *J. Comput. Phys.*, vol. 23, p. 276–299 (1977).

[80] J. P. Vila, Méthodes particulaires régularisées. Développements récents et nouvelles applications, Actes du 29eme Congrès d'Analyse Nulérique : CANUM'97, ESAIM : PROC., Vol. 3, p. 131–146, (1998).

[81] J. Von Neumann, R.D. Richtmyer, A method for the numerical simulation of hydrodynamics shocks , *J. Appl. Phys.*, 21, (1950).

[82] F. de Vuyst, J.-M. Ghidaglia et G. Le Coq, On the numerical simulation of multiphase water flows with changes of phase and strong gradients using the Homogeneous Equilibrium Model, *Int. J. Finite Volumes*, (2005).

[83] M.L. Wilkins, Calculation of elastic plastic flow Methods, *Computationnal Physics* (3), (1964).

[84] C.T. Wu, J.H. Ferziger, D.R. Chapman, Simulation and modeling of homogeneous turbulence, Dept. of mechanical engineering, *Stanford Univ.*, (1985).

[85] D.L. Youngs, Time-Dependent multi-material flow with large fluid distortion, *Numerical Methods for Fluid Dynamics*, edited by K. W. Morton and M. J. Baines, p. 273–285, (1982).

[86] D.L.Youngs, Modelling turbulent mixing by Rayleigh-Taylor instability. *Advances in fluid turbulence* (Los Alamos, NM, 1988), no. 1-3, 270–287 Phys. D 37 (1989).

[87] D.L.Youngs, A Numerical Technique for 2D Compressible Multiphase Flow *Paper presented at the workshop Numerical methods for multimaterial flows*, Paris, September 23-25 (2002).

[88] D.L. Youngs, Numerical simulation of mixing by Rayleigh-Taylor and Richtmyer-Meshkov instabilities, *Laser and Particle Beams* Vol. 12, p. 725-750 (1994).

[89] F. Zhang et al, Explosive Dispersal of Solid Particles, *Shock Waves*, 11, 431-443, (2001).

[90] O.C. Zienkiewicz, The finite element method in engineering science, *Mac Graw Hill*, (1977).

Table des figures